ABSTRACT

Title of dissertation: PRESSURE-BASED PREDICTION OF SPRAY COOLING HEAT TRANSFER

Bahman Abbasi, Ph.D., 2010

Directed by: Professor Jungho Kim, Department of Mechanical Engineering

One of the main challenges of spray cooling technology is the prediction of local and average heat flux on the heater surface. It has been suggested that spray cooling heat transfer depends on the local spray mass flux. However, in this work it is hypothesized and demonstrated that local single-phase and boiling heat transfer can be predicted within ±25% of the measured values from the local normal pressure produced by the spray. In the single-phase study, hollow cone, full cone, and flat fan sprays operated at three standoff distances, five spray pressures, and two nozzle orientations were used to identify the relation between impingement pressure and heat transfer coefficient. PF-5060, PAO-2, and PSF-3 were used as test fluids, resulting in Prandtl number variation between 12-76. A 7×7 mm^2 micro-heater array consisting of 96 platinum resistance heaters operated at constant temperature was used to measure the local heat flux. A separate test rig was used to make impingement pressure measurements for the same geometry and spray pressure. The heat flux data were then compared with the corresponding impingement

pressure data to develop a pressure-based correlation for single-phase spray cooling heat transfer.

Hollow cone and full cone PF-5060 sprays at three subcooling levels were used for the two-phase heat transfer study. The conventional wisdom is that the temperature at which critical heat flux (CHF) is observed changes with the droplet impact velocity, droplet number density, and droplet size. However, the present measurements indicate that although the magnitude of CHF is strongly dependent on the spray characteristics, the temperature at which CHF occurs lies within a very narrow band (about ±5°C) for smooth flat surfaces. This was also observed from local measurements at various radial distances using hollow cone and full cone spray nozzles where the local mass flux varies dramatically. This observation along with liquid properties and subcooling were used to develop a correlation to predict local CHF for PF-5060 sprays. The single-phase and CHF correlations were combined to predict local spray cooling curve within ±25% of the measured valued over the sprays impingement zones.

PRESSURE-BASED PREDICTION OF SPRAY COOLING HEAT TRANSFER

By

Bahman Abbasi

Dissertation submitted to the Faculty of the Graduate School of the

University of Maryland, College Park, in partial fulfillment

of the requirements for the degree of

Doctor of Philosophy

2010

Advisory Committee:

Professor Jungho Kim (Advisor/Chair)

Professor Marino di Marzo

Professor Andre Marshall

Professor Reinhard Radermacher

Professor Tien-Mo Shih

Professor Kenneth Yu

To my parents

ACKNOWLEDGEMENTS

First and foremost, I would like to acknowledge the guidance and support of my advisor, Professor Jungho Kim. This dissertation would have not been possible without his insight and valuable suggestions. I also appreciate the suggestions of my advisory committee members, Dr. Marino di Marzo, Dr. Andre Marshall, Dr. Reinhard Radermacher, Dr. Tien-Mo Shih, and Dr. Kenneth Yu. Furthermore, I appreciate Dr. Andre Marshall and the Fire Protection Engineering Department who generously allowed me to work with the Malvern Laser Analyzer system in their laboratory facilities. This dissertation benefited from the assistance of many people in the Department of Mechanical Engineering. I would like to specially thank the department's Chair, Dr. Bar-Cohen, and the department's machine shop manager and my friend Mr. Al Aaron.

I was very fortunate to work alongside a number of wonderful friends and distinguished current and former students: Dr. Payam Delgoshaei, Dr. Rishi Raj, Micheal Siemann, Dr. Jack Coursey, Dr. Greg Anderson, Dr. Kevin Moore, Steve Fuqua, etc. In particular, I have to thank my friends Payam, Rishi, Michael, and Greg for their invaluable help in many occasions, spirited discussions about the research, and more importantly for their friendship and support. Also, I want to thank Jack for his great help in designing and building the experimental apparatuses.

A number of great student interns also helped me in conducting the experiments. I like to acknowledge Patrick Schrimpf, Funda Karakas, Markus Nicklas, and Martin Karch for their hard work and valuable help. Specially, I would like to thank my good friend Patrick for working tirelessly on the pressure measurement and droplet size analyzer apparatuses.

As always, my greatest gratitude and appreciation is to my parents for their everyday inspiration and encouragement and unspeakable sacrifices without which I could never stand here. My brother has always been there for me and I cannot thank him enough for that. And I want to specially thank my lovely wife, Shafagh, whom every moment with, is a beautiful memory.

TABLE OF CONTENTS

LIST OF FIGURES

LIST OF TABLES

NOMENCLATURE

a	Absorbance
A	Heater surface area (m^2)
A_0	Orifice surface area (m^2)
c_p	Heat capacity (J/kgK)
Ca	Capillary number - $(\mu/\sigma)\left(\sqrt{P/\rho}\right)$
CHF	Critical Heat Flux (W/m^2)
d	Diameter (m)
d_0	Nozzle orifice diameter (m)
d_{32}	Sauter Mean Diameter (m)
D	Liquid dispersion (mm^3/mm^2s)
Ec	Eckert number - $V^2/c_p\Delta T_{sat}$ or $P/\rho c_p\Delta T$
f_{inj}	Spray injection frequency (Hz)
h	Heat transfer coefficient (W/m^2K)
h_{fg}	Latent heat of vaporization (J/kg)
H	Pressure-based Stanton number - $h/(\rho P)^{0.5}c_p$
Ja	Jacob number - $c_p\Delta T_{sat}/h_{fg}$
k	Thermal conductivity (W/mK)
l	Distance (m)
La	Laplace number - $\rho\sigma d_{32}/\mu^2$
m''	Local mass flux (kg/m^2s)
$\dot{m}$	Local mass flow rate (kg/s)

MAE	Mean absolute error
N	Droplet number density (#/m^3)
Nu	Nusselt number - $c_p\mu/k$
ONB	Onset of nucleate boiling
P	Local spray impingement pressure (Pa)
ΔP	Pressure change across the nozzle (Pa)
Pr	Prandtl number - $c_p\mu/k$
q''	Heat flux (W/m^2)
Q''	Local volumetric flux (m^3/m^{2}s)
$\overline{Q}''$	Area-averaged volumetric flux (m^3/m^{2}s)
Re	Reynolds number - $\rho Vd/\mu$
RSME	Root mean square error
R_{DP}	Digital potentiometer resistance (Ω)
s	Standoff distance (m)
SMD	Sauter Mean Diameter - d_{32}
St	Stanton number - $h/\rho Vc_p$
Δt_{inj}	Time interval between two successive injections (s)
T	Temperature (K or °C)
Tr	Laser transmission (%)
ΔT	T_w - T_f (K or °C)
ΔT_{sub}	T_{sat} - T_f (K or °C)
ΔT_{CHF}	T_{CHF} - T_f (K or °C)
V	Velocity (m/s)

We	Weber number - $\rho V^2 d/\sigma$

Greek Symbols

α	Nozzle inclination (degrees)
δ_T	Thermal boundary layer thickness (m)
δ_v	Viscous boundary layer thickness (m)
λ	Droplet flux - log[$\rho V/m''$]
μ	Dynamic viscosity (Pa.s)
σ	Surface tension (N/m)
ρ	Density (kg/m^3)
θ	Spray cone angle (degrees)
ψ	Attenuation (%)

Subscripts

1-ϕ	Single-phase
2-ϕ	Two-phase
CHF	Critical heat flux conditions
f	Liquid
g	Gas
ONB	Onset of nucleate boiling conditions
s	Spray
sat	Saturation conditions
w	Wall

CHAPTER ONE: INTRODUCTION

1-1- Motivation

The high heat dissipation rate of future electronics necessitates efficient removal of the generated waste heat. Natural and forced convection systems using air are the basis of most current cooling systems in the electronic industry. However, the limited capacity of these systems have led to implementation of liquid cooling systems in some of the more advanced systems. Submerged cooling of electronic devices using dielectric liquids has been tried in some systems and has been proven to be far more capable than the forced air systems. Bar-Cohen, et al. (2006) presented a review of the technical aspects and performance of different direct liquid cooling systems for high heat flux electronic components. Among these techniques, spray cooling technology is a particularly promising tool to provide a long term solution to the problem of overheating electronic components. As liquid is forced through a small orifice, inertia forces overcome the surface tension and inter-molecular forces and disperse the liquid into a large number of fine droplets that vary in size and velocity depending on the ejection pressure and liquid properties. Upon impact, the droplets spread on the surface and remove heat through single-phase and two-phase mechanisms. In the single-phase regime the forced convection due to the flowing thin liquid film is enhanced through agitation by the impacting droplets and quick replacement of heated liquid with cooler incoming liquid.

Boiling heat transfer in the two-phase regime can remove even larger amounts of heat from a target surface. The heat removed by evaporation is often far greater than single-phase (due to the evaporation latent heat). So it is often more desirable and cost efficient

to operate in the two-phase regime. In the two-phase regime, heat removal is largely due to thin film evaporation, secondary nucleation, and contact line evaporation. A review of spray cooling is given in Kim (2007) and a review of high heat flux cooling technologies including spray cooling can be found in Manglik and Jog (2009).

An important goal in spray cooling research is to develop simple and reliable methods to predict local and average heat transfer from the heater. The highly complex fluid dynamics and heat transfer phenomena in spray cooling makes it especially difficult to make such predictions. Although there are several models available to predict spray cooling heat transfer, they almost always rely on droplet velocity, size, and number concentration data. These measurements are expensive and tedious to acquire. Also, almost all of the correlations in the literature are valid only for one fluid (or occasionally a few fluids). In the two-phase regime, there are very few models available for the heat flux at the CHF point and even fewer for the entire spray cooling curve. Almost all the models for either heat transfer regimes are area-averaged and have not been validated at local levels.

1-2- Hypothesis

It is the thesis of the current work that the spray heat transfer depends primarily on the *kinetic energy* of the incoming droplets rather than just the flow rate of liquid through the nozzle (which is often the assumption in other studies on spray cooling). The droplets transfer this energy to the liquid film in the form of thinning of the boundary layer and increased agitation, the amount of which is related to the dynamic pressure exerted by the droplets onto the surface. This connection is also suggested by studies of droplets striking

free liquid surfaces. For example, Oguz and Prosperetti (1990) and Prosperetti and Oguz (1993) showed that the depth to which a liquid mass penetrated a deep pool of liquid depended on its initial kinetic energy at impact. They used the Froude number and Weber number (both representing the droplet kinetic energy) to predict the radius of a hemispherical cavity in the liquid layer created by droplet impingement. Zhu, Oguz, and Prosperetti (2000) and Fedorchenko and Wang (2005) also used the droplet kinetic energy described in terms of the Weber and Froude number to estimate the droplet penetration length. A similar approach has been implemented in numerical studies such as those of Weiss and Yarin (1999) and Jossenard and Zaleski (2003), where different combinations of Froude, Weber, and Reynolds numbers were used to study droplet impact on films. These studies indicate that the kinetic energy of the droplets (manifested in form of the impingement pressure), and not the mass flux, is widely regarded as important in describing the droplet impact phenomena. It is expected to be just as important in heat transfer.

The local impingement pressure is hypothesized to be the controlling parameter for spray cooling heat transfer in the single-phase region. If such a connection can be established, the local and average heat transfer coefficients can be predicted from the easily measured local impingement pressure and liquid properties. A major advantage of this method is that it can account for nozzle and spray characteristics, spray-to-heater distance, nozzle inclination, spray pressure, number of sprays, etc. According to this hypothesis,

$$h_{1-\phi} = f(P, \rho, \mu, c_p, k) \tag{1}$$

Nondimensionalizing yields

$$H = \frac{h_{1-\phi}}{(\rho P)^{0.5} c_p} = CPr^a \tag{2}$$

or

$$h_{1-\phi} = C_1 P^{0.5} \qquad C_1 = C' \rho^{0.5} c_p Pr^a \tag{3}$$

The nondimensional group *H* can be viewed as a pressure-based Stanton number.

It is hypothesized that local impingement pressure remains the driving parameter throughout the process until the CHF condition is reached. It is assumed that CHF is a function of fluid properties, local impingement pressure, and subcooling:

$$q''_{CHF} = f(P, \rho, \mu, k, c_p, h_{fg}, \sigma, \Delta T_{CHF}) \tag{4}$$

It is hypothesized that pressure drives the heat transfer, *Ja* accounts for the effect of subcooling, and a proper combination of fluid properties in form of a constant *C* summarizes the effects of fluid properties. Therefore,

$$q''_{CHF} = CP^{c_1} Ja_{CHF}^{c_2} \tag{5}$$

Experimentation under different conditions is needed to verify these hypotheses and calculate the constants and coefficients. A schematic of spray impingement on liquid film is given in Figure 1.

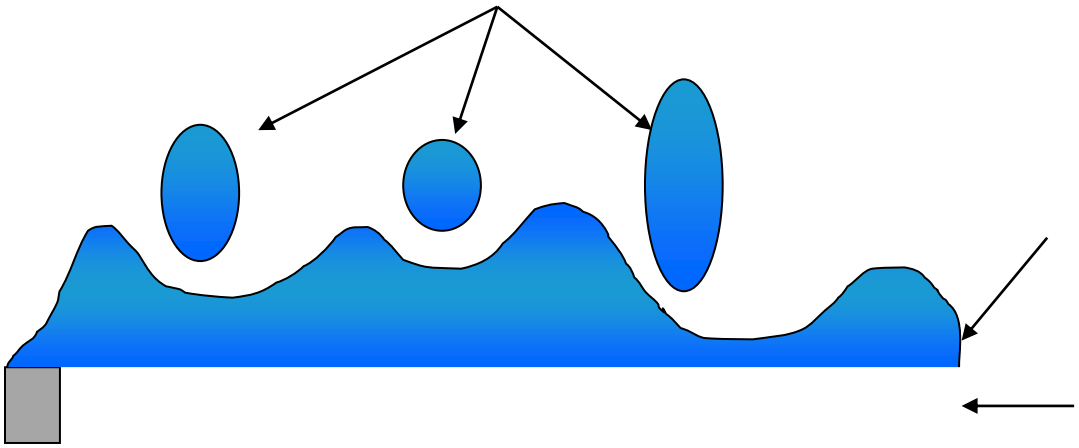

Figure 1. Schematic of droplet impingement on liquid film

1-3- Research Objectives and Approach

Developing accurate, inexpensive, and easy-to-use models that are valid for a reasonable range of fluids is an important requirement in thermal management using spray cooling. A review of the literature reveals some major areas in the field that deserve more attention. One of these areas is predicting local heat flux from spray cooling. Large localized heat dissipation in many electronic components requires predicting both area-averaged and local heat removal. Another major area that requires further investigation is two-phase heat transfer regime. Boiling heat transfer mechanisms have not been

accurately identified and the effects of different parameters have not been adequately characterized. This work was targeted to fill these gaps:

1. Investigate the hypothesis that local impingement pressure is the driving parameter in spray cooling heat transfer. In other words, all the hydrodynamic factors, geometrical specifications, and spray characteristics will translate into local impingement pressure.
2. Propose a unified model to predict the entire local spray cooling curves. The model has to be independent of spray pattern, geometry, and should be valid for a wide range of fluids. Such model will also be valid for area-averaged predictions.
3. Identify the heat transfer mechanisms in single- and two-phase regimes. Review the suggested heat transfer mechanisms and use the experimental data to narrow down the possible dominating mechanisms.

Three experimental setups were designed to investigate the link between local impingement pressure and heat transfer. One setup was used to acquire impingement pressure data for many spray conditions and fluids. The exact same conditions were used to produce the same sprays in another setup, where the heat fluxes were measured. The data from the two systems allowed for examination of the basic hypothesis of this work. To further study the hydrodynamic effects of the sprays a third experimental setup was designed and the range of droplet sizes and number density were measured.

Developing the correlations comprised the largest part of this thesis. The work was divided into two parts for the two heat transfer regimes. A separate test matrix was designed for each regime where the impingement pressure and heat flux data for many test cases were acquired and used to develop a correlation for the single-phase regime and

for the CHF conditions. The two correlations were then combined using a non-dimensional weighting function to predict the local spray cooling curves from single-phase through CHF.

1-4- Chapter Summary

Excessive thermal dissipation is a major limiting factor in the advancement of electronic systems. Spray cooling has gained much attention as a technique to provide a long term solution to the problem. Complexity of the spray systems has made it difficult to predict the local heat removal rate of the cooling systems. The current correlations that are used to predict heat flux rely on expensive and tedious measurements, are limited to very few fluids, and do not capture the underlying mechanisms that dominate the heat transfer. This dissertation is developed to provide physics-based, simple, and accurate predictions of heat transfer in the single- and two-phase regimes with a wide validity range.

CHAPTER TWO: THE STATE OF THE ART

There is a large body of literature available on spray cooling heat transfer. This chapter is provides a review of some of the major studies and discuss different approaches to the problem. Due to fundamentally different aspects and processes, the discussion is divided into two parts, corresponding to the two heat transfer regimes. Another section provides a review of two-phase heat transfer mechanisms in pool boiling as well as spray cooling.

2-1- Single-phase Heat Transfer Correlations

It has been suggested that local volumetric flux is the controlling parameter in single-phase spray cooling heat transfer. Ashwood and Shedd (2007) and Shedd (2007) assumed that the spray produced a liquid film on the surface that could be described through a two-layer model where a turbulent liquid layer flowed over a thin viscous sublayer of thickness δ_v. The heat transfer coefficient could be expressed as

$$h = \frac{k}{\delta_T} = \frac{k}{\delta_v} Pr^n \tag{6}$$

where δ_T is the thermal boundary layer thickness. In the sublayer, the non-dimensional velocity profile $u^+=y^+$ can be manipulated to yield $\delta_v = \beta\nu/\sqrt{\tau/\rho}$. The heat transfer coefficient could then be written

$$h = \frac{k}{\beta \nu}\sqrt{\frac{\tau}{\rho}}Pr^{n} \tag{7}$$

where β is a dimensionless sublayer thickness. Since the shear stress τ was not known, he assumed that it could be related to the volumetric flow rate, $\overline{Q}''$ [m^3/m^2-s], of droplets striking the surface. The final form of his correlation was

$$h = C_{sys}\rho c_p \overline{Q}''^{0.5} Pr^{-0.5} \tag{8}$$

The value of C_{sys} depended on the spray system geometry. They used various spray configurations with FC-72, FC-74, FC-40, HFE-7000, HFE-7100, and their mixtures to estimate C_{sys}. For single nozzle conical sprays, C_{sys}=0.149 $m^{0.5}s^{-0.5}$, while their four-nozzle arrays were about 14% less efficient, resulting in C_{sys}=0.129 $m^{0.5}s^{-0.5}$. The droplet size and velocity were not assumed to have significant influence on the heat transfer.

Estes and Mudawar (1995), Rybicki and Mudawar (2006), and Visaria and Mudawar (2008) conducted various studies and proposed a number of models for Sauter Mean Diameter, single and two-phase heat transfer, and CHF. They suggested that d_{32} for FC-87, FC-72, and water could be calculated from

$$\frac{d_{32}}{d_0} = 3.07\left[\frac{\rho_v^{0.5}\Delta P d_0^{1.5}}{\sigma^{0.5}\mu}\right]^{-0.259} \tag{9}$$

and the droplets mean velocity was given by

$$V = \left[V_{tube}^2 + \frac{2\Delta P}{\rho} - \frac{12\sigma}{\rho d_{32}} \right]^{0.5} \tag{10}$$

Also, they suggested that the single-phase *Nu* for PF-5052 spray could be predicted with an absolute error of 13.1% from

$$Nu_{d_{32}} = 4.70 Re_{d_{32}}^{0.61} Pr^{0.32} \tag{11}$$

where $Nu_{d_{32}} = \left[q'' / T_{surface} - T_{liquid} \right] \left[d_{32} / k \right] = h d_{32} / k$ and $Re_{d_{32}} = \rho \overline{Q}'' d_{32} / \mu$. This correlation also assumed that the heat transfer coefficient depended on the volumetric flow rate of droplets onto the surface.

Both of the above correlations assume the spray cooling heat transfer depends primarily on the local volumetric flux. For simplicity, consider a spray containing droplets of uniform diameter (*d*). The volumetric flux is given by

$$\overline{Q}'' = \frac{1}{6} \pi d^3 N V \tag{12}$$

Shedd's correlation suggests that the heat transfer coefficient remains constant if $\overline{Q}''$ remains constant, irrespective of large variations in *d*, *V*, and *N*. Similarly, the Rybicki

and Mudawar (2006) correlation yields constant heat transfer coefficient if the quantity $\overline{Q}''^{0.61}/d_{32}^{0.39} \propto N^{0.61} d_{32}^{1.44} V^{0.61}$ remains constant.

Single-phase heat transfer coefficient depends on the fluid properties and hydrodynamics of the spray, in other words

$$h = f(V, d_{32}, N, \rho, c_p, \mu, k) \tag{13}$$

and through dimensional analysis:

$$Nu_{d_{32}} \propto Re_{d_{32}}^{d} Pr^{e} (d_{32}^{3} N)^{f} \tag{14}$$

Pursuing this approach requires knowledge of all the above parameters which are very difficult to obtain and even then at least four different fluids are needed to calculate the correlation constants. On the other hand, the effects of velocity, Sauter Mean Diameter, and droplet density can be summarized in the dynamic pressure in the following form,

$$P = \frac{1}{2} \rho_{effective} V^2 = \frac{1}{2} \left[\frac{\pi d_{32}^3}{6} \rho N \right] V^2 \tag{15}$$

Bratuta and Ivanowsky (1982) recommended the following correlation to estimate the heat flux in water spray cooling.

$$\dot{q}'' = 4.616^{6} \Delta T^{0.1} D^{0.4} \tag{16}$$

Karwa, et al. (2007) suggested the following correlation for average *Nu* in the single-phase heat transfer regime based on data collected from full cone water spray impingement on a constant heat flux heater at various pressures. The correlation claimed to predict *Nu* within ±7.3%.

$$Nu = 20.344\, Re^{0.659} \tag{17}$$

R-134a sprays were used by Hsieh and Tien (2007) to develop the following correlation for average *Nu* for non-boiling regimes with an accuracy of ±10%:

$$Nu = 933 We^{0.36} (d_{32}/d_0)^{0.25} (\Delta T/T_s)^{0.027} \tag{18}$$

In a study of the cooling effects of fuel injection on the internal combustion engine intake valves, Panao and Moreira (2005), Moreira, et al. (2007), and Panao and Moreira (2009) carried out a series of studies on single and two-phase heat transfer in gasoline spray heat transfer analytically, numerically, and experimentally. They argued that

$$h = f(d_{32}, V, \rho, k, \mu, c_p, \sigma, h_{fg}, \Delta T_{sat}) \tag{19}$$

which after nondimensionalizing reduces to

$$Nu = aRe^m Pr^n We^p Ja^q Ec^w \tag{20}$$

By ignoring *We* and *Ec*, they proposed the following correlation for gasoline-like fluids for temperatures between 50-150°C with an uncertainty of ±26%.

$$Nu = 3.4 \times 10^{-5} Re^{1.51} Ja^{-0.254} \tag{21}$$

In order to account for the intermittency of the injections in an internal combustion engine they refined their hypothesis and proposed an alternate correlation for *Nu* designed for gasoline-like liquids with an absolute error of 30%.

$$Nu = 0.052 \lambda^{0.59} La^{0.521} Ca^{0.932} \tag{22}$$

They also presented other correlations for different stages of fuel injection.

Acroumanis and Chang (1993) developed a correlation for diesel sprays impinging on surfaces between 150–205°C in the single-phase regime.

$$Nu = 0.34 Pr^{-0.33} Re^{-0.53} We^{0.94} \tag{23}$$

Some et al. (2007) studied single-phase heat transfer for PF-5060 with one and two overlapping hollow cone nozzles and proposed that

$$h = 10^4 \left[2.598 + 0.908 \ln\left(\frac{P}{248.9} + 0.2 \right) \right] \tag{24}$$

with RMSE of 12.6%.

Landero and Watkins (2008) combined some empirical spray and heat transfer models and through detailed mathematical and numerical analysis developed a code to model steady-state heat transfer of water sprays. Their code incorporated a spray impingement heat transfer model that was claimed to handle both single and two-phase regimes over a heater temperature range of 373 K-573 K. Their simulations were accurate to within 10% of the experimental data for some of their test cases and several times higher in others. They attributed the large discrepancies to assumptions they made in the spray impingement model.

An analytical solution to the spray cooling governing equations was presented by Jia, et al. (2008). Using a velocity and pressure model as well as liquid film model (on the heater), they proposed an analytical relation for the heat transfer coefficient. They reported that the results from their analytical and numerical models were consistent to within 16%. Transient spray cooling for highly heated surfaces using water sprays was numerically modeled by Mzad and Tebbal (2009). They used a combination of correlations and numerical methods to discretize the heat conduction equation and studied the effects of different parameters on the heat transfer coefficient and surface heat flux.

2-2- Two-phase Heat Transfer Correlations

Considerably more heat transfer can occur in the two-phase regime due to the latent heat of vaporization. As the wall temperature increases, two-phase heat transfer can be characterized by an increase in slope of the spray cooling curve. This curve reaches a

local maximum (CHF) at a certain temperature (T_{CHF}) and then drops as the temperature is increased further. Although spray cooling CHF has been the subject of several studies, there are only a few correlations available to predict its value and they often have limited range and are difficult to use.

Estes and Mudawar (1995) and Rybicki and Mudawar (2006), Visaria and Mudawar (2007, 2008, 2008), and Mudawar et al. (2009) conducted a series of studies on CHF in spray cooling and developed correlations to predict the CHF value. They argued that volumetric flux and Sauter Mean Diameter (d_{32}) were the controlling parameters in spray cooling heat transfer. They suggested that local volumetric flux for a given nozzle could be determined using purely geometrical considerations and a correlation to predict d_{32}. The following correlation was proposed for CHF value for upward, downward, and inclined full cone sprays.

$$q''_{CHF} = 2.3\rho_g h_{fg} Q'' \left(\frac{\rho_f}{\rho_g}\right)^{0.3} \left(\frac{\rho_f Q''^2 d_{32}}{\sigma}\right)^{-0.35} \left(1+\beta\frac{\rho_f c_p \Delta T_{sub}}{\rho_g h_{fg}}\right) \quad (25)$$

where β is 0.0019 for PF-5052, FC-72, FC-87, and water with a mean absolute error (MAE) of 12.6%. In a later study, Visaria and Mudawar (2009) included the effects of spray inclination and proposed that β is 0.0050 with a MAE of 16.3%. d_{32} for FC-87, FC-72 and water could be calculated from Equation 9. The local volumetric flux (Q'') could be determined based on average volumetric flux over the entire sprayed surface ($\overline{Q}''$).

$$Q'' = 0.5\overline{Q}''\left[1+\cos(\theta/2)\right]\cos(\theta/2) \tag{26}$$

Moreira and Panao (2006), Moreira et al. (2006), and Panao and Moreira (2009) studied single- and two-phase heat transfer for intermittent gasoline-like sprays in internal combustion engines and presented a few correlations for single-phase *Nu* and two-phase heat transfer rate. They assumed that the liquid mass flux striking the heater surface was the driving parameter for heat transfer and suggested the following correlation for total time-averaged heat flux in the nucleate boiling regime for T_w between 125-175°C and injection frequency between 10-30 Hz.

$$q'' = \frac{\dot{m}_f h_{fg}}{A}\left[0.17\left(\Delta t_{inj} f_{inj}\right)\frac{T_w}{T_f} - 0.284\left(\Delta t_{inj} f_{inj}\right) + 0.046\left(1 - 0.112\frac{T_w}{T_f}\right)\frac{T_w}{T_f} - 0.077\right] \tag{27}$$

Puterbaugh et al. (2007) studied the effect of dissolved air in spray cooling of FC-72 and developed a correlation for two-phase heat flux for surface temperatures between T_{sat} and T_{CHF}. They assumed a parabolic profile for the heat flux in the boiling regime and developed the correlation for chamber saturation pressure of 69-82.7 kPa, subcooling of 2-12°C, flow rate of 6.31-10.5 ml/s, and volumetric air content of 1-20%. Using this correlation requires the knowledge of heat flux at the saturation conditions and critical as well as CHF temperature.

$$q''_{2-\phi} = -\left[\frac{q''_{sat}}{\Delta T_{sub}^2} + \frac{q''_{CHF} + \frac{q''_{sat}\Delta T_{CHF}^2}{\Delta T_{sub}^2} - q''_{sat}}{\Delta T_{sub}\left(\Delta T_{CHF} - \frac{\Delta T_{CHF}^2}{\Delta T_{sub}}\right)}\right]\left(T_w - T_{sat}\right)^2 + \left[\frac{q''_{CHF} + \frac{q''_{sat}\Delta T_{CHF}^2}{\Delta T_{sub}^2} - q''_{sat}}{\Delta T_{CHF} - \frac{\Delta T_{CHF}^2}{\Delta T_{sub}}}\right]\left(T_w - T_{sat}\right) + q''_{CHF} \quad (28)$$

One of the earlier correlations for CHF in air-assisted water sprays with mass flux between 1.12-6.75 kg/m^{2}s was proposed by Chow et al. (1996). The correlation was also used to reproduce data from other studies with R-113 and LN_2 with ±30% accuracy. The same group also studied the effects of different parameters on CHF and concluded that higher spray flow rate and subcoolings had considerable effects on increasing the CHF value, Yang et al. (1993). They hypothesized that CHF depended on droplets velocity, spray pressure, d_{32}, and fluid properties. Although they obtained the data for 0-50°C subcooling, the CHF correlation was developed only for saturated liquid.

$$q''_{CHF} = 0.38\left(\rho_f V h_{fg}\right)\left(\frac{\sigma}{\rho_f V^2 d_{32}}\right)^{1/3}\left(\frac{\rho_f}{\rho_g}\right)^{0.5}\left(\frac{P_s}{P_0}\right)^{0.25} \quad (29)$$

Cabrera and Gonzalez (2003) conducted a study on boiling heat transfer and CHF for full cone water sprays with uniform droplet sizes and velocities for nozzle mass flow rates between 4.4×10^{-4}-7.0×10^{-4} kg/s, ΔT_{sub} between 22-78°C, test chamber pressures in the range of 1 to 1.8 bar, and surface roughness between 5.0-79.4 μm. They proposed the following correlation for two-phase spray cooling heat flux with accuracy of ±19%.

$$q''_{2-\phi} = 2450\left(\rho V h_{fg}\right)\left(\frac{\Delta T_{sub}}{\Delta T}\right)^{0.491}\left(\frac{\rho\sigma\dot{m}''}{\mu^3}\right)^{0.133}\left(\frac{\varepsilon}{d}\right)^{0.0213}\left(\frac{P_{ch}}{P_0}\right)^{0.291} Ja^{1.038} \quad (30)$$

They presented a simplified relation for CHF value with ±15% error.

$$q''_{CHF} = 1.623\left(\frac{\varepsilon}{d}\right)^{0.0465} We^{-0.315} \quad (31)$$

Water spray impingement on high temperature surfaces was studied by Wendelstrof et al. (2008). They used full cone nozzles with orifice diameters between 300-400 μm to spray water at 291 K on a wall heated to 473-1373 K. Local mass flux was measured to be 3-30 kg/m^{2}s and average droplet velocity was between 13-15 m/s. They postulated that two-phase heat flux was a function of local mass flux and surface temperature and proposed a correlation on that basis. The "±" symbol in this correlation represents 95% confidence intervals for the curve fit to the data.

$$h_{2-\phi} = 190 \pm 25 + \tanh\left(\frac{\dot{m}''}{8}\right)$$
$$\left[140 \pm 4\dot{m}''\left(1 - \frac{\dot{m}''\left(T_w - T_f\right)}{72000 \pm 3000}\right) + 3.26 \pm 0.16\left(T_w - T_f\right)\left[1 - \tanh\left(\frac{T_w - T_f}{128 \pm 1.6}\right)\right]\right] \quad (32)$$

Silk, et al. (2006) developed an energy conservation-based form for the two-phase spray cooling Nusselt number. They suggested that,

$$Nu_{2-\phi} = n_1 \mathrm{Re}^{n_2} Pr^{n_3} \left[\frac{n_4 Ja_{sub} + 1}{\left(\rho_f / \rho_g\right)^{n_5} Ja} \right] \left(\frac{\pi}{6} Nd_{32}^3 \right)^{n_6} \tag{33}$$

They determined n_1 to n_6 for several sets of data from different studies and proposed the following correlation for CHF value for PF-5060, FC-72, FC-87, methanol, and water within ±30% of the original experimental data with an average mean error of ±18%.

$$q''_{CHF} = 5.3 Re^{0.55} Pr^{0.33} \left[\frac{0.8Ja + 1}{\left(\rho_f / \rho_g\right)^{0.4}} \right] \left(\frac{\pi}{6} Nd_{32}^3 \right)^{0.09} \left(\frac{k_f}{d_h} \right) \left(\frac{h_{fg}}{c_{p,f}} \right) \tag{34}$$

2-3- Two-phase Heat Transfer Mechanisms

To discuss two-phase spray cooling mechanisms, it is advantageous to review a few major works on pool boiling mechanisms. Ha and No (1997) postulated that when the number of bubbles reaches a critical limit in a pool of liquid, they prevent the supply of fresh liquid to certain regions on the heater. Nucleation in the trapped liquid results in formation of dry spots that leads to CHF occurrence. Arik and Bar-Cohn (2003) experimented with FC-72 and attributed formation of the local dryouts to spontaneous local hot spots on the heater surface. This assumption was examined by Demiray and Kim (2004) using a constant temperature micro-heater array. The heater array prevented any temperature gradient on the heater surface and thus formation of the hot spots. They obtained time- and space-resolved data from FC-72 single bubbles and proved that parameters other then local hot spots drive pool boiling heat transfer and cause CHF.

Bang et al. (2005) visualized pool boiling CHF and burnout processes in alumina/water nano-fluid. They suggested a seven-stage process from ONB to CHF: initiation of nucleation, growth of bubbles and entrapment of liquid under those bubbles, coalescence of the bubbles, nucleation in the interleaved liquid layer underneath the vapor cloud, spontaneous break up of the liquid film due to the formation of new bubbles, extension of the dry spots because of continuous evaporation at the rim of the "vapor holes," and complete dryout on the heater, and burnout. In a more recent study, Delgoshaei and Kim (2010) used a constant temperature micro-heater array to study pool boiling of pentane and suggested that bubble growth time was the dominant factor in determining heat transfer mechanisms in pool boiling. Single-phase mechanisms (transient conduction and micro convection) were identified as dominant mechanisms for bubbles with shorter growth time (<78 ms) and two-phase mechanisms (micro-layer and three phase contact line evaporation) were dominant for slower growing bubbles (>78 ms).

Horacek, et al. (2003, 2004, 2005) used total internal reflection (TIR) technique to visualize FC-72 spray cooling process in order to study heat transfer mechanisms and evaluate the effects of subcooling and dissolved gas concentration on heat transfer rate and CHF. Heat flux at the CHF point increased with increasing subcooling due to the additional sensible heat required to boil the liquid. They also found a direct relation between the three-phase contact line length and heat flux and argued that two-phase heat transfer rate is directly related to the contact line length rather than the extent of the wetted area. They presented a number of boiling curves for FC-72 where it appeared that for a given liquid and surface type (specifically, smooth flat surfaces) the temperature at which CHF occurred was independent of spray characteristics (spray type, pattern, angle,

inclination, pressure, liquid temperature, etc). Those spray cooling curves were developed using single and overlapping hollow cone sprays with flow rates up to 50 ml/min and standoff distances between 7 and 17 mm. In all of the test cases, CHF occurred at around 31°C superheat (wall temperature of 86°C). Moreno et al. (2007) reported similar observations with respect to critical heat flux temperature. Previously, Nishio et al. (1998) had visualized pool boiling of R-113 and reached the same conclusion on the relation between the contact line density and two-phase heat flux. In a liquid film, the three-phase contact line length is directly related to the liquid film break up which could be caused by external means (incoming droplets) or by local dryouts.

Heat flux at the CHF point in water sprays were by Chen et al. (2002). They investigated the effects of droplet velocity (V), d_{32}, and droplet number flux (N) on two-phase heat transfer and CHF of the sprays. Data mining technique was used investigate the effect of surface nuclei and droplet flux to assess bubble formation and characteristics. For the water sprays, N was between 7.3×10^6-29.0×10^6 /cm^2, V between 4.64-24.1 m/s, and Sauter Mean Diameter was in the range of 62.2-191.4 μm. They found that droplet velocity had the largest effect on heat transfer followed by droplet number flux and d_{32}. They also suggested that in two-phase spray cooling, droplet number flux did not affect bubbles number density or mean bubble diameter, however, increased N decreased mean bubble peak diameter and mean bubble diameter. At high droplet fluxes, the number of surface nuclei did not influence droplet number density because secondary nucleation overwhelmed surface nucleation.

Every major work spray cooling in boiling regime relates two-phase heat transfer mechanisms to the breakup of the liquid film on the heater. This brings a lot of attention

to film breakup mechanisms and related phenomena. The rupture of liquid films on smooth surfaces has been the subject of numerous studies, albeit at temperature much lower than T_{sat}. Sharma and Ruckenstein (1989) developed a notable energy-based criterion for rupture of stationary liquid films and dewetting of solids which was used by Dhiman and Chandra (2008) to propose the criteria for rupture of radially spreading liquid films upon being punctured by an external mean (such as incoming liquid droplet). The growth of dry regions during nucleation of non-wetting liquids on smooth surfaces was studied by Kheshgi and Scriven (1991) where they identified external disturbances as the most likely cause of liquid film rupture. There are other hydrodynamic effects that can result in the breakup of liquid films, for instance, hydrodynamic instabilities. These effects have also been extensively studied, however, they are very minor compared to the turbulences induced by incoming droplets (for more details refer to Lin and Jiang (2003)). Once the film ruptures at different locations, liquid rivulets start to rapidly form, move, and evaporate and two-phase heat transfer is suspected to be driven by this phenomena. The fundamental mechanisms are likely to be transient conduction and microlayer and contact line evaporation. Determining the exact mechanisms and contribution of each to the total heat flux require further investigation.

2-4- Critical Heat Flux Temperature

In the works of Horacek et al. (2003, 2004, 2005) that was discussed in the previous section, they also studied the effects of dissolved gas and liquid subcooling on CHF in FC-72 sprays. They observed an increase in T_{CHF} for gassy sprays which was considered to be a direct consequence of increased T_{sat} in those cases. They presented a number of

spray cooling curves for subcoolings between 2.1-35.6°C where the wall superheat at which CHF occurred stayed within about ±7.5°C. The required wall superheat for CHF occurrence slightly decreased with increased subcooling which was attributed to the change in dissolved gas level. The present study confirms that local CHF tends to occur around the same temperature irrespective of the spray characteristics, however, it contradicts the works of Rybicki and Mudawar (2006) and Visaria and Mudawar (2010) where it is suggested that T_{CHF} significantly drops with increased liquid subcooling. It also contradicts the study by Cabrera and Gonzalez (2003) where *Ja* at which CHF occurs appeared to increase with subcooling. El-Genk and Parker (2004) also reported a considerable increase in pool boiling CHF temperature at higher subcoolings for smooth as well as enhanced surfaces.

Effect of heater surface enhancement on spray cooling CHF was studied by Coursery et al. (2005, 2007). They investigated the heat transfer from small-pitched straight-finned heaters with 360 μm channel width, 500 μm fin width, and fin heights of 0.5-5 mm on 30°C to PF-5060 sprays and reported lower T_{ONB} and T_{CHF} than those of flat heaters. A connection between the fins height and ONB and CHF temperatures could not be established, however, they suggested that highest cooling efficiency was achievable using 1-3 mm fin heights. Similar results were reported by Bostanci et al. (2008) for ammonia sprays on micro-structured surfaces. They recorded substantially higher heat fluxes at lower heater temperatures as the surface structure became more complex. Increased range of cavity sizes and nucleation sites, secondary nucleation, and increased surface area were considered responsible for higher heat flux. These observations were in agreement

with pool boiling study of HFE-7100 by El-Genk and Parker (2004) where T_{ONB} was shown to decrease and resulted in earlier occurrence of CHF.

Coursey and Kim (2007, 2008) studied the effect of nano-fluids and surface oxides on spray cooling and pool boiling heat transfer. They experimented with alumina/water nano-fluid on copper and copper oxide heaters and reported that the heat transfer enhancement that could be achieved using nano-fluids in pool boiling strongly depended on fluid/surface wetting characteristics. Substantial CHF enhancement was reached for non-wetting fluid/surface combinations by adding nano-particles (as much as 37%). Whereas, for already wetting fluid/surface combinations introducing nano-particles to the system did not have significant effect on the CHF. They concluded that the main mechanisms responsible for CHF enhancement were those directly related to the wettability of the fluid/surface pair. Even though adding nano-particles did not have considerable effect on the CHF value, it shifted T_{CHF} to as much as 20°C below that of pure fluid. Same observations were made by Duursma et al. (2009) for CHF in nano-fluid spray cooling. They showed that, similar to the pool boiling, adding nano-particles reduced the spreading time but did not have notable effects on critical heat flux temperature or value.

2-5- Chapter Summary

Some of the correlations used to predict single- and two-phase heat transfer in spray cooling were reviewed in this chapter. The dominant heat transfer mechanisms in spray cooling in the two-phase regime are largely unknown. A review of some studies on pool boiling and two-phase spray cooling was presented to provide insight into the problem.

There is general agreement that the formation of local dryouts on the heater surface precedes CHF occurrence and that heat transfer mechanisms at the CHF point can be explained on that basis. The effects of subcooling, surface enhancement, nano-fluids, and nozzle orientation in the peak heat flux were also discussed. Some of the works on CHF temperature were cited and explained. The data on T_{CHF} are contradictory. While some of the studies show that CHF occurs around the same temperature for various spray characteristics, others show large variations in T_{CHF}.

CHAPTER THREE: EXPERIMENTAL METHODOLOGY

This chapter introduces the working fluids and experimental setups. For each test rig the components and operation methods as well as the data acquisition system are explained. Data reduction techniques and uncertainty analysis are also discussed.

3-1- Fluids and Nozzles

The experiments were carried out using three fluids chosen based on their applicability to the electronic cooling industry, diversity of thermo-physical properties, and availability:

1. PF-5060 (3M Performance Fluid 5060 - C_6F_{14}): This fluid has the same chemical formula and properties as FC-72 but it contains different isomers of the same molecule. It is a widely used in boiling studies and has a relatively low boiling temperature. Very high dielectric factor makes it especially attractive for electronic cooling systems. PF-5060 is inert but very volatile and its vapor is a greenhouse gas. Even though at regular temperatures it is not hazardous for human health, if heated to over 250°C the dangerous acidic component, HF, can be synthesized.
2. PSF-3 (Clearco Products Co. Pure Silicone Fluid 3cSt): Silicone oils come in variety of grades and purity levels, ranging from very heavy lubricants to food grade silicone oils. This particular oil is one of the lightest industrial level grades, it highly dielectric, and exhibits desirable thermal properties for single-phase heat transfer studies. The boiling temperature for this fluid is over 200°C which is beyond the capacity of the heater in this study.

3. PAO-2 (ExxonMobil Spectrasyn/Polyalphaolefin 2): Alpha-olefins are a type of olefins (also known as, alkenes) which have an alpha bond, meaning that the molecule starts with a C=C double bond. Polyalphaolefins are synthetic polymers made for specific purposes, e.g., flexible foams, lubricants, coolants, etc. They can be made with very different properties, however, the one used in this study is a very light one which is common in heat transfer studies. Also, along with the other two liquids, it provides a wide range of fluid properties that adds to the validity range of the correlations that will be developed.

A summary of the fluid properties at atmospheric conditions is given in Table 1. The sprays were produced using four nozzles:

1. Spraying Systems LLN-1/4 1.5 hollow cone nozzle: This nozzle was used for PF-5060 and PSF-3. The orifice diameter was about 0.5 mm and the cone angle was between 65-70° at different pressures.
2. Spraying Systems LLN-1/4 3 hollow cone nozzle: This nozzle had a bigger orifice (1 mm) which was more suitable for the thicker liquid, PAO-2. The cone angle was varied between 65-70° at different spray pressures.
3. ISR prototype full cone nozzle: PF-5060 and PSF-3 were sprayed through this nozzle. Since it was a prototype nozzle, the geometry had not been documented, but the orifice diameter was photographed and measured to be 110 μm.
4. Spraying Systems H1/4VV flat fan nozzle: A rather large rectangular orifice made this nozzle a good candidate for the thicker operating fluid, PAO-2. PF-5060 was also tested with this nozzle.

Sample photographs of the hollow cone, full cone, and flat fan PF-5060 sprays are shown in Figure 2.

Table 1. Fluid properties

Fluid	**PF-5060**	**PSF-3**	**PAO-2**
ρ **(kg/m^3)**	1680	898	791.7
μ **(Pa-s)**	0.64×10^{-3}	2.69×10^{-3}	4.61×10^{-3}
c_p **(J/kg-K)**	1050	1970	2301.2
k **(W/m-K)**	0.057	0.113	0.140
σ **(N/m)**	12.1×10^{-3}	19.2×10^{-3}	28.0×10^{-3}
Boiling temperature (°C)	56	> 200	> 200
Pr	11.8	46.9	75.8
h_{fg} **(kJ/kg)**	88	-	-
Refraction coefficient	1.25	-	-

Hollow cone Full cone Flat fan

Figure 2. Photographs of spray produced by three nozzle types operating at 344 kPa (the photographs are courtesy of Mr. Michael Siemann)

3-2- Spray Measurement Apparatus

A Malvern laser analyzer system was used to study spray characteristics for different geometries (Figure 3). The system consisted of a laser generator that emitted a red collimated laser beam with a diameter of 10 mm. The collector was made of several concentric fringes. The diameter of each fringe was designed to collect light from certain range of refraction angles based on the droplet size and refraction coefficient. This way the fraction of droplets that were within a certain range in diameter could be determined. There results could be obtained in terms of d_{10}, d_{50}, and d_{90} that reflected the diameters of which 10%, 50%, and 90% of the droplets were smaller. Sauter Mean Diameter was also calculated by the equipment. Transmission percentage, attenuation, and droplet number concentration were other outputs of the system.

For each test, the nozzle was placed in an airtight Plexiglas chamber and the liquid was circulated via a Cole Parmer gear pump (model number: 75211-10). There were two pressure gauges on the outside of the chamber. One gauge was mounted on the feed line to the nozzle and the other was used to measure the chamber pressure. The imperfections on the Plexiglas chamber resulted in excessive scattering even without an operational spray. Therefore, two cutouts were needed at the exact locations where the laser beam crossed the chamber walls. The windows were covered with extra smooth microscope glass slides with thickness of 2 mm and sealed with silicone sealant. The glass slides substantially reduced the scattering and allowed for more accurate measurements. For the recirculation line to be able to suck the liquid out of the chamber, a certain level of liquid had to accumulate at the bottom of the chamber. Impact of the spray on the accumulated liquid resulted in droplet rebound and formation a strong mist in the chamber. An opaque

diaphragm with a large circular hole in the middle was placed below the nozzle to allow droplets to travel to the bottom of the chamber while preventing the mist from bouncing to the upper section and interfering with the measurements.

The system had an external data acquisition system which was used to power the laser, read the signals, and transfer the data to a data acquisition board mounted in a desktop computer. RTSizer Spraytec was the standard software package that paired with the system and interpreted the data. The output could be saved either in standard format of the software package or in form two text files. The text files contained detailed data from the sprays and could be analyzed with any software with statistical analysis capability (for example, Microsoft Excel or Matlab).

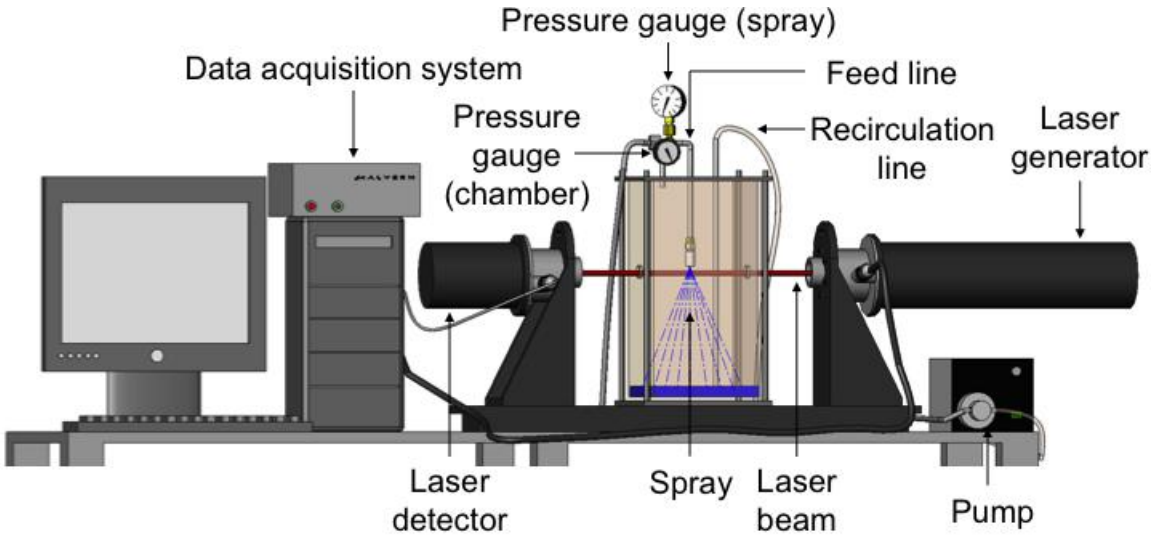

Figure 3. Malvern laser analyzer setup for spray measurements

3-3- Pressure Measurement Apparatus

A schematic of the pressure measurement setup is shown in Figure 5. Local impingement pressure was measured using two differential pressure transducers (All sensors 20 INCH-D-4V for lower spray pressures and All sensors 5 PSI-D-4V for higher spray pressures). One port of the pressure transducer was exposed to the test chamber and the other port was connected to a 3.2 mm channel drilled half way through one cross section of a Plexiglas plate through a liquid trap. This small channel was connected to a 0.1 mm pressure tap carefully drilled in the bottom of the plate (Figure 4). Since the plate was sprayed from the bottom, the length of the tap created a small head and that needed to be minimized, so the length of the pressure tap was only 5 mm.

The Plexiglas plate was connected to a set of two orthogonal stages (Zaber T-LS13M, 13 mm strokes and 0.1 μm accuracy) via an aluminum traverse. The stages enabled the plate (thus the pressure tap) to survey the entire spray impingement area in form of a 32×32 matrix with 350 μm steps. A set of three-dimensional orthogonal stages with an accuracy of 25 μm was used to coordinate of the nozzle with respect to the Plexiglas plate. The relatively small movement span of the Zaber system necessitated such high accuracy for the three-dimensional stages so that pressure readings were possible for the entire extent of the sprays. Standoff distance was an important factor in local impingement pressure that further amplified the importance of using precise instruments.

Liquid was pumped into the system using a Cole Parmer gear pump (model number: 75211-10). Particulate contamination could clog the nozzle so a Swagelok SS-4FW-2 2 μm filter was placed after the pump and before the nozzle to clear the liquid of the particles. After being sprayed on the bottom of the Plexiglas plate, a large potion of the

fluid was collected at the bottom of the chamber and drained back to the fluid reservoir via a drain line. A small portion of the liquid that entered the pressure tap traveled through the channel and was collected in the liquid trap. The liquid trap was used to transfer the pressure information to the pressure transducer while keeping it from coming in actual contact with the liquid. It was sealed at the top with only two ports going out. One port was connected to the Plexiglas plate and was the liquid entrance and the other one was connected to a port on the pressure transducer outside of the chamber. At different steps, where the pressure tap on the Plexiglas plate was placed on an area with higher impingement pressure, liquid started to move into the plate and liquid trap until the pressure in air/vapor gap at the top of the trap was balanced with the impingement pressure, at which point the flow stopped. As the plate proceeded to a step with lower impingement pressure, the liquid in the plate flowed in the reverse direction until a new equilibrium was reached.

The delay time required at each step for the pressure to stabilize was determined by increasing the delay time until no further change in pressure was observed. The delay time varied between 5-10 s depending on the spray pressure. For some test cases with the flat fan spray this delay time was as high as 20 s. Delay time was greatly influenced by the volume of air/vapor gap at the top of the liquid trap, the smaller the gap the shorter the delay time. Experiment duration for each test case was between approximately 85-170 minutes so even a slight decrease in the delay time could translate into several hours in saved experiment time. Hence, the air/vapor gap volume was maintained at a minimum at all times. This was made possible by using a solenoid valve placed inside the chamber with the entrance port connected to the bottom of the liquid trap and the exit port exposed

to the chamber. As the accumulated liquid in the trap reached a certain level the solenoid valve was manually opened to allow for the liquid to exit and provide space for the incoming liquid from the spray. This opening time had to be very short and precise to avoid any interference with pressure measurement. Upon completion of one column, the Zaber stages moved to the next column, providing a few seconds to drain the liquid trap and achieve a desirable liquid level. This process proved to have minimal effect on the pressure measurements. For high spray pressures and low standoff distances this process was needed to be performed several times during each measurement while for lower spray pressures and larger standoff distances it was not necessary to drain the trap until the measurement was complete.

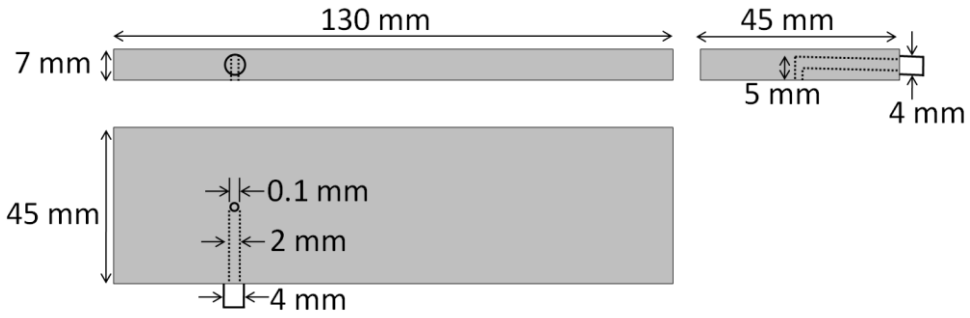

Figure 4. Schematic of the pressure plate and pressure tap geometry

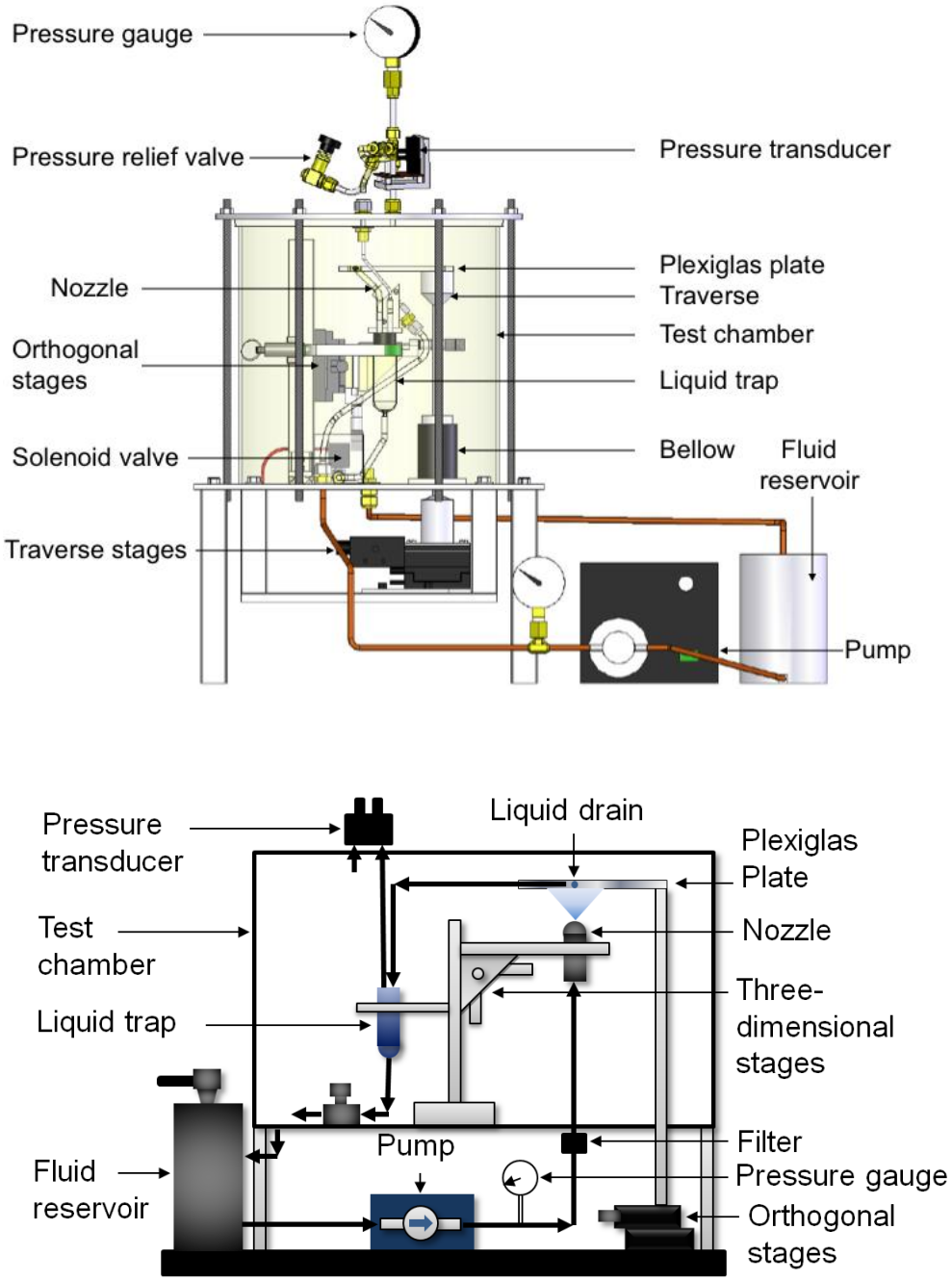

Figure 5. Pressure measurement apparatus (top: three-dimensional model of the setup, bottom: schematic of the setup)

3-4- Heat Transfer Measurement Apparatus

An array of 96 microheaters was used to measure the spatial heat transfer distribution on the surface. Each heater element (Figure 6) was nominally 700 × 700 μm2 in size and consisted of a 200 nm thick by 7 μm wide serpentine platinum resistance heater and titanium adhesion layer sputtered onto a 500 μm thick quartz substrate. Thicker gold leads were deposited up to the edge of the array to ensure minimal lead resistance (< 1 Ω). The entire array was covered with a 1 μm SiO_2 passivation layer to provide a uniform surface energy. The individual heater elements were maintained at a uniform specified temperature using 96 Wheatstone bridge feedback circuits. The temperature of each element was selected through the use of a 20 kΩ digital potentiometer with 512 discrete steps. When combined with the other resistor elements in the circuit, the array temperature could be set from 30-115°C with a nominal resolution of 0.2°C. The frequency response of the combined heater/bridge circuit was approximately 15 kHz. Each heater was capable of dissipating 2.0 W, or a maximum surface heat flux of about 4.1 MW/m^2. Additional details regarding the working principles of the micro-heater array are available by Rule and Kim (1999) and Bae et al. (1999).

The feedback control circuit for one heater is shown in Figure 7. The operation principals of this circuit are similar to those of hot wire anemometry. Cool liquid striking a heater decreased the resistance of that heater resulting in an imbalance in the Wheatstone bridge. The Op-Amp sensed the imbalance and sent a signal to the transistor to allow for larger current to flow in the circuit from the 28 V source. The digital potentiometer resistance (R_{DP}) changed to shift the circuit back to a new state of equilibrium. This process repeated for each heater at a frequency of 15 kHz.

The heater temperature was increased in 5°C increments from 40°C to 115°C, and the local heat transfer from each of individual heater was measured for 2 s at each temperature. In the case of the hollow cone spray with PF-5060 for standoff distances of 5 and 7 mm, the spray impact region was larger than the heater size. To acquire data for the entire region the spray was positioned over the four corners of the middle 8×8 heaters and the heat transfer data for a quarter of the spray was collected. The data sets were subsequently merged to create the full heat transfer distribution pattern in form of a 16×16 matrix.

A schematic of the heat transfer measurement apparatus is shown on Figure 8. The working fluid was pumped from the fluid reservoir through a positive displacement pump (Cole Parmer Gear pump, model number: 75211-10), a flow meter (Omega flow meter, model number: FLR1000BR), a heat exchanger (API Heat Transfer, model number: SB1-20), a filter (Swagelok, model number: SS-4FW-2, 2 μm), and then through the nozzle. The atomized liquid impacted the heater array located at the bottom of the test chamber. Excess liquid drained from the spray chamber back to the fluid reservoir by gravity. The standoff distance between the heater and the spray was adjusted using a set of three orthogonal traverses with an accuracy of 25.4 μm. A black and white CCD camera mounted on a tripod head and fixture below the chamber and projected onto a TV screen allowed the spray axis to be adjusted over the center of the heater with an accuracy of approximately 0.2 mm. A thermocouple placed before the nozzle orifice monitored the liquid temperature to assure constant temperature throughout the data acquisition process.

The data acquisition systems consisted of two data acquisitions boards mounted inside a desktop computer (each for 48 heater) and a Visual Basic code that connected to

the heater array and controlled the heat temperatures and measurement durations. The output of the system was a set of data files consisting of Wheatstone bridge voltages for each heater at each set temperature. These data files were imported in a Matlab code where they were translated into heat flux and combined to give a complete map of heat flux distribution on the heater at various temperatures.

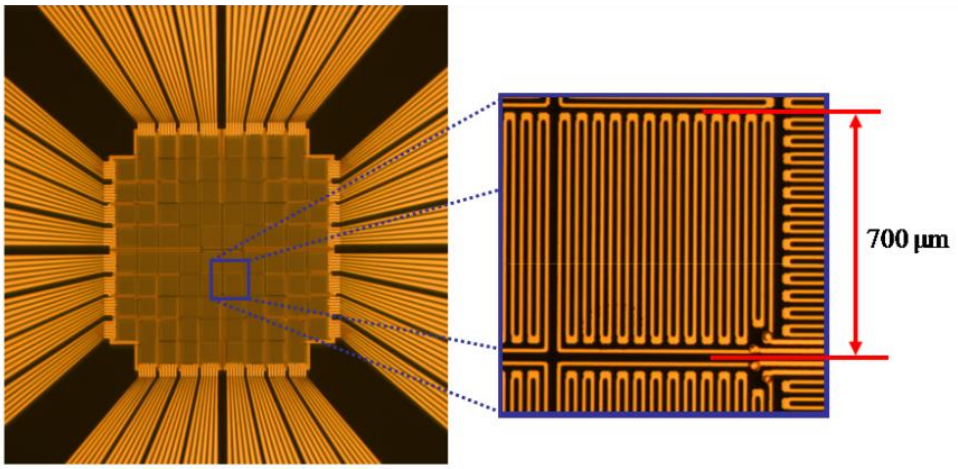

Figure 6. Photograph of the micro-heater array used to measure heat flux distribution

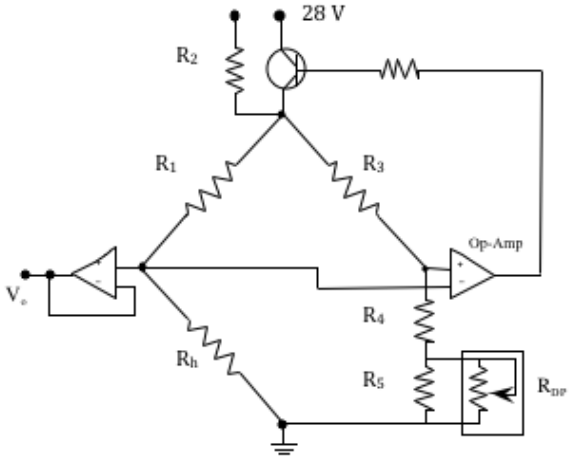

Figure 7. Feedback circuit schematic

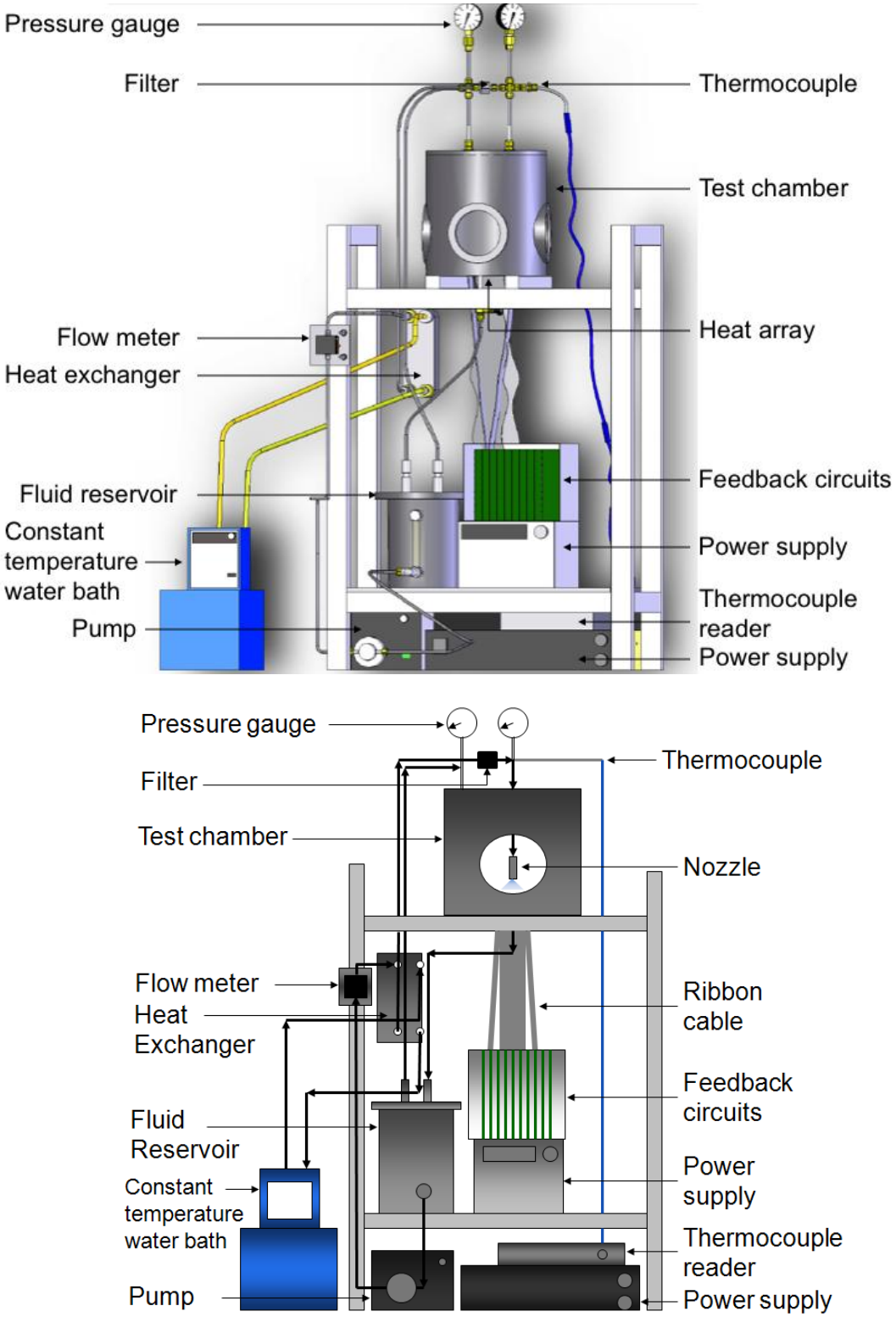

Figure 8. Heat transfer measurement apparatus (top: three-dimensional model of the setup, bottom: schematic of the setup)

3-5- Data Reduction and Uncertainty Analysis

The uncertainties in the readings from each experimental setup are discussed in details.

3-5-1 Spray measurement apparatus. The most important source of error for the Malvern laser setup was in the calibration and alignment of laser generator and detector. The laser generator in Figure 3 was quite heavy and the Malvern design was such that the large mass created a moment that caused alignment difficulties. The back had to be held upright and the system was so delicate that the slightest misalignment could cause erroneous readings. Considerable effort was put into calibration and alignment to achieve a noise level in compliance with the systems specifications. Another source of uncertainty was ambient light that was minimized by dimming all the surrounding lights. The mist created by spray impingement on the liquid at the bottom of the chamber was a source of uncertainty that was compensated for by abruptly shutting off the spray at different pressures and measuring the mist characteristics and subtracting them from the readings. Multiple scattering, which was a result of droplets interference with the laser beam at multiple locations, would cause excessive scattering of the laser and would result in unrealistically small droplet sizes. This issue prevented performing droplet size measurements with the full cone nozzle. But the data for the hollow cone and flat sprays were modified using an empirical correlation (for details refer to Chapter 4). Quantification of the error associated with these measurements was not possible due to complexity of the system and the shortcomings of the operating software. The uncertainties are expected to be minimal since all the major sources were carefully eliminated.

3-5-2- Pressure measurement apparatus. The Zaber orthogonal stages were capable of sampling data over a 13×13 mm^2 area and the heater array was 7×7 mm^2. To obtain matching data, the impingement pressure data were sampled in form of 32×32 matrices in 350 μm increments (11.2×11.2 mm^2). Each increment was designed to correspond to one quarter of an individual heater in the heater array. Several of the rows and columns in each set of pressure data were then cropped to obtain a 20×20 matrix with the same area as the heater array. Cropping of the matrices was also designed to make the locations of pressure and heat flux coincide. To achieve that, the center of each data set was determined by counting the number of pixels in the horizontal and vertical directions and finding the coordinates of the center. The number of cropped rows and columns were changed until the centers of the pressure/heat flux distributions were exactly the same. The data were then radially averaged to double check the occurrence of the peaks of pressure and heat transfer at the same radii. The next step was coarsening the data over 2×2 cells to obtain 10×10 matrices with the same resolution as the heat transfer data. As discussed earlier, for hollow cone sprays at 5 and 7 mm standoff distances the spray was larger than the heater array and the data were in form of 16×16 matrices with each cell 700×700 μm^2. Efficient processing of the data required the same size for all of the data matrices. Therefore, for cases with the regular 10×10 size, 3 rows and 3 columns were added to the top, bottom, right, and left of the data matrices, thus increasing the size of each data set to 16×16. The value of added elements to the data were zero so they had no influence on post-processing.

Figure 9 illustrated the above procedure for hollow cone PF-5060 spray at 3 mm standoff distance and 689 kPa spray pressure. “A” is the original pressure distribution in

32×32 format. 7, 3, 5, and 6 rows and columns were cropped from top, bottom, right, and left respectively and replaced with zeros to maintain the size of the matrix, "B." The data is averaged over 2×2 pixels in "C" to match the resolution of pressure and transfer data. "D" is the corresponding heat flux distribution at 90°C wall temperature. The black square in "B" shows a subset of the data that was averaged to one element in "C."

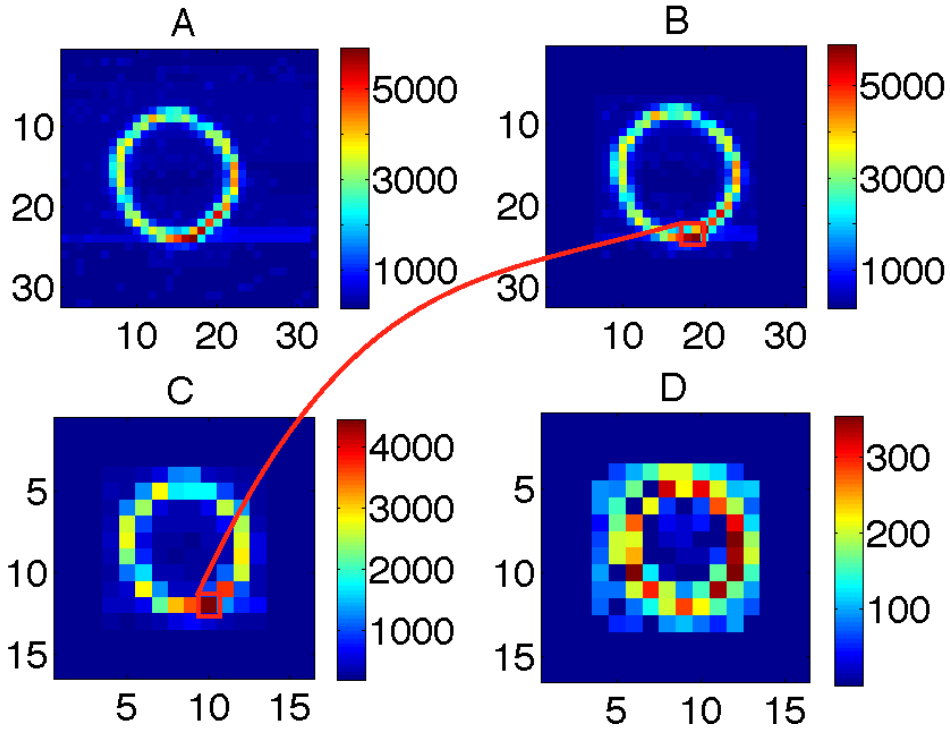

Figure 9. Data reduction for pressure distribution of hollow cone PF-5060 spray at 3 mm standoff distance and 689 kPa spray pressure; A: original pressure distribution (Pa) in 32×32 format, B: Cropped pressure distribution (Pa), C: Coarsened pressure distributions (Pa), and D: Heat flux distribution at 90°C wall temperature (W/cm^2)

Two differential pressure transducers with nominal ranges of 0-5 kPa and ±34.4 kPa were used to collect the data for different cases. Each of the transducers had a nominal

linearity and hysteresis error of ±0.5% of their full scale, which corresponded to uncertainties of ±25 Pa and ±172 Pa for the smaller and larger transducer, respectively. The other major sources of uncertainty in the pressure measurement apparatus was due the pressure tap length which created a reverse head and caused up to 49 Pa pressure reduction in the measurements. The uncertainty in standoff distance was approximately one mark on the orthogonal traverse set (±25 μm).

3-5-3- Heat Transfer measurement apparatus. The heater array was calibrated using a constant temperature oven. The heater was placed in the oven at a set temperature and when the temperature stabilized the digital potentiometer values that balanced the Wheatstone bridge were recorded. Ideally, resistance values had to increase linearly as heater temperature increased. The heater was calibrated from 40°C to 100°C. The recorded resistance values were used to determine the digital potentiometer values and set the heater array at the desired temperatures. The heater could potentially drift from the calibrated values, so room temperature calibrations were performed periodically to ensure heater stability and consistency. Room temperature calibration was similar to the regular calibration, except that the heater did not need to be placed in the over. Rather, it was exposed to the ambient temperature and the digital potentiometer values were recorded for that specific temperature and the linearity of the resistance values were compared to the calibrated values. If the values had drifted by several units, recalibration was necessary. Figure 10 is sample of calibration curves for heaters 61-70. The room temperature was about 23°C and the calibration was done for temperatures between 40 and 100°C as described above. The results were completely linear and the intermediate

resistances for temperature other than those calibrated for could be determined by a simple interpolation. Heater 65 was a non-regulating heater and the resistance values were fixed at 512 Ω. This was the maximum resistance that could be attained by the digital potentiometer and the limiting factor for the operation temperature of the heater array. Above 115°C several of heaters needed resistances above 512 Ω to regulate properly which was beyond the possible range and therefore was the limiting factor. Heater 64 had slightly drifted over time from its original calibration, so the slope of the calibration curve had changed between the room temperature and 40°C. The rest of the heaters showed remarkable consistency and very few full calibrations were needed throughout the course of research.

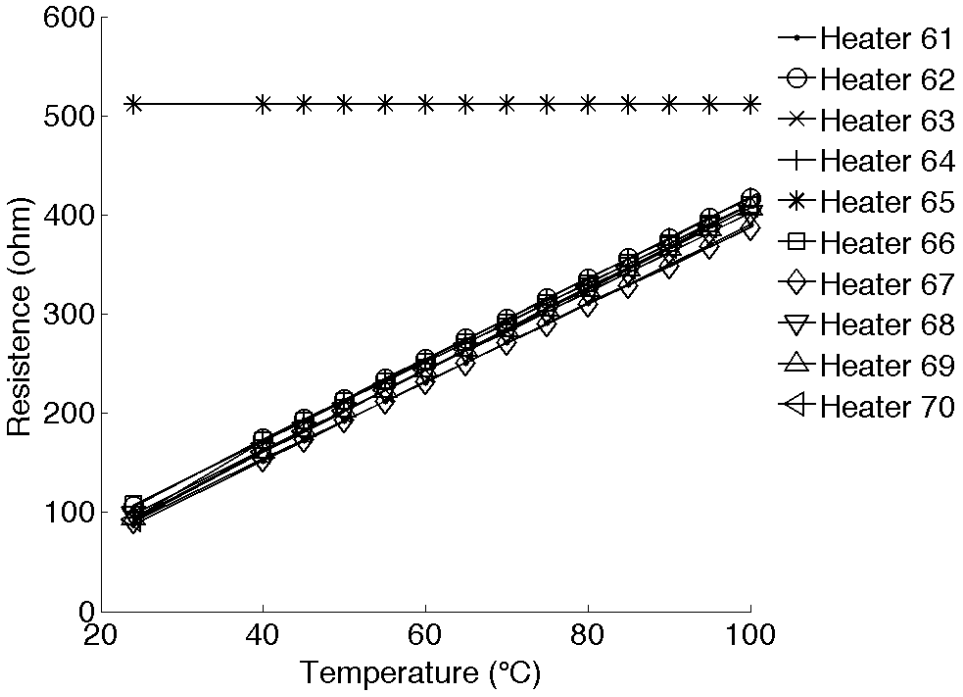

Figure 10. Calibration curves for a subset of heaters

As mentioned before, for hollow cone sprays at 5 and 7 mm standoff distances, the spray area was larger than the heater. So the nozzle was placed at four corners of the heater and data was taken for heat quarter separately. Then the four sets were merged to provide the complete map in form of 16×16 matrices. A CCD camera was placed underneath the heater and provided an enlarged imaged of the heater on a TV set. This setup was used to position the nozzle at the desired locations. Figure 11 shows the above procedure for a hollow PF-5060 spray at 5 mm standoff distance, 689 kPa spray pressure, 90°C heater temperature, and 25°C liquid temperature. Data from the four quarters were taken separately and are shown in their respective locations. The solid lines indicate the contribution of each quarter to the complete distribution map. The continuity of the heat flux profile is another indication of excellent accuracy in positioning the nozzle with respect to the heater.

A detailed uncertainty analysis for the heat transfer measurement apparatus was presented by Horacek et al. (2005). Uncertainties in voltage and heater resistance measurement in the feedback circuitry along with substrate conduction could result in up 3% error in the acquired heat flux data. Other sources of uncertainty included spray pressure (±3.5 kPa - 0.4 to 1.5% - between two marks on the dial pressure gauge), standoff distance (±25 μm - 0.3 to 0.8% - one mark on the three-dimensional stages), and heater temperature (0.4°C - 0.4 to 1% - the difference between two positions on the digital potentiometer). These factors could potentially result in a maximum uncertainty of 6.3% in the heat transfer coefficient data).

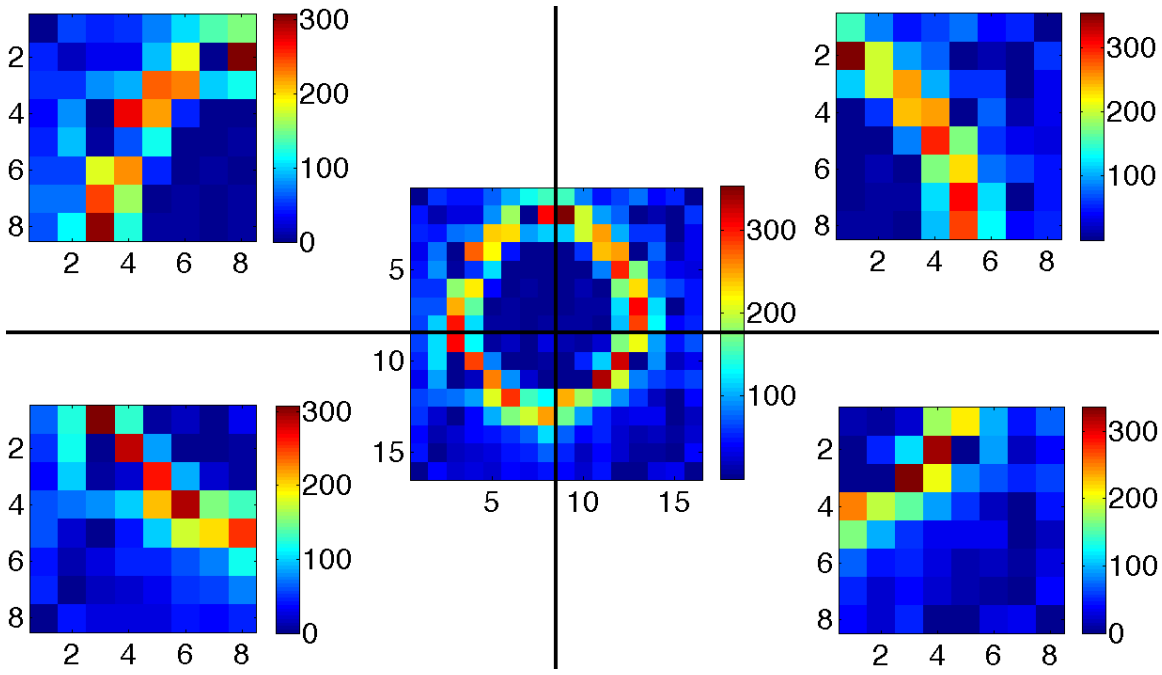

Figure 11. Sample plot for merging the four quarter of heat flux data for hollow cone PF-5060 spray at 5 mm standoff distance, 689 kPa spray pressure, 90°C heater temperature, and 25°C liquid temperature; the color bars show the heat flux values in W/cm^2

3-6- Chapter Summary

Three experimental setups were used in this study: - Spray measurement apparatus, - pressure measurement apparatus, and - heat transfer apparatus. The measurement concepts, design characteristics, components, and operation methods for each system were discussed. Several figures from the setups and individual components were presented. Details of data reduction for trivial, as well as, more complicated procedures were discussed and illustrated. The major uncertainties associated with readings from each system were also reviewed and quantified.

CHAPTER FOUR: SPRAY ANALYSIS

Studying the spray properties and characteristics provides important insights into the range of parameters under discussion. They can be used to identify the parameters that are more likely to have significant impact on the heat transfer performance. This chapter explains the test conditions and spray analysis results and also presents discussions on the importance of different heat transfer variables.

4-1- Test Matrix

Flow rates through the nozzles were measured for all three fluids and droplet size analysis was preformed using the Malvern laser system for hollow cone and flat fan PF-5060 sprays. Multiple scattering problems associated with the full cones nozzle prevented laser measurements for those sprays. PF-5060 could provide the required information for the purpose of this study and eliminated the need to repeat the experiments with the other liquids. Table 2 summarizes the test conditions for spray measurements. In total, 52 experiments were performed to obtain the required information from the sprays. Each test was carried out a minimum of two times to ensure repeatability of the experiments.

Table 2. Test matrix

Fluid	**Experiment type**	**Nozzles**	**P_s (kPa)**	**s (mm)**
PF-5060	Flow rate	Hollow cone, full cone, flat fan	206, 344, 482, 689	-
	Spray droplet measurement	Hollow cone, flat fan	206, 344, 482, 689, 896	8, 10
PSF-3	Flow rate measurement	Hollow cone, full cone	206, 344, 482, 689, 896	-
PAO-2	Flow rate measurement	Hollow cone, flat fan	206, 344, 482, 689, 896	-

4-2- Flow Rate Results

An Omega flow meter (model number: FLR1000BR) was used to measure the mass flow rate through the nozzles at different pressures (Table 3). The output of the flow meter was a voltage value. Since calibration curves were not available for the liquids in this study, Therefore, preliminary tests were conducted to obtain the calibration curves and convert the voltage into flow rate. In theory, the flow rate through the nozzle changes with the square root of spray pressure.

$$\dot{m} = A_0\sqrt{2\rho P_s} \tag{35}$$

Power law models were calculated for each nozzle to investigate the proximity of the theory and experimental results. The models are presented in Table 4. With the exception of flat fan PF-5060 sprays, the experiments where within 16% of expected values.

The hollow cone nozzle that was used for PAO-2 had the largest orifice and therefore had the largest flow rate; followed by flat fan nozzle, hollow cone nozzle that was used for PF-5060 and PSF-3, and full cone nozzle. Figure 12 is a comparison between flow rates of different fluids through the nozzles at various pressures. The symbols represent the measured values while the lines correspond to the models in Table 4.

Table 3. Summary of nozzle flow rates; flow rate in ml/s

Fluid	**PF-5060**			**PSF-3**		**PAO-2**	
Pressure (kPa)	Hollow	Full	Flat fan	Hollow	Full	Hollow	Flat fan
206	1.04	0.28	2.17	1.77	0.61	3.24	2.93
344	1.28	0.36	2.63	2.12	0.80	4.15	3.73
482	1.56	0.43	2.94	2.44	1.01	4.90	4.48
689	1.72	0.54	3.33	2.83	1.17	5.93	5.52
896	-	-	-	3.43	1.39	6.38	6.02

Table 4. Flow rate fits for each nozzle and fluid, spray pressure in kPa

Fluid	**Nozzle**	**Flow rate (ml/s)**
PF-5060	Hollow cone	$0.110P^{0.42}$
	Full cone	$0.014P^{0.55}$
	Flat	$0.335P^{0.35}$
PSF-3	Hollow cone	$0.129P^{0.48}$
	Full cone	$0.026P^{0.58}$
PAO-2	Hollow cone	$0.233P^{0.49}$
	Flat	$0.169P^{0.53}$

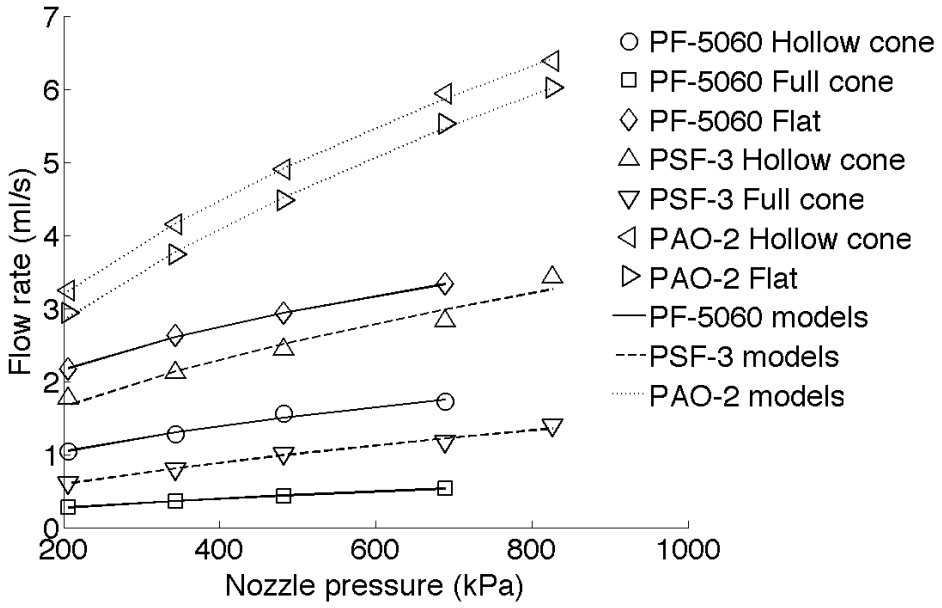

Figure 12. Flow rate of different liquids through the nozzles at various pressures

4-3- Spray Droplet Measurement Results

Calibration and alignment of the Malvern laser equipment was an involved process. It included careful adjustment of the laser generator and detector, eliminating the ambient light, and building small windows on the test chamber to minimize the scattering off the chamber walls as the beam was going through. For each specified condition the data were collected for 10 s intervals at a frequency of 100 Hz and was averaged over the number of measurements. Each test was carried out twice to ensure repeatability and in case of any significant mismatch, third and fourth iterations were made to acquire repeatable and reliable data. Splash of the sprays on the accumulated liquid at the bottom of the experimental chamber created a mist in the enclosure. The same set of tests was performed to analyze the mist effect in the chamber. In each case the spray was abruptly shut off and measurements were made in a similar manner to the regular tests. Since mist

formation was a transient phenomenon and died down relatively quickly, only 1 s of the data was used for mist analysis.

The output of the system was a list of droplet size ranges with the percentage of the droplets that fell within certain diameters. Sauter Mean Diameter (SMD or d_{32}) was defined as

$$d_{32} = \frac{\sum d_v^3}{\sum d_s^3} \text{ or } d_{32} = \frac{\sum n_i d_i^3}{\sum n_i d_i^2} \tag{36}$$

where d_v and d_s are equivalent droplet diameters based on volume and surface area, respectively, and n is the fraction of droplets within certain droplet size ranges, Lefebvre (1989). Multiple scattering of laser beam passing through the hollow cone nozzle necessitated modifying d_{32} from its basic definition to obtain more accurate results. Gulder (1990) presented and empirical correlation to compensate for multiple scattering in dense sprays via a correlation factor. According to the model,

$$d'_{32} = d_{32}\left(1.35e^{F_1+F_2}\right) \tag{37}$$

where

$$\begin{aligned} F_1 &= -0.1184\left(\frac{d_{32}}{100}\right)^2 + 13.122\frac{\psi}{d_{32}} - 5.7474\frac{\psi}{d_{32}^{0.5}} \\ F_2 &= 2.2389\psi^8 - 2.6077\psi^9 \\ \psi &= 1 - Tr \end{aligned} \tag{38}$$

Details of droplet size analysis and related topics can be found in Lefebvre (1989).

Droplet number concentration was calculated using the Beer-Lambert law.

$$\frac{I}{I_0} = e^{-al} \text{ where } a = \frac{-1}{l}\ln(Tr) \tag{39}$$

It basically states that the laser beam intensity logarithmically attenuates as it passes through the spray field. *a* is the particles absorbance which is a function of transmission and travel length. Some manipulation yields,

$$C_v = \frac{-2000\ln(Tr)}{3l\sum\frac{\eta_i v_i}{d_i}} \tag{40}$$

where C_v is in ppm, and *i* represents droplets with different diameter ranges. C_v can be divided by 10000 to indicate the volume concentration of particles per unit volume of the spray. Details discussion on this topic can be found in Leong (2000), Cabra et al. (2002), and Malvern Spraytec RTSizer software manual.

Table **5** presents the droplet measurement results. For the full cone sprays, d32 was calculated from Equation 9 and for all of the cases *V* was calculated from Equation 10. Sauter Mean Diameter decreased with increase of pressure. As spray pressure increased, there was higher momentum flux through the nozzle and a larger force to disperse the liquid and shatter the jet into droplets. The larger force resulted in smaller droplet sizes with increasing spray pressure. This trend continued until the cumulative surface tension forces of the droplets canceled the increasing force and the change in droplets sizes

evened out. Smaller droplet sizes required increasing droplet number concentration (C_v) to maintain continuity. Figure 13 and Figure 14 show the changes in d_{32} and C_v with spray pressure. The variations are very modest in the figures, largely because the sprays were fully developed. The maximum drop in SMD between higher and lower spray pressures was only 6.4 μm while droplet number concentration initially changed but flatted out at higher spray pressures.

It should be noted from Table **5** that the droplets velocities for all three nozzles are the same. Equation 10, which was used to determine droplet velocity, depends on liquid velocity in the tube (mass flow rate), spray pressure, d_{32}, and fluid properties. Since the fluid properties were the same and flow rates and droplet sizes were relatively close, the most dominant parameter in droplet velocity was the spray pressure. This should be kept in mind since it implies very similar heat transfer from all sprays if the driving parameter in heat transfer was the droplet velocity. In the future chapters it will be shown that heat transfer from different sprays were hugely different, highlighting the inconsistency of previous works assumptions with the experimental results.

Table 5. Spray measurements, *: d_{32} was calculated using Equation 9, V was calculated using Equation 10

Nozzle	**Pressure (kPa)**	**Flow rate (ml/s)**	***s* (mm)**	d_{10} **(µm)**	d_{50} **(µm)**	d_{90} **(µm)**	d_{32} **(µm)**	C_v **(ppm)**	***V* (m/s)**
Hollow Cone	206	1.04	8	6.3	18.4	105.9	29.2	178.7	15.7
	344	1.28	8	7.0	21.6	116.4	30.0	225.0	20.2
	482	1.56	8	4.6	15.6	114.4	27.5	235.8	23.9
	689	1.72	8	3.9	15.9	125.0	27.4	241.1	28.6
	896	2.00	8	3.4	19.1	141.2	26.3	283.1	32.6
	206	1.04	10	5.2	15.0	79.8	25.3	141.6	15.6
	344	1.28	10	4.3	14.1	89.5	24.9	143.9	20.2
	482	1.56	10	3.7	11.9	86.0	24.7	195.1	23.9
	689	1.72	10	3.1	11.0	119.5	23.6	188.5	28.6
	896	2.00	10	2.4	10.4	136.7	23.6	214.0	32.6
Flat Fan	206	2.17	8	14.0	82.3	129.1	39.3	559.3	15.7
	344	2.63	8	12.7	77.0	122.1	39.0	621.2	20.2
	482	2.94	8	10.0	69.5	116.7	37.8	617.2	23.9
	689	3.33	8	8.5	59.6	111.6	37.2	623.3	28.6
	896	3.85	8	6.4	58.8	113.4	36.0	595.3	32.6
	206	2.17	10	14.2	77.4	121.9	39.5	528.3	15.7
	344	2.63	10	11.1	69.1	120.1	38.5	502.0	20.2
	482	2.94	10	8.6	60.3	114.4	38.4	425.9	23.9
	689	3.33	10	7.0	54.0		37.0	454.2	28.6
	896	3.85	10	5.7	50.0	111.0 110.0	35.7	455.9	32.6
Full Cone	206	2.79	-	-	-	-	58*	-	15.7
	344	3.57					51*		20.2
	482	4.30					47*		23.9
	689	5.43					43*		28.6
	896	6.25					40*		32.6

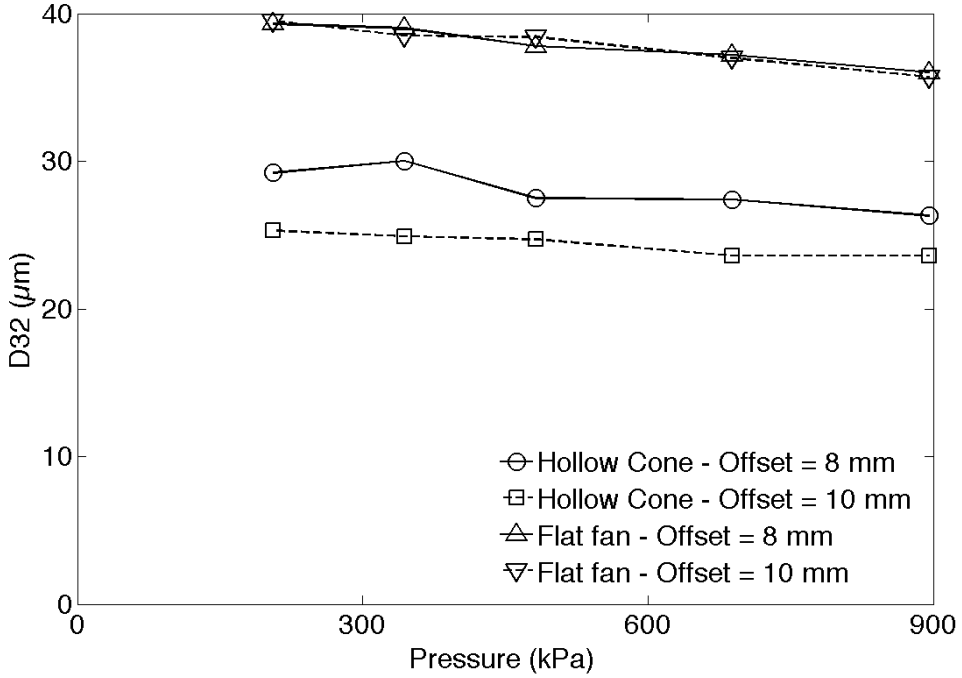

Figure 13. Sauter Mean Diameter against spray pressure for hollow cone and flat PF-5060 sprays

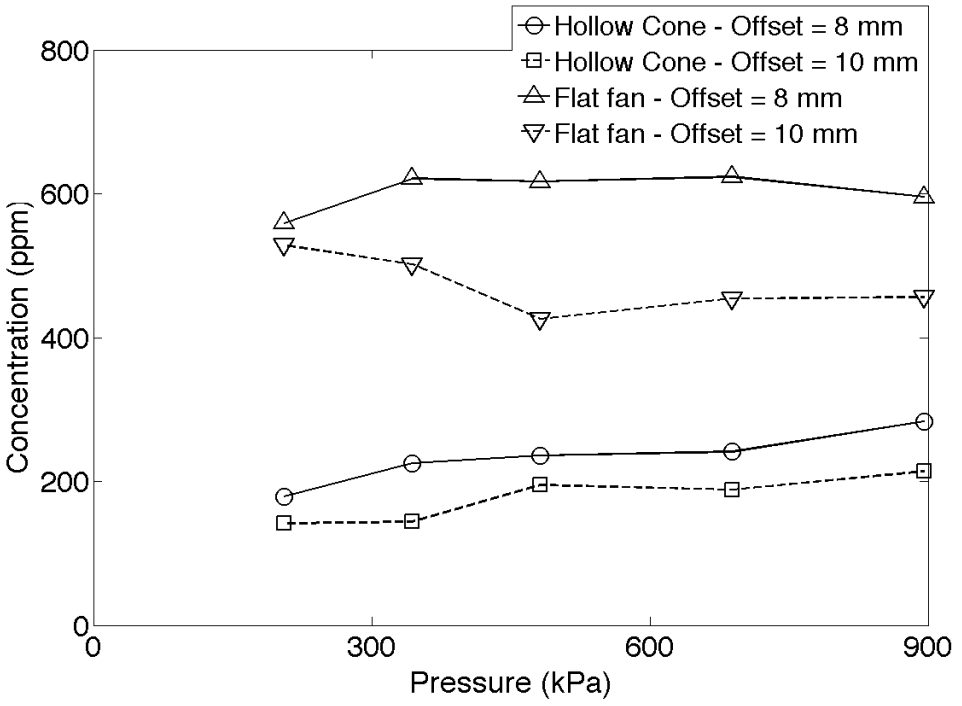

Figure 14. Droplet number concentration against spray pressure for hollow cone and flat PF-5060 sprays

4-4 Chapter Summary

Flow rate through the nozzles for all operating fluids and pressures were measured and the experimental and theoretical trends were in good agreement. Curve fit techniques were used to present simple equations for flow rate in each nozzle and for each fluid. A Malvern laser analyzer was used to measure droplet sizes, volumetric concentration, transmission, and attenuation in PF-5060 hollow cone and flat fan sprays. It was seen that the Sauter Mean Diameter and droplet number concentration did not change significantly near the fully developed conditions (higher pressure). It was also seen that droplet velocities were very similar for all sprays at similar pressures. As was discussed in Chapter 2, all of the available correlations for spray cooling are based on droplet velocity and d_{32}. Therefore, heat flux would be relatively similar from all sprays, which was not the case. These findings emphasize the importance of the basic premise of the present work in challenging the common wisdom and presenting a new approach in the study of spray cooling studied.

CHAPTER FIVE: SINGLE-PHASE HEAT TRANSFER

Heat transfer results are presented in two chapters, one for each regime. This chapter presents the single-phase results. Details of the experimental procedure are given and results are discussed. A correlation to predict single-phase heat transfer in spray cooling is developed and evaluated.

5-1- Test Matrix

Table 6 summarizes the test matrix for the single-phase study. As was shown in the hypothesis, there were two unknown parameters the general equation for single-phase heat transfer coefficient and two fluids were required to determine those. The third fluid in the table is added to provide additional confidence in the data and correlation. There are 96 test cases listed in the table. PF-5060 was studied for heater temperatures between 40°C and 55°C and the other two fluids were studied for temperatures between 40°C and 90°C, all with 5°C increments.

Table 6. Test matrix

Fluid	**PF-5060**	**PSF-3**	**PAO-2**
Spray type	Hollow cone, full cone, flat fan	Hollow cone, full cone	Hollow cone, flat fan
***s* (mm)**	3, 5, 7	3, 5	3, 5
P_s (kPa)	206, 344, 482, 689	206, 344, 482, 689, 896	206, 344, 482
α (deg)	45, 90	45, 90	45, 90
T_w (°C)	40 to 55	40 to 90	40 to 60

5-2- Single-phase Heat Transfer Results

Pressure and heat transfer data were collected for a total of 96 test cases (48 with PF-5060, 30 with PSF-3, and 18 with PAO-2). Three samples of the data for each fluid and nozzle are presented in Figure 15, Figure 16, and Figure 17. The left column in each figure is the pressure and the right column is the heat transfer coefficient distribution for the same conditions. There were a number of "non-regulating" heaters that are indicated by their dark blue color in the heat transfer coefficient plots. A non-regulating heater required its neighboring heaters to dissipate more heat so the non-regulating heaters along with their surrounding heaters were excluded from the postprocessing.

The flat fan spray (Figure 15) produced the largest local impingement pressure (up to 20 kPa). The result was very high heat fluxes that were occasionally beyond the capacity of the heater array and were therefore discarded. As expected, the spray diameter increased with increasing pressure and standoff distance when using the full-cone and hollow-cone nozzles (Figure 16 and Figure 17). The locations of the peak impingement pressure and heat flux were similar, which was consistent with the hypothesis in this work. However, there was a region of low pressure and relatively high heat transfer on the outskirt of the sprays due to the horizontal flow over the heater array. Hollow and full cone sprays had wider distribution and more modest maxima of about 10 kPa in impingement pressure.

In absence of direct impingement, horizontal flow controls the heat transfer. This effect can be seen on the top right corner of heat transfer distribution plots in Figure 15. While there was no impingement on that area, the inclined spray resulted in horizontal flow to the upper right corner resulting in significant convective heat transfer denoted in

green color. Same observation was made for the full cone and hollow cone sprays. After impingement, the liquid flowed outward resulting in relatively high heat transfer. In the case of hollow cone sprays, some of the liquid got trapped in the inner zone and exhibited considerably lower heat transfer compared to the impingement zone or even the outer zone. The imperfections in the full cone ISR prototype nozzle resulted in an unexpected spray patter, Figure 16. However, the almost identical correspondence between the pressure and heat transfer distributions was a reassurance for the validity of the basic assumption of the work.

Developing a model to evaluate the contribution of horizontal flow in overall heat transfer or using one of the standard model requires the knowledge of liquid film thickness and velocity which are very difficult to measure in spray problems. These contributions were proved to be several times smaller than that of direct impingement. The pressure-based model can be developed for the impingement zones only.

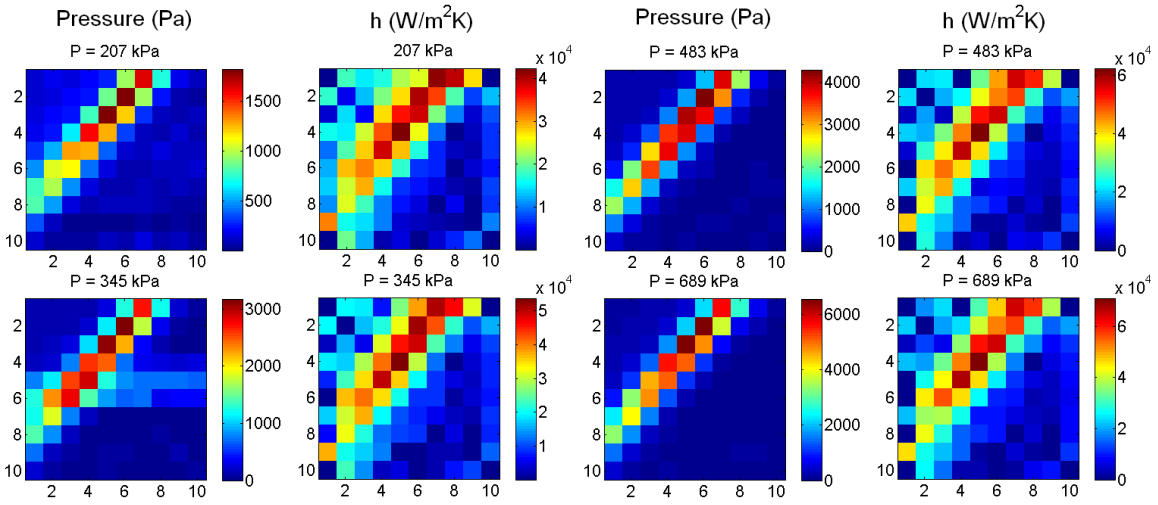

Figure 15. Pressure and heat transfer coefficient distribution for PF-5060 flat fan spray at 45° or orientation

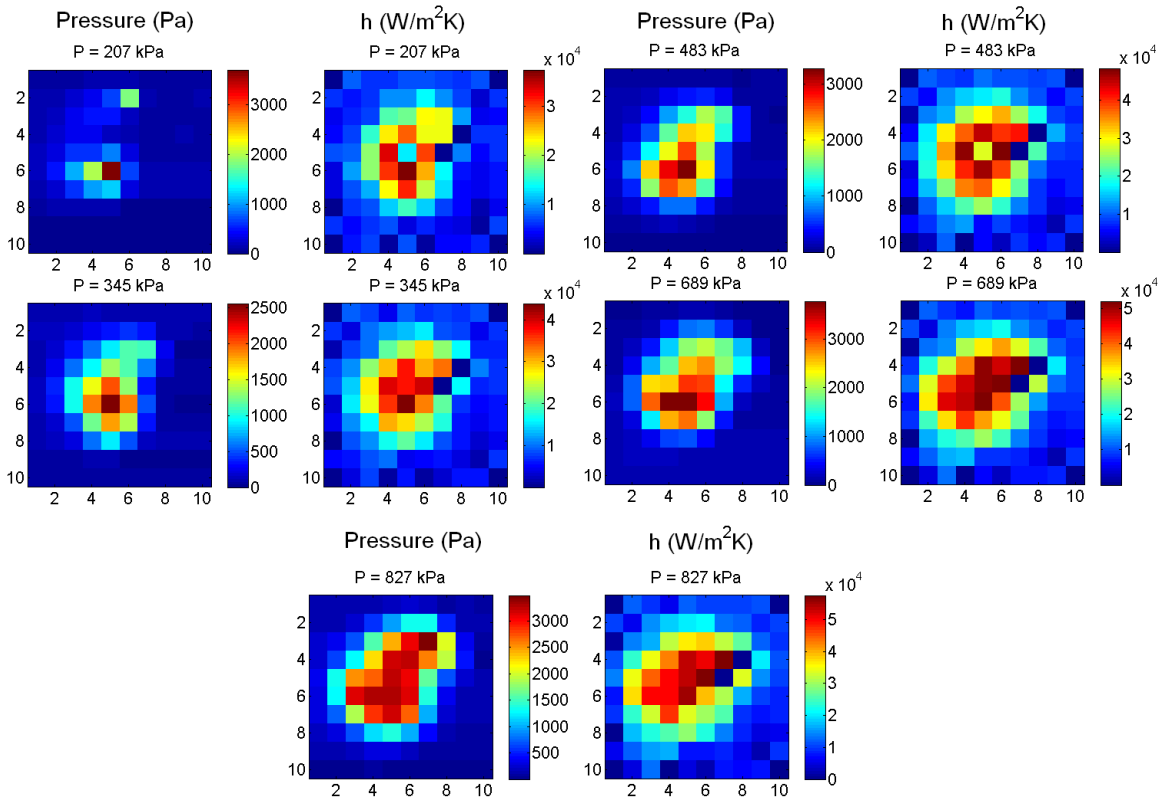

Figure 16. Pressure and heat transfer coefficient distribution for PSF-3 full cone spray at 5 mm standoff distance

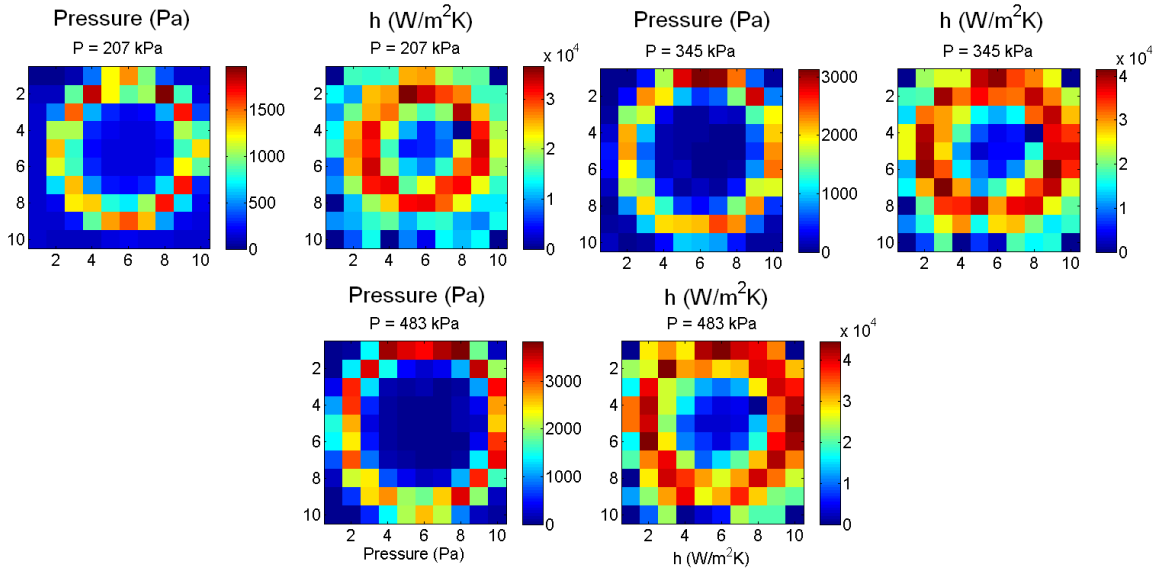

Figure 17. Pressure and heat transfer coefficient distribution for PAO-2 hollow cone spray at 5 mm standoff distance

Samples of radially averaged pressure and heat transfer coefficient plots are presented in Figure 18 and Figure 19. The circles and triangles represent pressure and heat transfer coefficient on the left and right ordinates respectively. In each case the center of the spray was determined and the readings were radially averaged. In both figures the peak locations for pressure and heat transfer coefficient were identical. The extent of the heat transfer distribution was larger than pressure due to the horizontal flow effects described above. Figure 18 is for the data with 3 mm standoff distance and therefore the peaks occurred at smaller radii compared to the 5 mm data in Figure 19. As expected, the pressure and heat transfer valued increased significantly with increasing spray pressure.

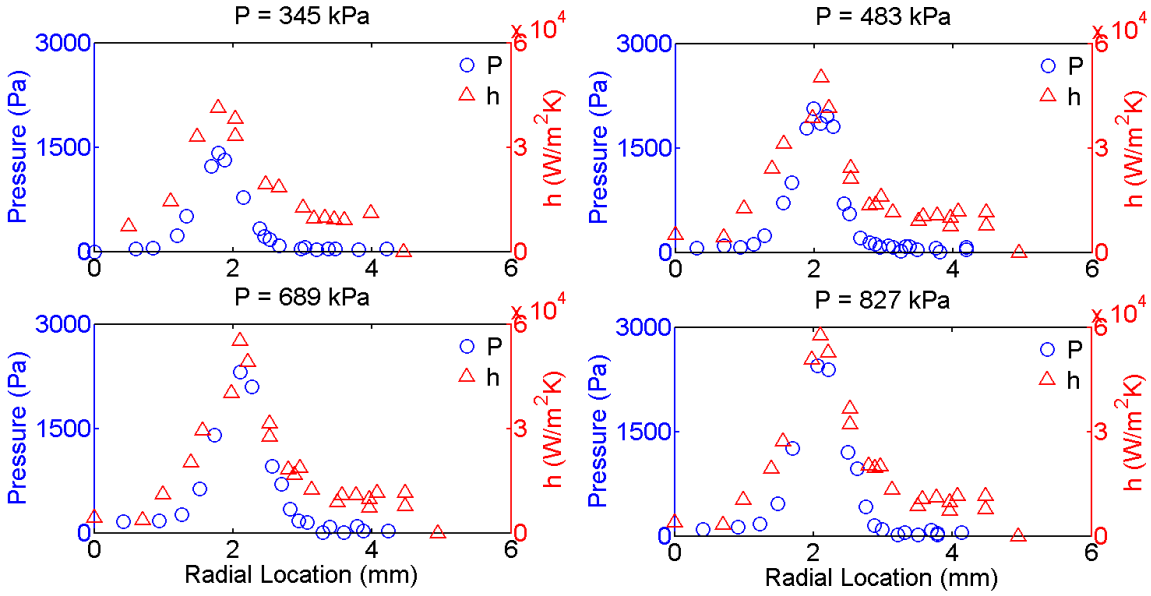

Figure 18. Radially averaged pressure and heat transfer coefficient for PSF-3 hollow cone spray at 3 mm standoff distance

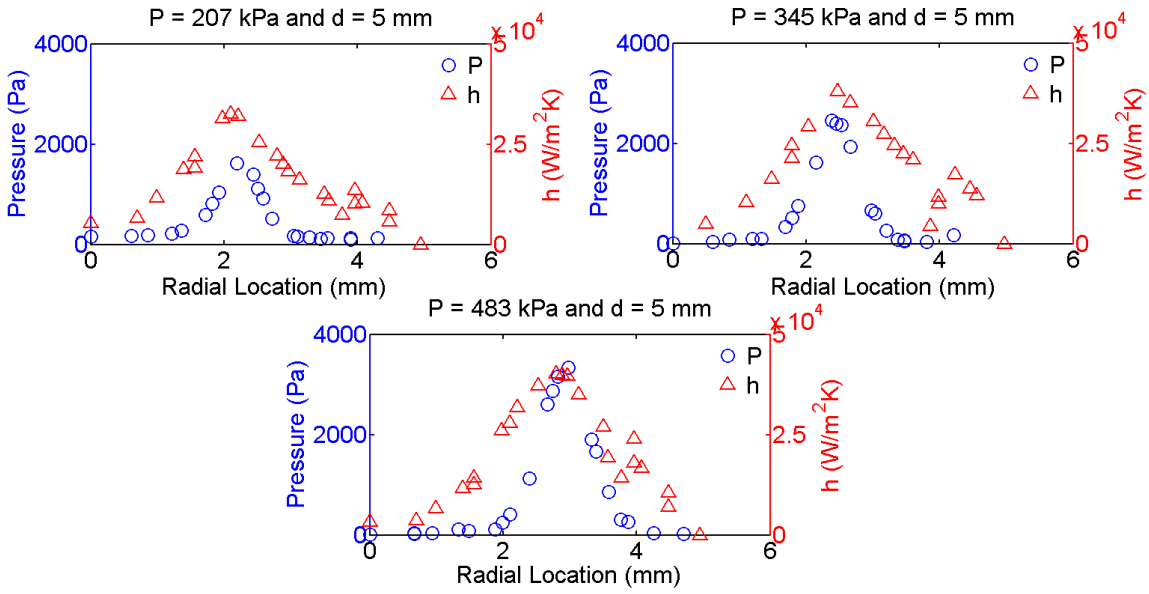

Figure 19. Radially averaged pressure and heat transfer coefficient for PAO-2 hollow cone spray at 5 mm standoff distance

5-3- Single-phase Correlation Development

In order to reduce the scatter, pressure and heat transfer data for full and hollow cone sprays were radially averaged and the flat fan spray data were averaged at different diagonal locations. The location of the center of the spray for a given pattern was chosen as the closest of the corners or center of a heater to the geometrical center of a corresponding circle. A radius scaling factor for each test case was introduced to compensate for the small mismatch between the radii of the hollow sprays for PSF-3 and PAO-2 to ensure the peaks in pressure and heat flux occurred at the same radius. This scaling factor was between 3-15%. Figure 18 and Figure 19 show the radial distribution of pressure and heat transfer coefficient for the cases to which the scaling correction was applied.

The local heat transfer data for each fluid were plotted against the corresponding local impingement pressure and were binned over 100 Pa increments. The binning process consisted of averaging the heat transfer coefficient and the impingement pressure of the data points that fell within the same increment. Binning eliminated the possibility of weighting the correlation toward the regions with disproportionately more data points and provided evenly distributed sets of data. Another benefit of binning was that the outlying data points were averaged. To develop a correlation between pressure and heat transfer coefficient, an appropriate form of the relation between the two parameters needed to be determined. The form suggested by the dimensional analysis (Equation 17) was chosen. Two constants, C and a need to be determined from the data. Taking the logarithm of both sides yields

$$\log(H) = \log(C) + a\log(Pr) \tag{41}$$

By averaging all H values from the binned data for each fluid and plotting them against the Prandtl numbers in log-log coordinates, a plot with three points was obtained through which a line was fit whose slope and y intercept represented a and $\log(C)$ respectively (Figure 20). The final correlation for fluids with Prandtl numbers between 12 and 76 and impingement pressures of below 20 kPa the heat transfer coefficient is given by

$$H = \frac{h}{(\rho P)^{0.5} c_p} = 0.042 Pr^{-0.33} \tag{42}$$

or

$$h = 0.042\rho^{0.5} c_p Pr^{-0.33} P^{0.5} \tag{43}$$

where SI unit system is used for all the parameters. In Figure 20 the average H values for each liquid is shown with solid symbols. The mean absolute error for the linear fit on these points is 4.3%.

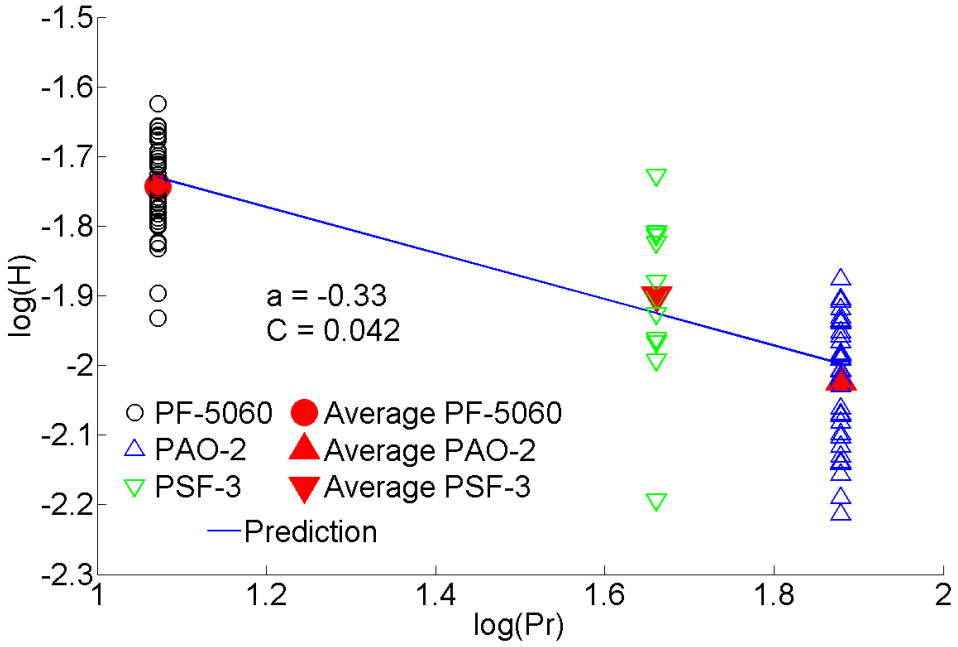

Figure 20. Linear fit on the average H values against Pr to determine the universal constants, a and C, in the correlation

5-4- Single-phase Correlation Verification

For PF-5060, the above correlation reduces to $h = 791.2P^{0.5}$ W/m^{2}K which is within 4.6% of the correlation the authors developed for PF-5060 sprays in Abbasi, et al, (2009), $h = 830.0P^{0.5}$. For PSF-3 the model yields $h = 688.2P^{0.5}$ W/m^{2}K (a fit on only the PSF-3 data yields $h = 797.6P^{0.5}$ W/m^{2}K). Likewise for PAO-2, the model predicts $h = 644.2P^{0.5}$

W/m^{2}K (a fit on only the PAO-2 data yields $h = 577.3P^{0.5}$ W/m^{2}K). A comparison of the binned data for each fluid with the prediction of Equation 38 is shown on Figure 21, Figure 22, and Figure 23. With the exception of a few outliers, all the average data points fall within ±25% of the predicted values.

Predicting radial variation of heat transfer coefficient in the hollow cone sprays is particularly important because they can be used to test the robustness of the correlation by capturing the variation in heat flux across the spray impingement region. Figure 24, Figure 25, and Figure 26 show the measured and predicted values for radially averaged heat transfer coefficient in hollow cone sprays for the three liquids. The peak locations and magnitudes as well as the extent of the impingement zones are accurately captured by the correlation. There was often somewhat higher heat transfer at radii smaller than the droplet impact zone and also the outskirt of the sprays where the mechanism driving the heat transfer wass not impingement pressure but the horizontal flow of liquid over the heater. This was expected since the correlation was developed from data within the droplet impact zone only.

Radially averaged pressure and heat transfer data for each fluid was compared against the corresponding models in Figure 27. The correlation was also used along with the measured pressure distribution data to obtain the area-averaged heat transfer from the surface and compared with the measured data (Figure 28). It is observed that the agreement is quite good, with almost all the data within ±25% of the correlation. The outliers are likely due to inaccurate prediction of the data outside of the droplet impingement zone.

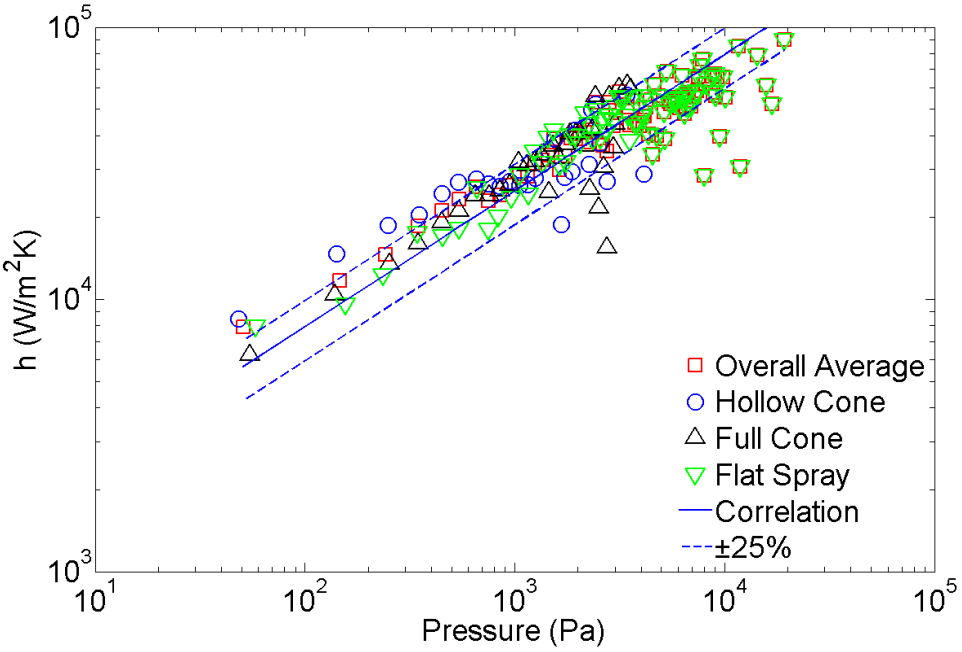

Figure 21. Pressure vs. heat transfer for PF-5060 experimental data and the prediction from the correlation

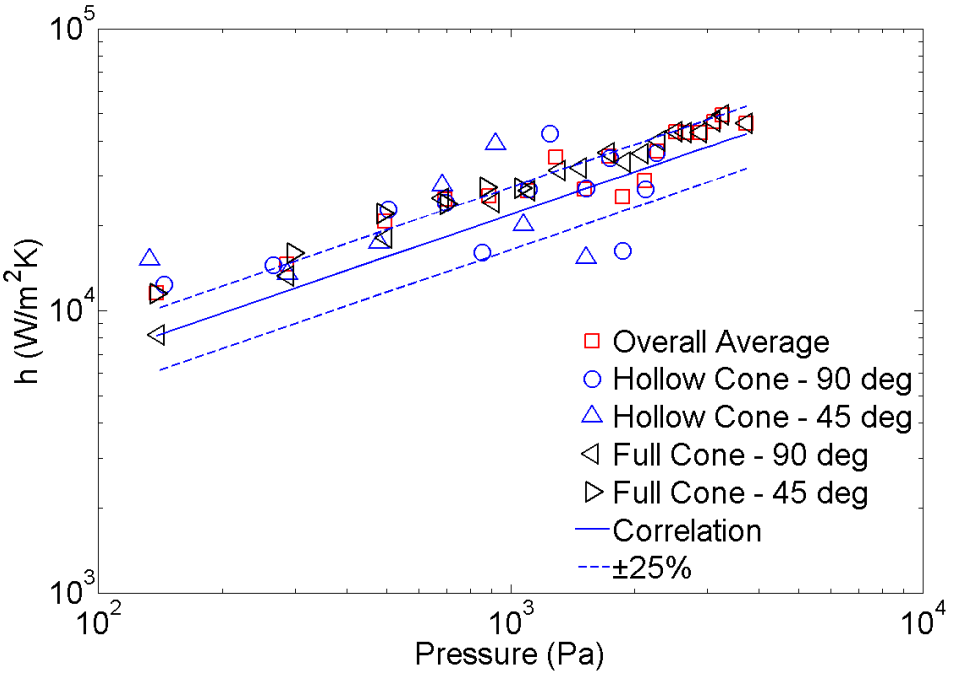

Figure 22. Pressure vs. heat transfer for PSF-3 experimental data and the prediction from the correlation

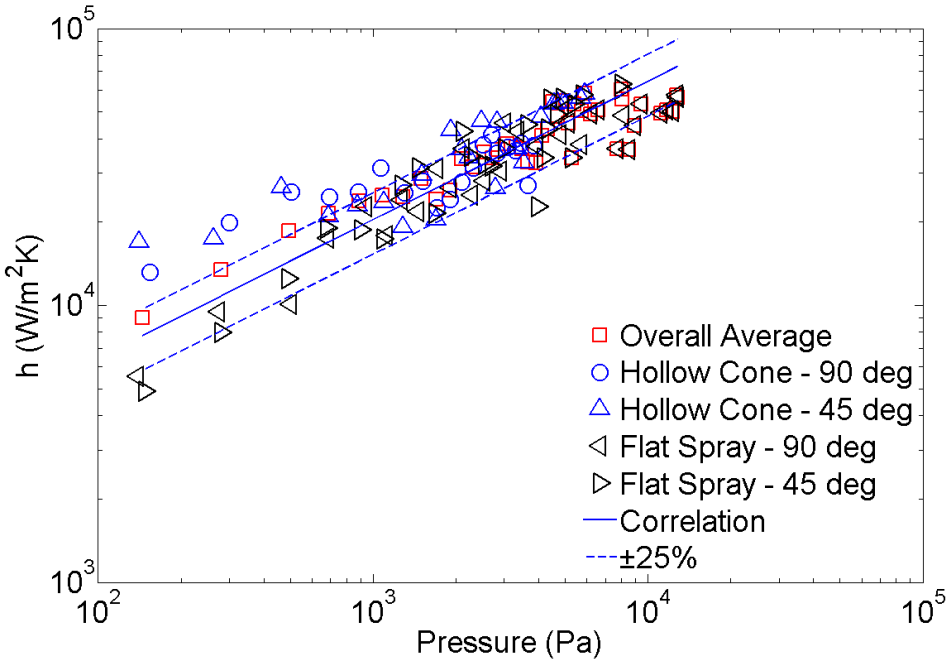

Figure 23. Pressure vs. heat transfer for PAO-2 experimental data and the prediction from the correlation

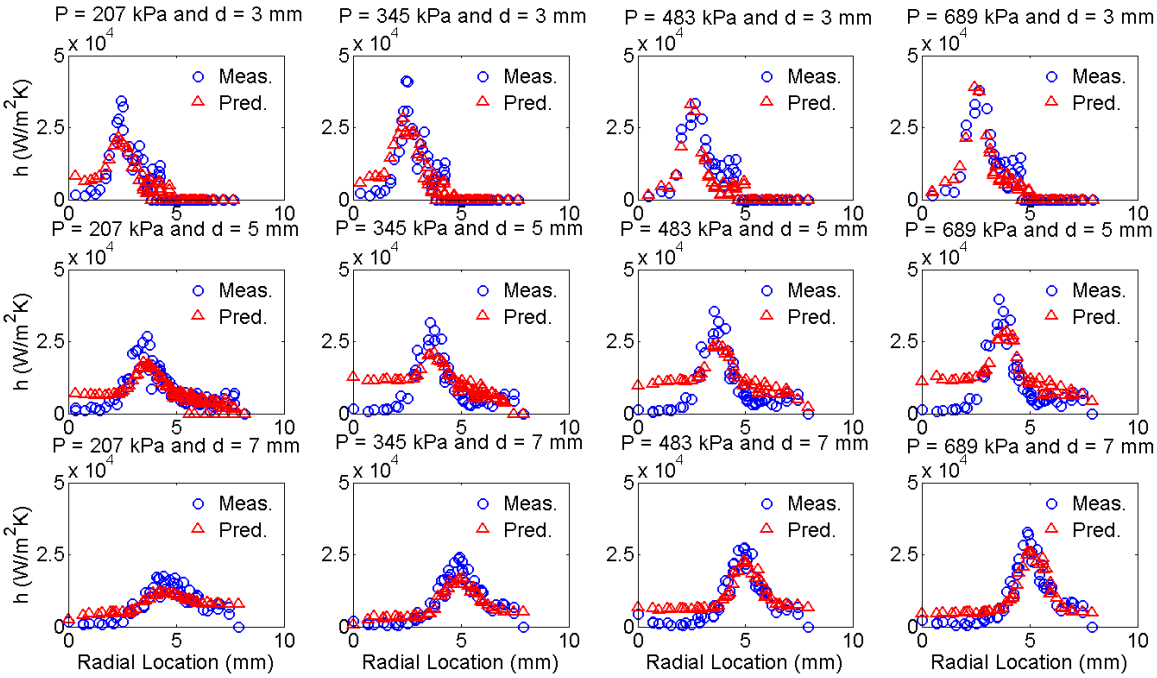

Figure 24. Measured vs. predicted radially averaged heat transfer coefficients for hollow cone PF-5060 data

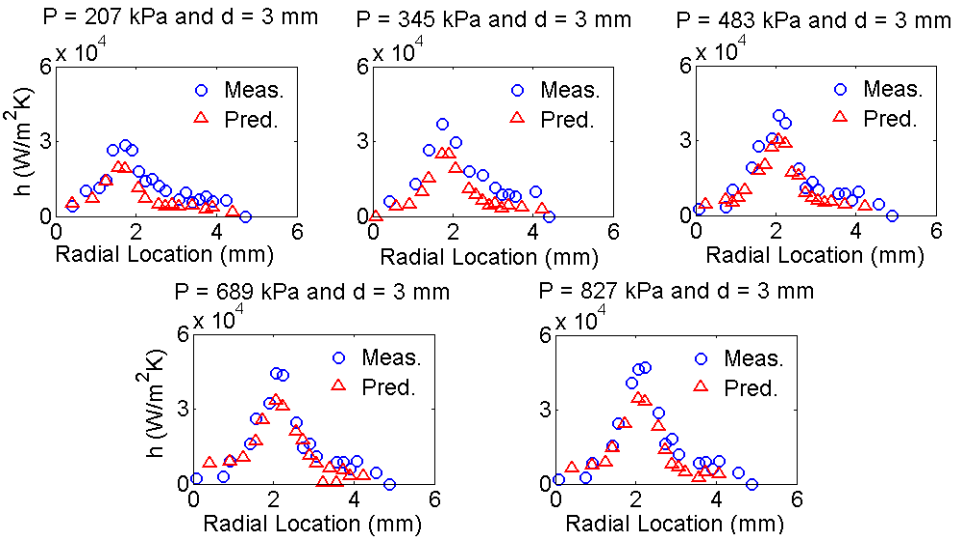

Figure 25. Measured vs. predicted radially averaged heat transfer coefficients for hollow cone PSF-3 data

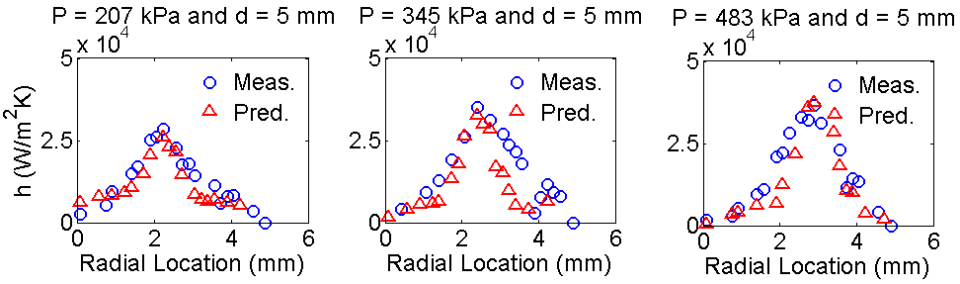

Figure 26. Measured vs. predicted radially averaged heat transfer coefficients for hollow cone PAO-2 data

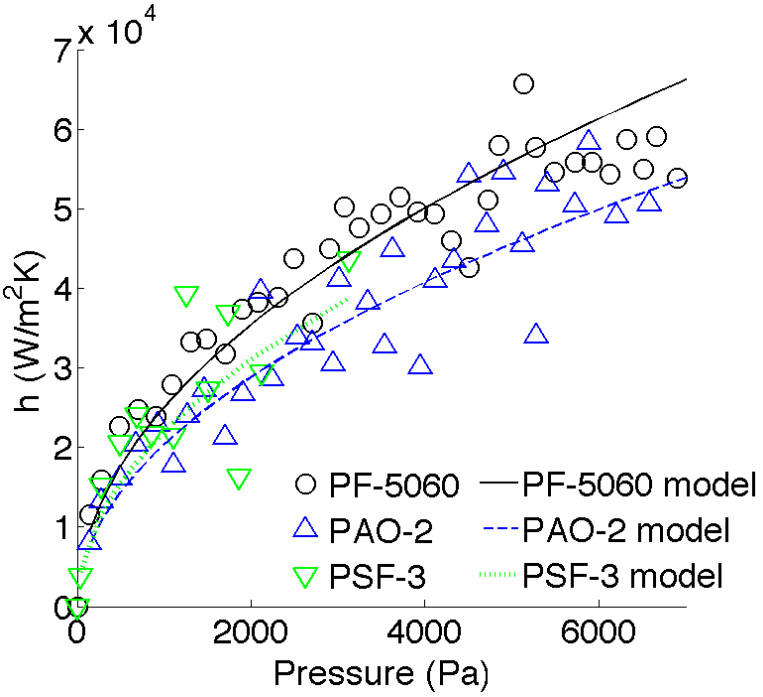

Figure 27. Radially averaged pressure and heat transfer for different liquids

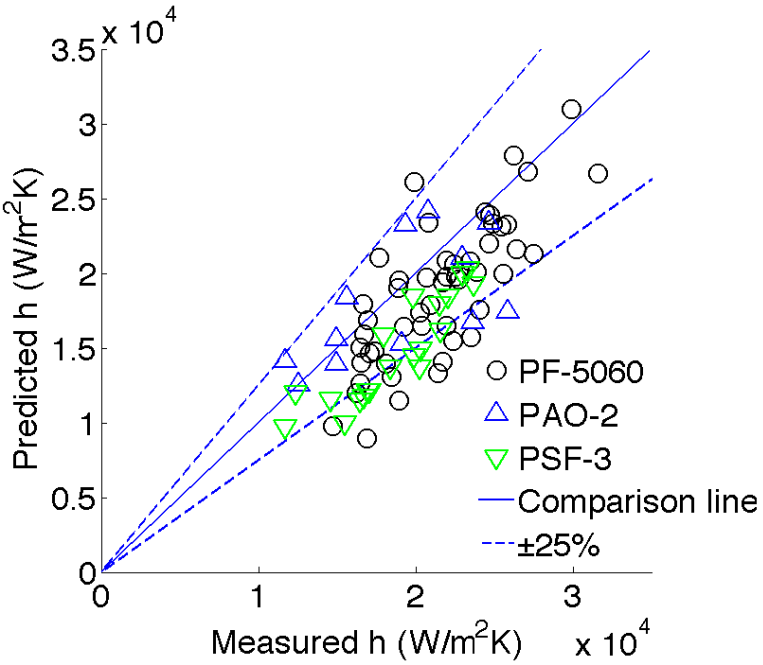

Figure 28. Predicted vs. overall average measured heat transfer coefficient for each test case

5-5- Comparison with Existing Correlations

Average heat transfer coefficients over the impingement area of PF-5060 full cone sprays were compared against the predictions obtained from correlations available in the literature (Figure 29). Even though Karwa et al. (2007) developed their correlation for water, it agreed with the present data better than other correlations. The Rybicki and Mudawar (2006) correlation was developed for PF-5052 whose Prandtl number is very close to PF-5060 (11.5 vs. 11.8). It is noteworthy that in this correlation h depends on $Pr^{0.32}$ which is in contrast with the findings of this study which indicate that h depends on $Pr^{-0.33}$. Although the comparison with Shedd's correlation (Equation 11) was made using their recommended values for system-specific constants, the agreement is quite poor. Some et al. (2007) used a different variation of pressure-based correlation that was based on a curve fit rather than a physics-based form for the correlation. Despite that deficiency, it performed well for higher h values. The predictions from the dedicated correlating for PF-5060 data (mentioned in the previous section) are also shown in the figure. This comparison highlights the advantages of using the pressure-based technique. While other correlations rely on system-specific constants and/or input parameters that are difficult to measure, the present work has no fudge factor and relies solely a single and easy-to-measure input parameter. The result is impressive agreement with the data for a variety of fluids.

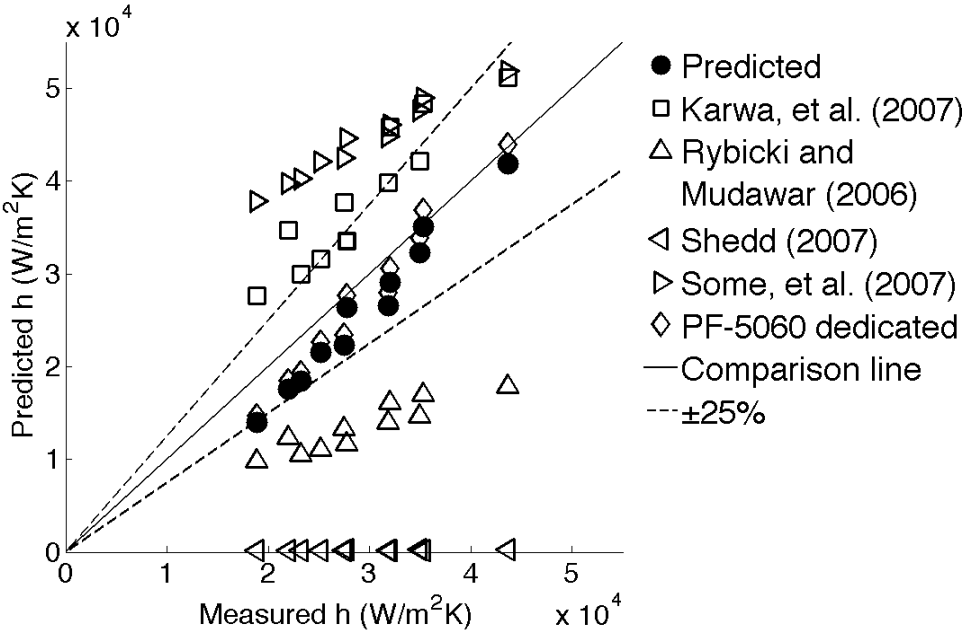

Figure 29. Measured versus predicted values for PF-5060 full cone spray heat transfer for various correlations from the literature

5-6- Error Analysis

Error analysis is very important for a versatile correlation like the one presented in this chapter. The errors in the predictions are results of various uncertainties, human error, and the randomness that is inherent to the problem. MAE and RSME are often used in this type of problems to represent the errors.

Table 7 summarizes the error analysis for different liquids and sprays. The errors were calculated using predictions based on binned pressure data. This method prevented weighting of the error toward regions with more data points and provided uniform distribution and more reliable analysis. Heat transfer coefficients values below 1 kW/m^2K were ignored for the purpose of this analysis because those points were almost always away from the impingement zone and less significant. They would have affected just a

few elements in the binned pressure vectors and would not have had much overall influence. However, discarding them allowed for more precise demonstration of the correlation performance.

PF-5060 had the best overall MAE of 11.8%, followed by PAO-2 with 17.2% and PSF-3 with 22.0%. The largest and least errors were in hollow cone PSF-3 and flat fan PF-5060 sprays with approximated values of 27.9% and 10.5% respectively. For all three operating liquids, the overall MAE was smaller than those of individual sprays. This emphasizes on the importance of the binning process, where various under- and over-predictions at the same pressure intervals were eliminated.

Table 7. Error analysis for the single-phase correlation; MAE in % and RMSE in W/m^2K

Fluid	**Spray pattern**	**Error type**	**Error value**
PF-5060	Total	MAE	11.8
		RMSE	7.6×10^3
	Hollow cone	MAE	17.5
		RMSE	6.5×10^3
	Full cone	MAE	16.9
		RMSE	6.8×10^3
	Flat fan	MAE	10.5
		RMSE	7.6×10^3
PSF-3	Total	MAE	22.0
		RMSE	6.9×10^3
	Hollow cone	MAE	27.9
		RMSE	7.5×10^3
	Full cone	MAE	22.6
		RMSE	5.2×10^3

PAO-2	Total	MAE	17.2
		RMSE	9.5×10^{3}
	Hollow cone	MAE	20.5
		RMSE	4.9×10^{3}
	Flat fan	MAE	21.6
		RMSE	10.5×10^{3}

5-7- Chapter Summary

A Malvern laser setup was used to measure droplet size and velocity for PF-5060 sprays. The data gave an insight into the range of parameters in the study and highlighted the need to incorporate the physical aspects of the process in proposing correlations. 96 different test cases were examined to discover the relation between local impingement pressure and heat transfer. It was seen that the spray impingement zone had the highest heat flux. The areas with high horizontal flow exhibited higher heat transfer than areas with stagnant liquid. Dimensional analysis was used to find the proper form for the correlation. There were two unknowns in the correlation and three fluids were used to determine the constants. The outcome was a correlation to predict the single-phase heat transfer coefficient for liquids with Prandtl number 12 and 76 and impingement pressure below 20 kPa within ±25% of the data.

CHAPTER FIVE: TWO-PHASE HEAT TRANSFER AND CRITICAL HEAT FLUX

Two-phase heat transfer and critical heat flux conditions are discussed in this chapter. The test matrix and the data are discussed and a pressure-based correlation for heat flux at the CHF point and for the entire local spray cooling curve is presented. The correlation is verified against the data and the correlations available in the literature.

6-1- Test Matrix

The test matrix for this part of the research is given in Table 8 and consists of 72 test cases. PF-5060 was chosen as the working fluid based on its applicability in the electronic cooling industry and availability and since PSF-3 and PAO-2 had very high boiling temperatures that were beyond the capacity of the heater. The sprays were produced using two nozzles: Spraying Systems LLN-1/4 1.5 hollow cone nozzle and an ISR prototype full cone nozzle. The extremely high local pressure and heat transfer produced by the flat fan nozzle exceeded the capacity of the heater to measure the heat flux and was therefore excluded from this part of the work.

Subcooling has significant effect on the two-phase heat transfer and critical heat flux. The available literature on the effect of subcooling on spray cooling heat transfer were discussed in Chapter 2. In the two-phase experiments, the water bath temperature was set to 33°C, 45°C, and 69°C to maintain the operating fluid at 25°C, 35°C, and 45°C respectively. It is important to mention that these are average temperatures and do not

reflect the exact values. In reality, liquid temperature increased as it flowed through the system and for one standoff distance the temperature increase from the lowest spray pressure to the highest spray pressure could be as much as 8°C. Therefore the actual liquid temperature varied from 23°C to 49°C. With the nominal saturation temperature being 56°C, the range of subcooling was 11°C-31°C.

Table 8. Test matrix

Fluid	PF-5060
Spray type	Hollow cone, full cone
***s* (mm)**	3, 5, 7
P_s (kPa)	207, 345, 483, 689
T_w (°C)	40 to 100
T_f (°C)	25, 35, 45

6-2- General Observations

Impingement pressure was measured with the liquid nozzle inlet temperature at room temperature (around 25°C). The measured pressure distribution was assumed to be the same as the other liquid inlet temperatures since fluid properties vary only slightly (usually 1-3%) as the liquid temperature changed. Samples of the heat flux distribution for the hollow and full cone sprays are shown in Figure 30 and Figure 31. Each pixel represents a heater in the micro-heater array. There were seven non-regulating heaters (distinguishable by their black color). Similar to the single-phase study, the non-regulating heaters as well as their neighbors were excluded from the postprocessing. Full

cone sprays had larger impingement areas than the hollow cone sprays. With increasing standoff distance and spray pressure, the spray covered a larger area of the heater resulting in higher overall heat flux compared to test cases with smaller standoff distance and lower spray pressures.

Heat flux values were averaged for heaters which were located within ±0.5 mm of specified radii and were plotted against heater temperature to obtain radially averaged spray cooling curves (Figure 32 and Figure 33). As expected, the curves were linear up to the saturation temperature (56°C). For temperatures above about 60°C, an increase in slope was observed. Heat flux also increased with increasing spray pressure and decreasing standoff distance (both resulting in higher impingement pressures).

Figure 32 and Figure 33 show the local spray cooling curves for hollow and full cone PF-5060 sprays for various configurations and subcoolings. The radial spray cooling curves for PF-5060 hollow cone sprays at 3 mm standoff distance are given in Figure 32. The heat fluxes in the inner zone of the spray (r=0 mm, r=1.5 mm) are low, but the heat flux sharply increases with radial distance and peaks at r=2.5 mm where the impingement pressure is highest. The heat flux then decrease as r increases beyond 2.5 mm. CHF occurs at around the same temperature regardless of the spray impingement pressure. This includes the inner zone of the spray (almost no droplet impingement where a pool boiling-type heat transfer process occurs), the impingement zone (where the driving mechanism for heat transfer is the local impingement pressure), and the outskirt of the spray (where radially outward flow drives the heat transfer). In spite of completely different heat transfer mechanisms, heat flux peaks at the same temperature. Similar patterns are observed for the full cone sprays (Figure 33). The heat flux is largest at the

center of the spray (r=0) where the local impingement pressure is at its maximum, then decreases with increasing r. As was seen for the case of hollow cone sprays, even where the dominant heat transfer mechanism is horizontal flow, CHF occurs at the same heater temperature of 87.5°C-92.5°C.

In this study the nozzle inlet liquid temperature varied between approximately 23°C to 49°C (subcooling between 7°C to 33°C). No specific pattern to suggest a connection between the subcooling and T_{CHF} could be identified. These plots clearly indicate that spray characteristics and the local heat transfer mechanisms have little to no influence on the CHF temperature. The points at which CHF occurs (q''_{CHF} vs. T_{CHF}) for the spray cooling curves in the impingement zone are plotted in Figure 34 for hollow cone and full cone sprays at the three standoff distances and nozzle flow rates tested (a total of 371 data points). The data range from CHF values as low as 50 W/cm^2 to the maximum reported CHF value of about 350 W/cm^2. Averaging T_{CHF} over all of the data yields that for PF-5060 sprays CHF occurs at an average temperature of 89.2°C.

At temperatures beyond T_{sat}, two competing parameters of incoming droplets and instabilities induced by vaporization determine the structure of the liquid film on the heater surface. The similar values of T_{CHF} for various spray conditions hints that as surface temperatures increases, vaporization (which is controlled by surface temperature) becomes more predominant than the incoming liquid droplets. This observation is in agreement with the study by Bernardin et al. (1997) who studied water droplets with $20<We<220$ striking a smooth heater at temperatures between 70-250°C and frequencies between 40 and 150 drops per minute. They visualized spreading of the droplets upon impact and reported that CHF occurred at ΔT_w between 100°C-110°C for all test cases

despite the significantly different spreading characteristics. They concluded that at high heater temperatures *We* had an important effect on the spreading of the droplets, however, CHF and Leidenfrost temperatures were insensitive to Weber number and impact frequency. It is important to note that although CHF *value* is dependent on the droplet impact characteristics as reported in Bernardin et al. (1997), the *temperature* at which CHF occurs does not change much. Elbaum (1995) provided a thermodynamic justification for the increased contact angle of droplets impinging on surfaces whose temperature was higher than T_{sat} for otherwise wetting liquids. A more extensive research on the underlying reasons for vaporization dominance on liquid film structure at high heater temperatures is needed.

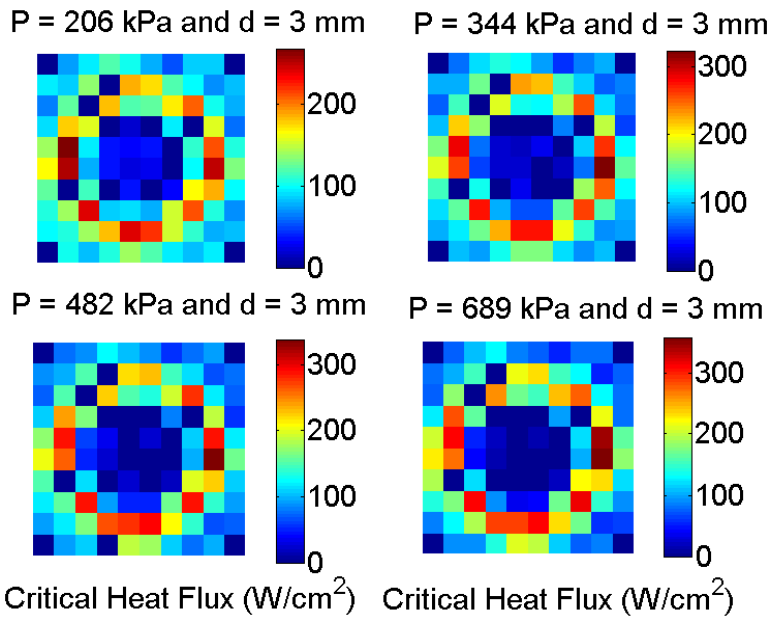

Figure 30. Heat flux distribution for the hollow cone spray at 90°C wall temperature and 3 mm standoff distance

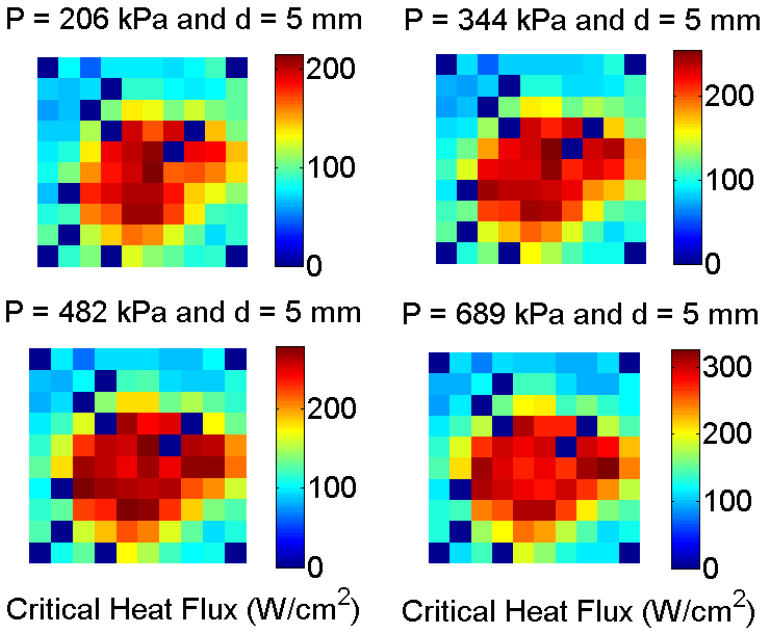

Figure 31. Heat flux distribution for the full cone spray at 90°C wall temperature and 5 mm standoff distance

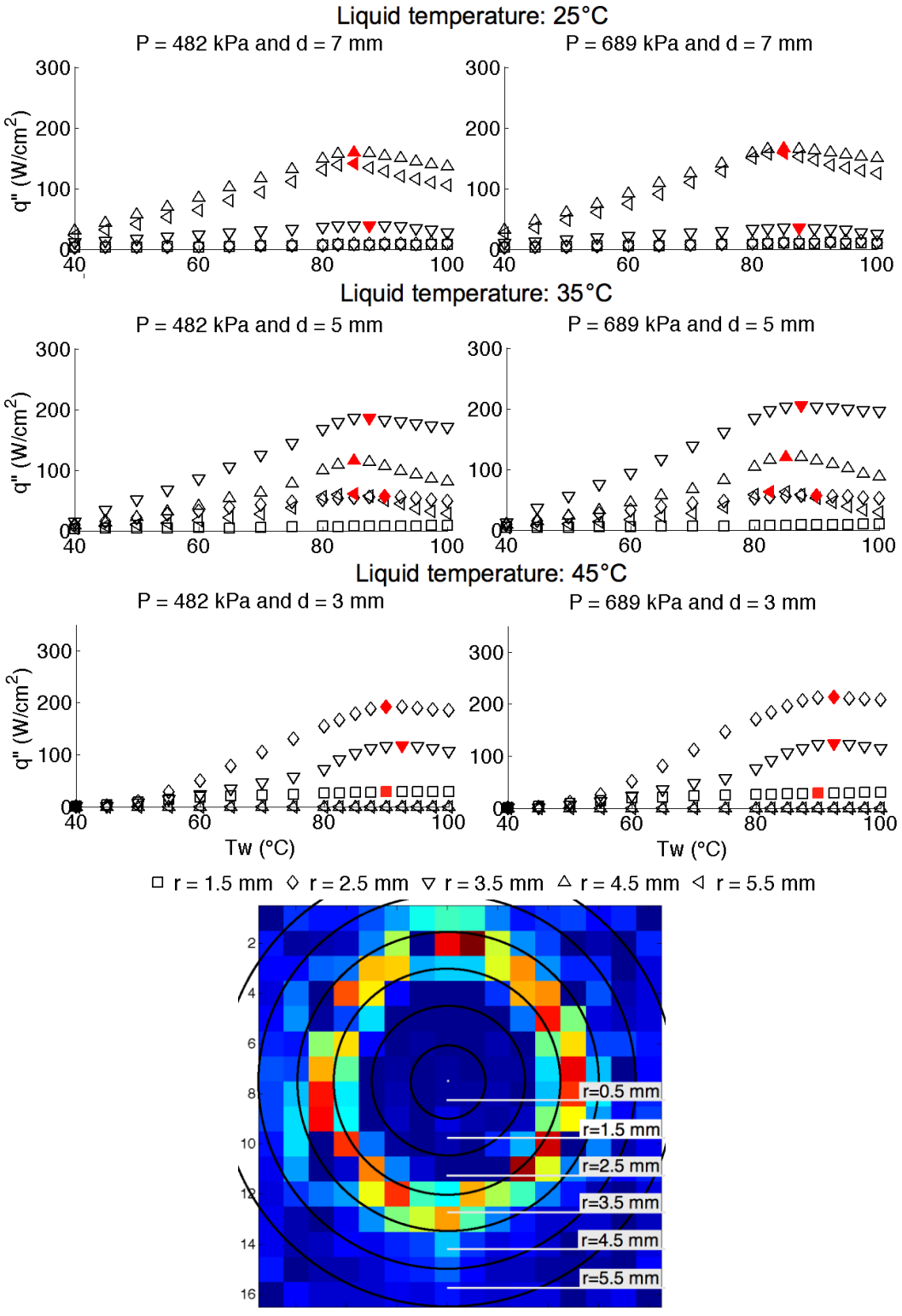

Figure 32. Radially averaged boiling curves for hollow cone sprays; the CHF location is designated using a solid symbol

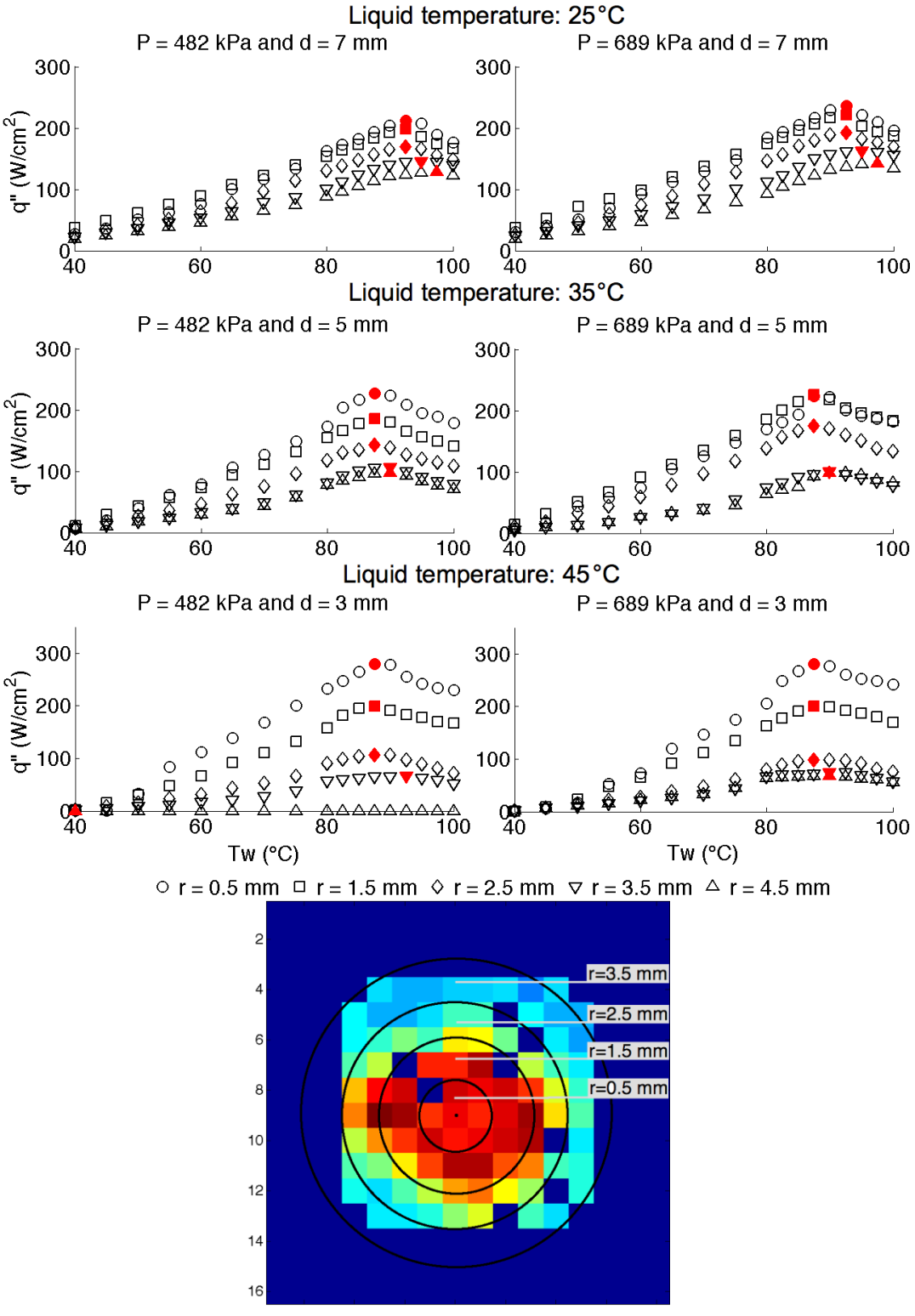

Figure 33. Radially averaged boiling curves for full cone sprays; the CHF location is designated using a solid symbol

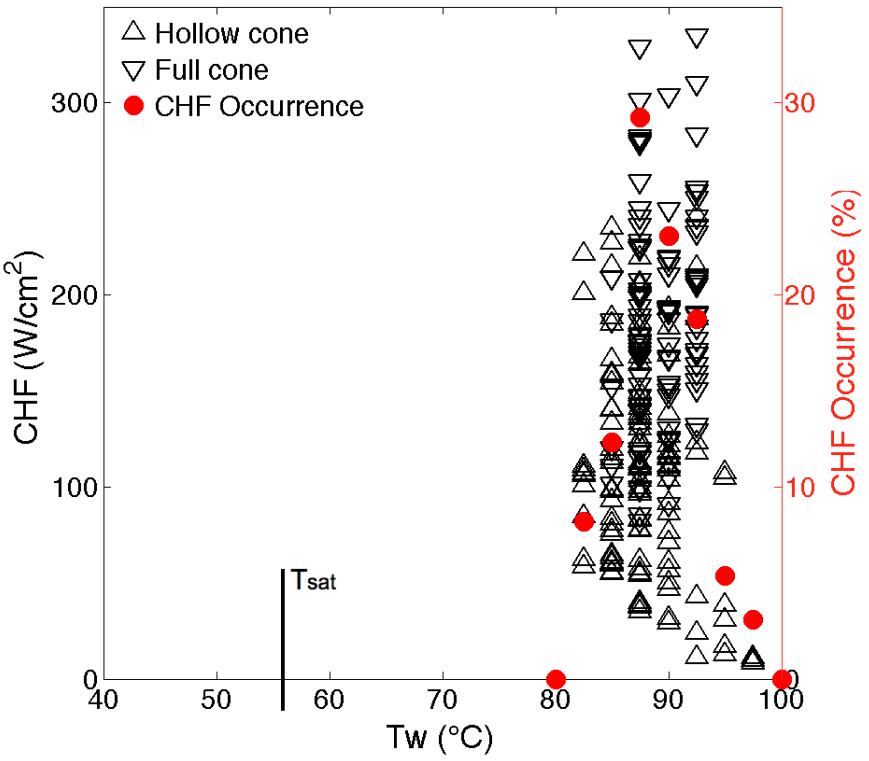

Figure 34. CHF value and occurrence temperatures at different wall temperatures

6-3- CHF Correlation Development

The single-phase study showed the strong connection between the local impingement pressure and heat transfer. That connection is investigated for the CHF conditions in Figure 35. For each data set, the impingement pressure was binned over 100 Pa intervals to evenly distribute the weight of the data points so the correlation is not weighted toward the intervals with more points. It is observed that CHF decreases with increasing liquid temperature and increases with increasing impingement pressure such that for different subcoolings the slope of the CHF increase with P is almost identical. The solid and dashed lines in Figure 35 represent separate fits to different test cases. The individual models for heat flux at the CHF point and pressure are given in Table 9. It is clear from

the figure and also the models that, similar to the single-phase regime, there is a strong connection between heat flux and local impingement pressure at the CHF point. It is assumed that CHF is a function of fluid properties, local impingement pressure, and subcooling:

$$q''_{CHF} = f(P, \rho, \mu, k, c_p, h_{fg}, \sigma, \Delta T_{CHF}) \tag{44}$$

where $\Delta T_{CHF} = T_{CHF} - T_f$. In the boiling studies it is very common to incorporate the effects of subcooling using *Ja*, several examples are cited by Carey (2008). Based on the those studies and the current single-phase work in can be hypothesized that:

$$q''_{CHF} = c_1 P^{c_2} Ja_{CHF}^{c_3} Pr^{c_4} \tag{45}$$

where c_1 is a combination of fluid properties with proper dimensions and $Ja_{CHF} = c_p \left(T_{CHF} - T_f \right) / h_{fg}$. Since only one fluid was used to obtain the data, the effect of *Pr* could not be studied. A more physically sensible form for the correlation can be proposed based on the remaining parameters, namely, a combination of fluid properties, local impingement pressure, and *Ja*. The effects of *Pr* and fluid properties have been absorbed into the constant, c_1. The following form was used to generate the following correlation for all of the test cases.

$$q''_{CHF} = c_1 P^{c_2} Ja_{CHF}^{c_3} \tag{46}$$

Using this form to obtain the best fit on the data resulted in:

$$q''_{CHF} = 1.45 \times 10^{5} P^{0.40} Ja_{CHF}^{0.52} \tag{47}$$

Some manipulation yields the final correlation for critical heat flux value for PF-5060 sprays:

$$q''_{CHF} = 9.15 \times 10^{4} P^{0.40} \left(1 + 2.42 Ja\right)^{0.52} \tag{48}$$

where all quantities are in SI unit system (heat flux in W/m^2, pressure in Pa, and the constant c in m/s).This correlation and the radially averaged pressure data were then used to predict the CHF value for different test cases. Figure 36 is a three-dimensional plot of the measure and predicted CHF values against radially averaged impingement pressure and incoming liquid temperatures. The variation in the incoming liquid temperature from about 23°C to 49°C and the drop in CHF value are also seen in this plot.

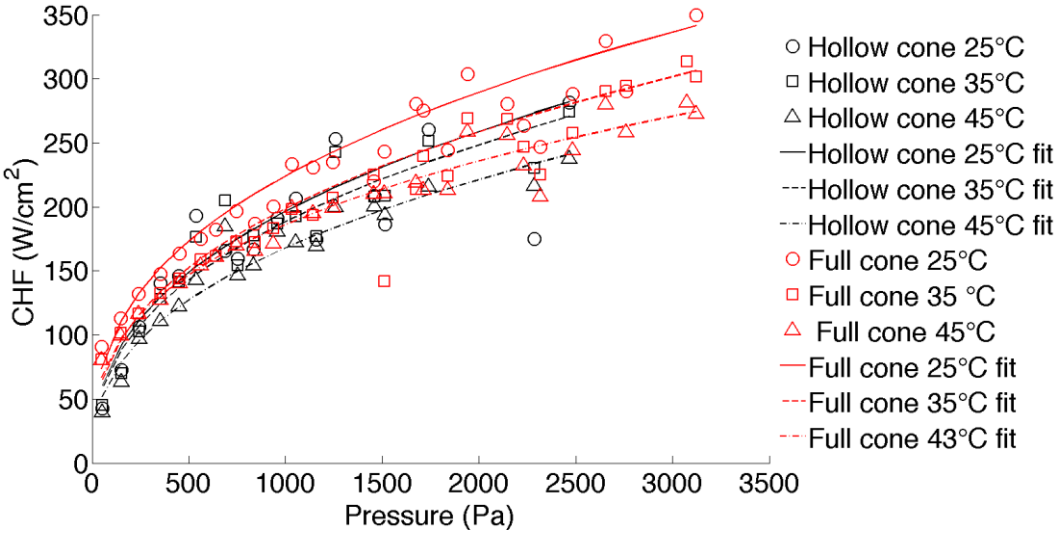

Figure 35. CHF vs. impingement pressure for different sprays and subcoolings

Table 9. CHF vs. pressure model for different subcoolings and sprays (P in Pa)

Spray pattern	**Liquid temperature** (°C)	q''_{CHF} **(W/m^2)**
Hollow cone	25	$1.24\times10^{5}P^{0.41}$
	35	$1.19\times10^{5}P^{0.40}$
	45	$1.06\times10^{5}P^{0.39}$
Full cone	25	$1.74\times10^{5}P^{0.37}$
	35	$1.44\times10^{5}P^{0.38}$
	45	$1.78\times10^{5}P^{0.34}$

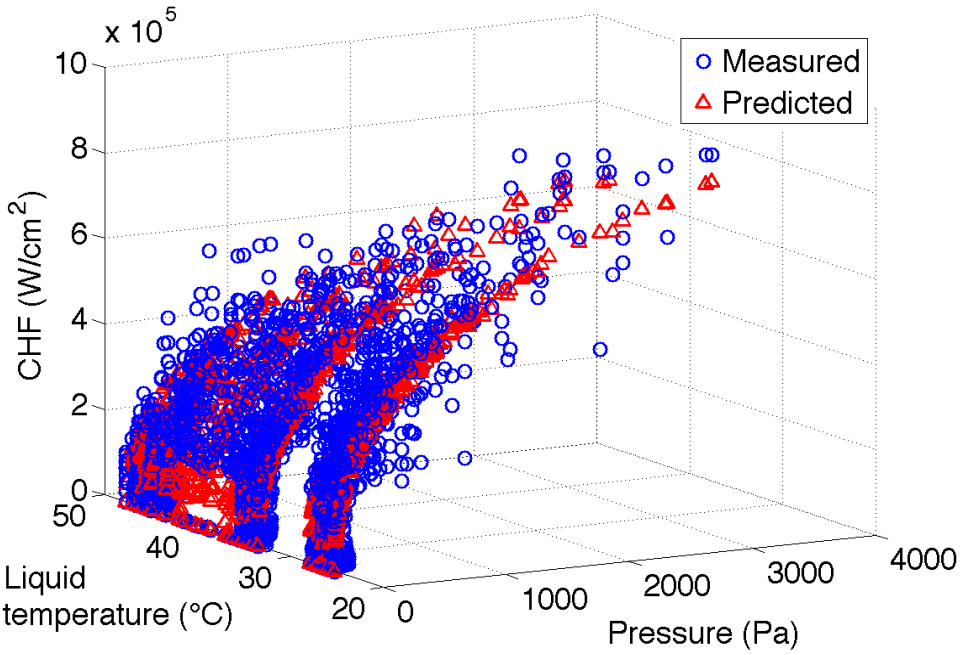

Figure 36. Measure and predicted CHF values against radially averaged impingement pressure and incoming liquid temperature for all the test cases

6-4- Two-phase correlation development

The observation of constant T_{CHF} along with the correlation for single-phase regime and CHF allow for prediction of the spray cooling curves from the single-phase region through the two-phase region up to CHF using the following technique. Consider the sample spray cooling curve shown in Figure 37. The single-phase portion is represented by the red line, while the location of CHF obtained from Equation 44 and T_{CHF}=89°C is indicated by a solid circle.

We can define a non-dimensional temperature T^* as

$$T^* = \frac{T_w - T_{ONB}}{T_{CHF} - T_{ONB}} \tag{49}$$

where T_{ONB} is the temperature at which the two-phase effects start to become important (onset of nucleate boiling). T^* varies from 0 to 1 as T_w varies from T_{ONB} to T_{CHF} and it incorporates the heater temperature range where two-phase effects is significant. In order to determine this temperature for the current study, T_{ONB} was varied from T_{sat} to T_{CHF} and using a RMSE minimization routine it was found out a value of T_{ONB}=59°C resulted in minimum error between the data and predictions. The heat flux in the two-phase regime between T_{ONB} and T_{CHF} can now be determined by combining the single-phase heat transfer contribution and the CHF value with the weighting function T^*.

$$q''_{2-\phi} = (1 - T^*) q''_{1-\phi} + T^* q''_{CHF} \tag{50}$$

where $q''_{1-\phi} = h_{1-\phi}\left(T_w - T_{ONB}\right)$ and $h_{1-\phi}$ is determined from $h_{1-\phi} = 0.042\rho^{0.5}c_p Pr^{-0.33}P^{0.5}$. When T_w=T_{ONB}, T^* is zero and $q''_{2-\phi} = q''_{1-\phi}$. If T_w=T_{CHF}, T^* is unity and $q''_{2-\phi} = q''_{CHF}$. The following summarizes the three models for the single-phase, two-phase, and CHF into one correlation that can be used for any wall temperature (heat transfer regime) for PF-5060 sprays.

$$q'' = \left[1 - \max\left(0, T^*\right)\right]\left(0.042\rho^{0.5}c_p Pr^{-0.33}P^{0.5}\right)\left(T_w - T_f\right) + \max\left(0, T^*\right)\left[9.15\times10^4 P^{0.40}\left(1+2.42Ja\right)^{0.52}\right] \quad \text{for } T_w \le T_{CHF} \tag{51}$$

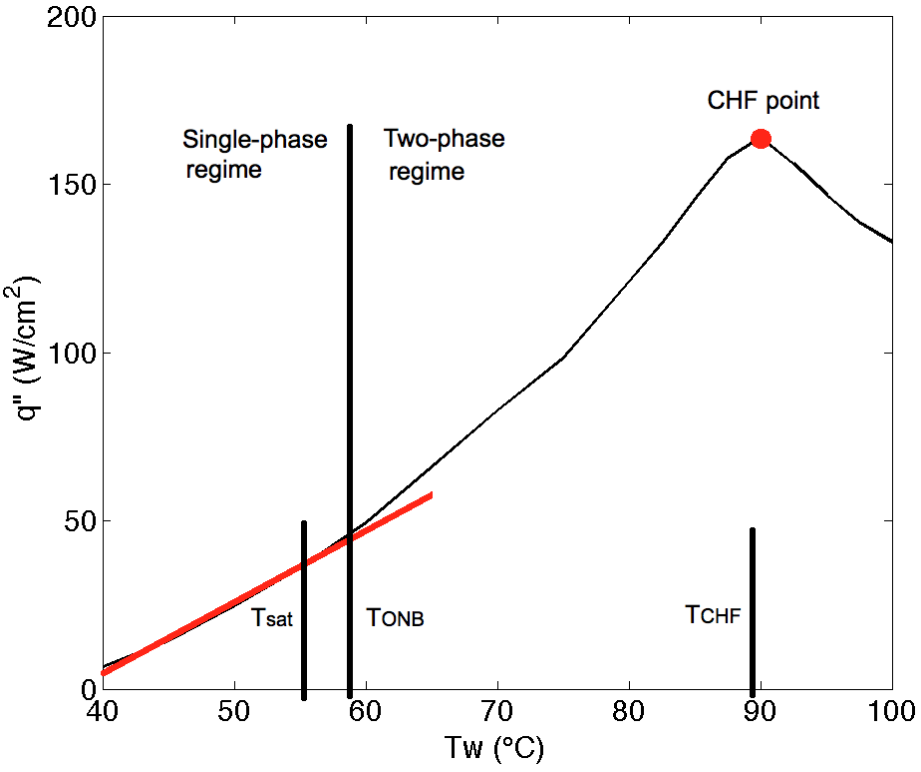

Figure 37. Sample spray cooling curve

6-5- Correlation Verification

Figure 38 and Figure 39 show the measured and predicted local spray cooling curves as well as single-phase and CHF contributions to the heat flux for the plots in Figure 32 and Figure 33. The CHF contribution was zero for heater temperatures below 59°C and then it started to increase and single-phase contribution dropped as wall temperature increased until the CHF point, where the single-phase contribution reduced to zero. For the hollow cone sprays at 25°C and 35°C liquid temperatures the local CHF temperature was 87.5°C but the model is based on CHF occurring at 89°C. Despite that difference, the model did quite well in capturing the spray cooling curves. CHF and spray cooling curve prediction for 45°C liquid were in very good agreement with the data (Figure 38). Full cone spray cooling curves are shown in Figure 39. At incoming liquid temperature of 25°C CHF occurs at 92.5°C and the model missed that point and slightly under-predicts the data, however, the prediction was excellent in the single-phase regime and quite good in the two-phase regime. The predictions for cases with liquid temperatures of 35°C and 45°C were also in good agreement with the data.

The predicted versus measured radially averaged heat flux at the impingement zone for all the test cases are presented in Figure 40 The top portion of the figure differentiates the data by the spray system configurations (spray pressure and standoff distance), spray pattern, and subcooling while the bottom portion shows the radial location and heat transfer regime. Combining the information from the two plots allows for exact identification of each data point and better evaluation of the predictions. Full cone 25°C spray at 689 kPa at the impingement zone and CHF point had the highest heat flux, followed by 35°C and 45°C. Single-phase heat transfer was considerably lower than the

two-phase and CHF and therefore the data points from that regime occupied the bottom of the plot. With a few exceptions, all the data points fall within ±25% of the measured values. For higher heat flux values this margin of error was significantly lower.

Figure 41 compares the area-averaged CHF for measured and predicted data over the impingement zone of the sprays. The predictions were made using the model presented in this work and that of Visaria and Mudawar (2008) from Equation 26. For smaller heat flux values the predictions from the two correlations had relatively similar accuracy, however, at higher heat fluxes the present correlations outperformed the mass flux-based correlation. The other relations discussed earlier were either inapplicable to the current data or there were insufficient input information to use them for the purpose of this comparison. Impingement frequency, droplet number concentration, system-specific constants, etc were required to use the other correlations which were not available for the present experiments. This fact further points out the unique advantage of the present work in being system independent. Several other comparisons are for radial spray cooling curves are presented in Appendix 2.

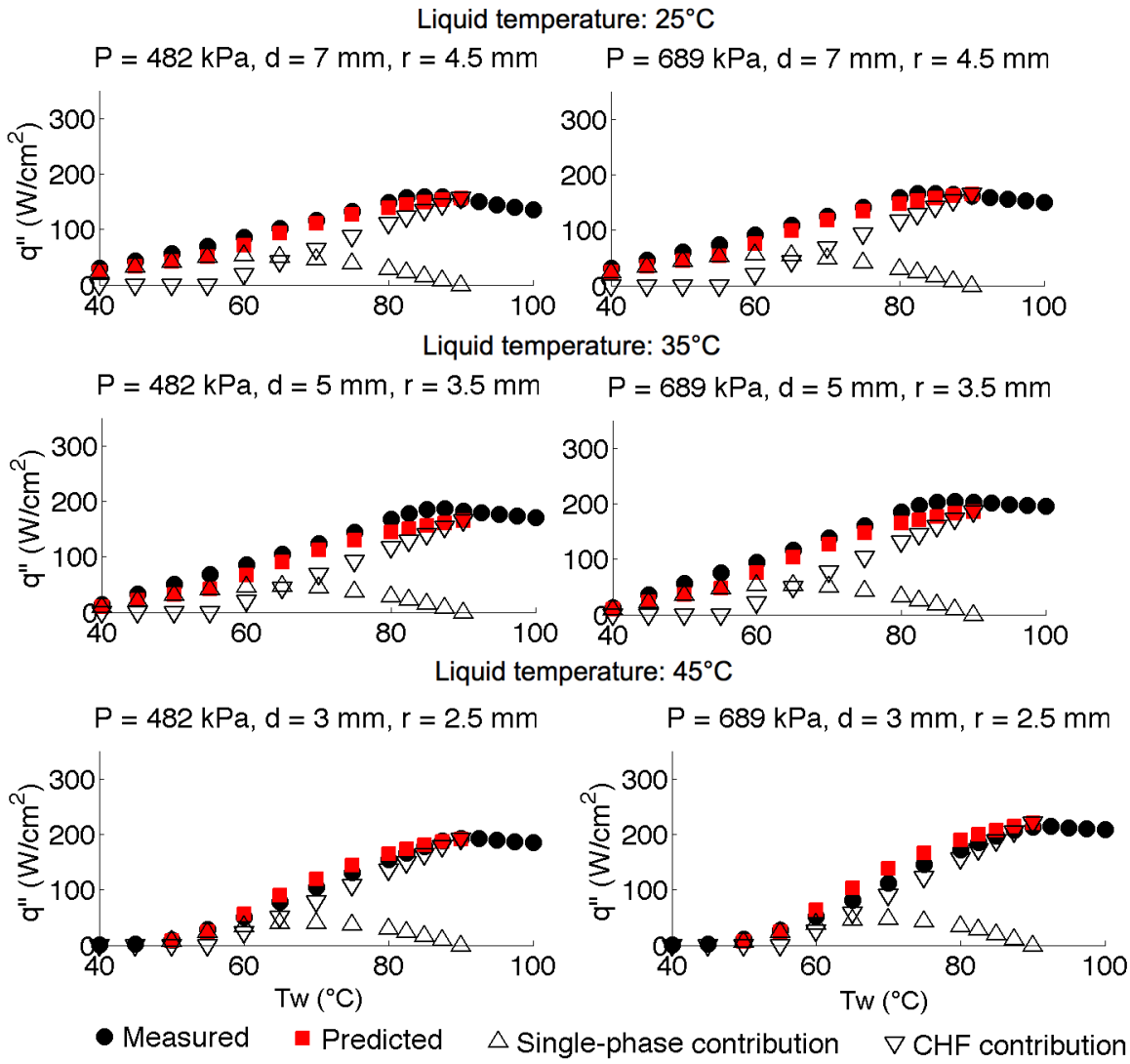

Figure 38. Measured and predicted hollow cone spray cooling curves at the impingement zone for different subcoolings, standoff distances, spray pressures, and radii

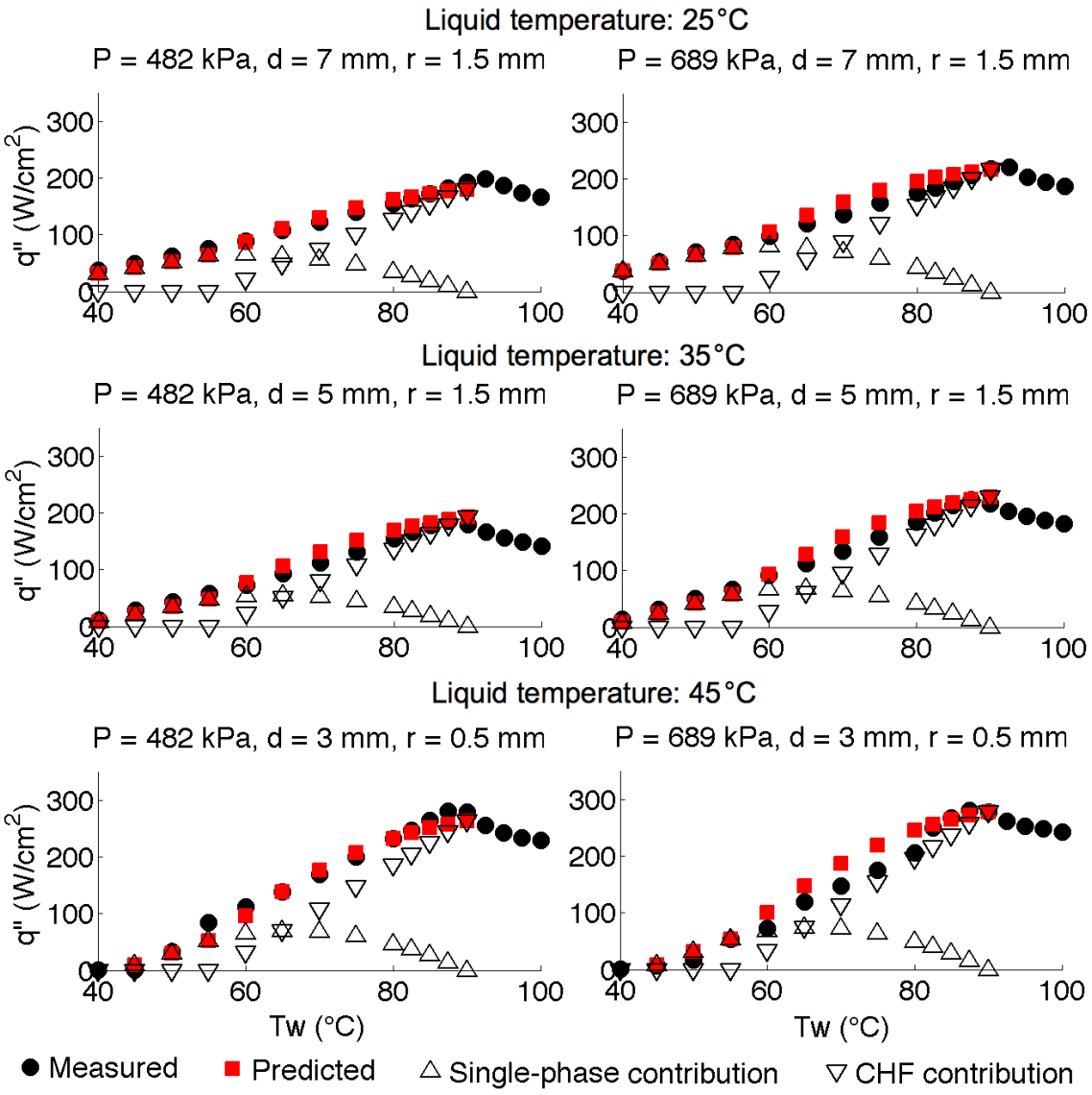

Figure 39. Measured and predicted full cone spray cooling curves at the impingement zone for different subcoolings, standoff distances, spray pressures, and radii

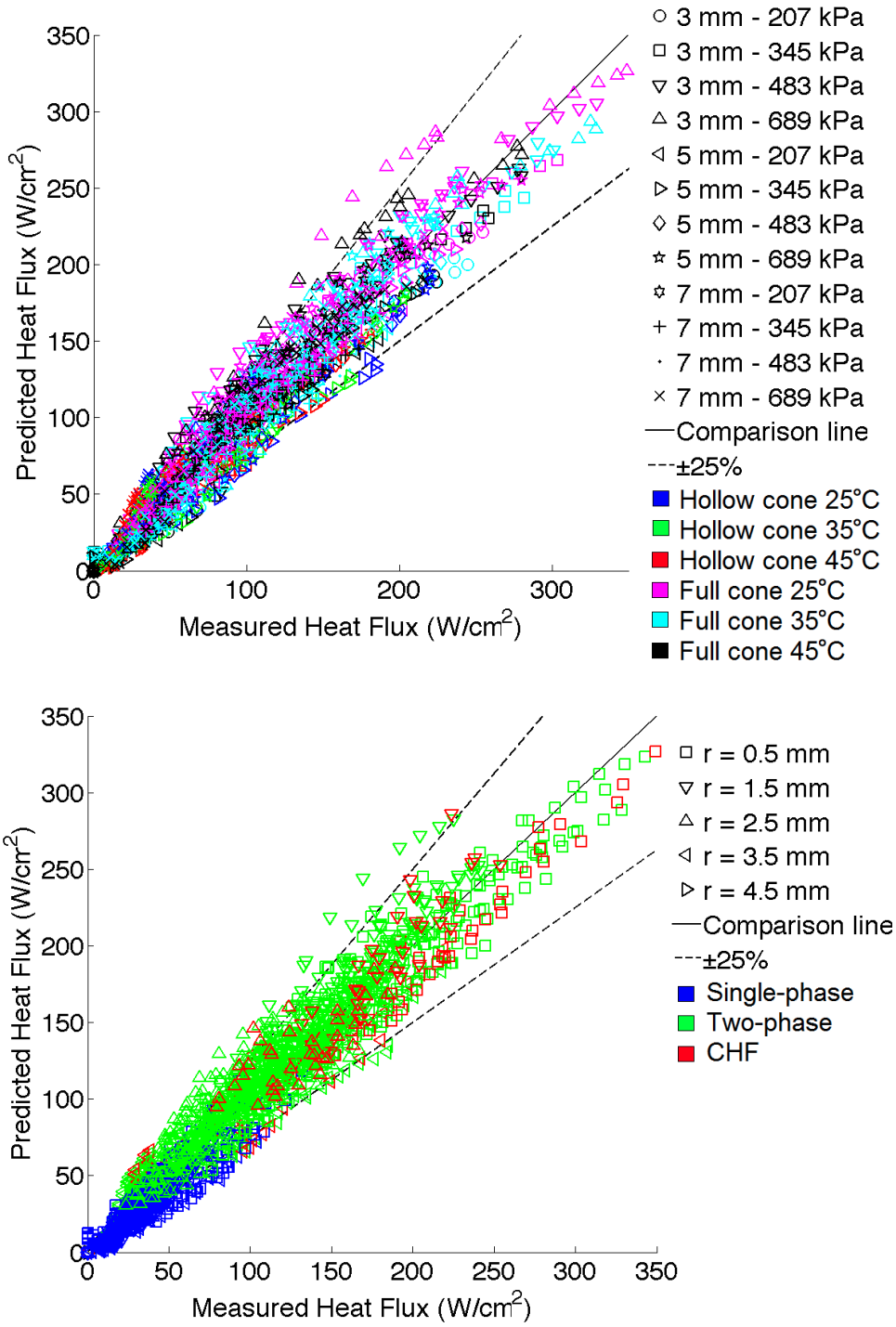

Figure 40. Measured versus predicted heat flux for all the data at the impingement zone for different sprays, subcoolings, and standoff distances (top) and different radii and heat transfer regimes (bottom)

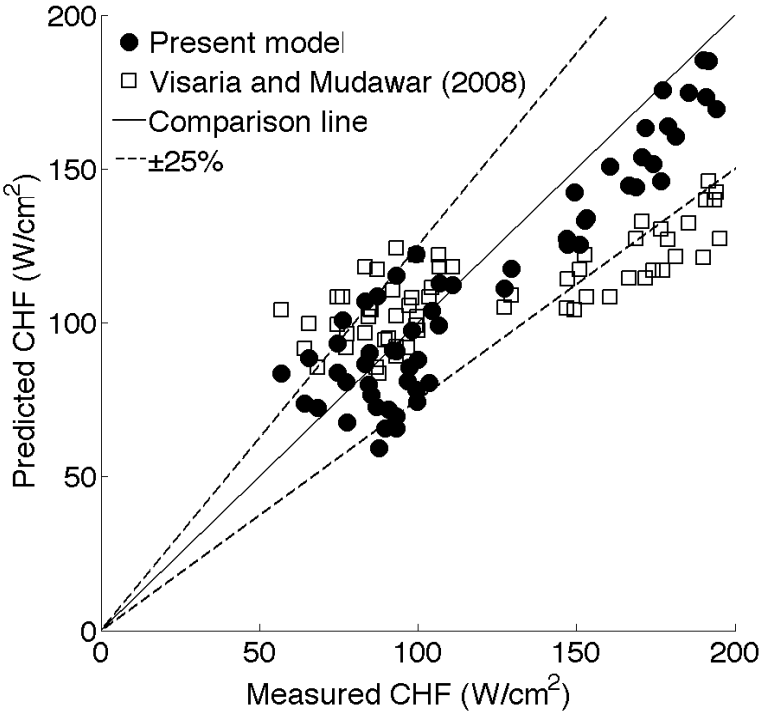

Figure 41. Comparison of area-averaged CHF predictions of the present model and that of Visaria and Mudawar (2008)

6-6- Error Analysis

The errors in heat flux predictions in spray cooling are usually presented in the form of a mean absolute error (MAE) and/or a root mean square error (RMSE) and often with insufficient details about where most of the error comes from. A more detailed discussion of the errors inspires more confidence in the accuracy of the correlations by pointing out the cases with larger errors and cases with higher accuracy.

Table 10 and Table 11 present MAE and RMSE for the single- and two-phase correlations. In Table 10, the single-phase correlation (for T_w between 40 and 55°C) errors for the two spray patterns and the combination of the both are presented. Hollow cone sprays had considerably larger errors than the full cone sprays (33.2% absolute error

in compared to 9.1% for the full cone). The combination of the both had an absolute error of 21.9%. The errors were mainly because the single-phase correlation was not developed exclusively for PF-5060, rather, it was developed for a range of liquids as explained in the previous chapter. The exclusiveness of the CHF correlation to PF-5060 could be responsible for lower errors in the CHF correlation. In several of the cases involving hollow cone sprays, CHF occurred at about 87.5°C which was lower than 89°C (average T_{CHF}) and on the other hand, there were a number cases with T_{CHF} at about 92.5°C in the full cone sprays. These two differences influenced the accuracy of the CHF correlation. But 21.7% absolute error for the hollow cone data, 11.8% for the full cone, and 16.7% for the combination of the both are considered quite reasonable for the boiling regime predictions.

Table 11 summarizes the errors for the complete local spray cooling curves as predicted from Equation 47. Perhaps the error values most reflective of the accuracy of this work are 20.0% MAE and 17.8 W/cm^2 RMSE for the both sprays for the entire spray cooling curves at different radii. The errors were also calculated for heat fluxes above 50, 100, and 150 W/cm^2. The continues decease in MAE indicated significantly better predictions for high heat flux cases, to the point that for heat flux value greater than 150 W/cm^2, MAE is only 6.7% which is considered to be a very impressive accuracy in boiling studies. The full cone sprays contribution to the error in this range of heat flux is only 4.7% and the hollow cone contribution is 17.3%. This indicates that there were many more full cone data point in this region than there were hollow cone data points. The reason, as explained earlier, was that the hollow cone nozzle produced considerable larger impingement pressures over a narrow band that often resulted in CHF values

beyond the capacity of the heater. Therefore, the data from those radial locations were discarded. That limitation in addition to smaller impingement area led to fewer points from the hollow cone sprays at higher heat fluxes. Since the ultimate goal is to design and build high heat flux spray cooling systems, such low errors prove very encouraging for efficient designs.

Table 10. Single-phase and CHF correlation prediction errors; MAE in % and RMSE in W/cm^2

Heat transfer regime	**Spray pattern**	**Error type**	**Error value**
Single-phase	Total	MAE	21.9
		RMSE	11.3
	Hollow cone	MAE	33.2
		RMSE	13.7
	Full cone	MAE	13.5
		RMSE	9.1
Two-phase	Total	MAE	19.5
		RMSE	19.4
	Hollow cone	MAE	22.0
		RMSE	21.7
	Full cone	MAE	17.4
		RMSE	16.8
Critical heats flux	Total	MAE	16.7
		RMSE	23.3
	Hollow cone	MAE	21.7
		RMSE	24.6
	Full cone	MAE	11.8
		RMSE	22.0

Table 11. Error analysis for the heat flux predictions; MAE in % and RMSE in W/cm^2

Spray pattern	**Error**	**Overall**	**Heat flux above 50 W/cm^2**	**Heat flux above 100 W/cm^2**	**Heat flux above 150 W/cm^2**
Hollow and full cone	MAE	20.0	14.9	9.1	6.7
	RSME	17.8	19.3	19.9	19.0
Hollow cone	MAE	25.0	17.8	16.6	17.3
	RSME	20.4	23.1	29.7	32.5
Full cone	MAE	15.8	13.3	6.3	4.7
	RSME	15.3	16.7	14.5	15.3

The percentage of the total data points within various error intervals are shown in Figure 42. It is observed that nearly 25% of all data points are within ±5% of the measured values, about 50% within ±10%, and almost 85% within ±25% of the experimental values. This plot includes all the data from the single-phase and two-phase heat transfer regimes for both nozzles and all radial locations in the impingement zone.

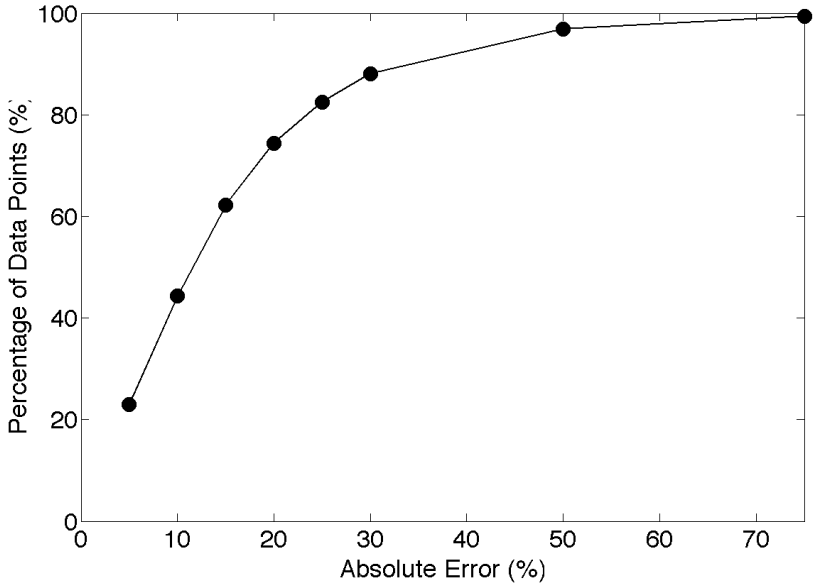

Figure 42. Percentage of data points within different error ranges

6-7- Chapter Summary

Two-phase heat transfer in spray cooling of PF-5060 was studied in detail. Boiling data were collected for many different conditions. It was observed that for a given pair of liquid/surface, local CHF occured at almost the same temperature. The CHF temperature was found to be 89°C for PF-5060 on smooth flat surfaces. A correlation was developed for the maximum heat flux based on fluid properties, local impingement pressure, and Jakob number. It was assumed that two-phase heat transfer is a combination of single-phase heat transfer and nucleation effects, peaking at the CHF point. Therefore, a dimensionless temperature-weighted combination of the single-phase correlation and the CHF correlation were used to predict the local spray cooling curves. The correlation yielded predictions with impressive accuracy, especially for high heat flux values which are the likely focus of real world applications.

CHAPTER SEVEN: CONCLUSIONS AND CONTRIBUTIONS

This chapter is provided to review the present work and summarize the findings of this research. The contributions that were made to the state of the art and advancements made possible by this work are discussed. Also, recommendations for future direction of spray cooling research are made.

7-1- Conclusions

Experiments were performed to study the spray cooling heat transfer mechanisms and develop correlations to predict the heat flux values. It was hypothesized that spray cooling heat transfer is primarily driven by local impingement pressure of the individual droplets on the heater surface. This assumption is supported by several droplet impingement studies and greatly accommodates the development of simple tools to predict spray cooling local heat transfer.

All of the available studies in this area assume that the local heat transfer depends on a combination hydrodynamic properties such as, local mass flux, droplet velocity, droplet size, and number density. However, the penetration depth of the incoming droplet in the liquid film on the heater is more dependent on the momentum flux of the droplets. This momentum flux translates into local impingement pressure and captures all the hydrodynamic effects of the spray. The clear trend of heat transfer increase with the increase of local impingement pressure indicated the validity of the hypothesis both in the single-phase and two-phase regimes. Therefore, it was established through this work that local heat transfer is primarily driven by local impingement pressure.

A test matrix was defined for the single-phase heat transfer regime study. Various spray patterns, standoff distances, orientations, spray pressures, and liquids were tested. The data were combined in a proper format and a correlation was proposed for the single-phase heat transfer coefficient. The correlation was based on fluid properties and local impingement pressure as input and predicted the radial distribution of heat flux. The predictions were in great agreement with the experiments. The correlation is valid for liquids with *Pr* between 12-76 and impingement pressure below 20 kPa with accuracy of ±25%.

Two-phase heat transfer regime and the critical heat flux were studied for PF-5060 sprays. It was seen that, similar to the single-phase regime, local impingement pressure drives the heat transfer in the two-phase regime. This observation was used to develop a pressure-based correlation for heat flux at the CHF point. The effects of subcooling were accounted for by inserting *Ja* into the correlation. The other finding with respect to the CHF point was its occurrence at the same temperature irrespective of spray configurations. This discovery allowed for the development of a non-dimensional temperature as weighting function that was used to combine the single-phase and CHF correlations in order to predict local spray cooling curves for PF-5060 with MAE of 20%. For the wall temperatures below T_{ONB} the single-phase correlation and at T_{CHF} the CHF correlation determined the heat flux. For temperatures between T_{ONB} and T_{CHF} a combination of the two was used so that as T_w approached T_{CHF} the single-phase contributions diminished and CHF contribution became more predominant.

Forced convection resulted from very high velocity incoming droplets assisted by increased agitation, and better mixing is considered to be the reason for high heat fluxes

in the single-phase regime. The underlying heat transfer mechanisms in the boiling regime is an area of ongoing debate. Several mechanisms regarding heat transfer have been postulated including, micro-layer evaporation, contact line evaporation, transient conduction, etc. Although this work was not defined to determine the dominant mechanism, the discoveries made here can shed light into the matter. At high wall temperatures a combination of incoming droplets and evaporation results in the formation of liquid rivulets that continuously form, evaporate, and move around on the heater. This process is believed to be responsible for the tremendous heat removal capacity for spray cooling systems. However, determination of the exact mechanisms remains beyond the scope of this work.

7-2- Intellectual Contributions

Spray cooling offers one of the highest heat removal capacities among the modern cooling technologies. However, predicting the local heat flux continues to be difficult and challenging. The literature review presented in Chapter 2 summarized the advancements that have been made as well as areas that require further investigation. This work was designed to fill some of those gaps. The contributions made to the state of the art via this work can be listed as follows:

1. Local impingement pressure was proved to be the driving parameter in the single-phase and two-phase heat transfer regimes. Prior works argued that local mass flux and a combination of spray properties were the dominant driving factors. But an in-depth review of the literature and many experiments presented in this work indicated that all of the hydrodynamic effects of the spray can be reflected in form

of the local impingement pressure (and this quantity can be used to predict the local heat transfer).

2. A simple, accurate, fast, and inexpensive setup was introduced to measure the local impingement pressure. The pressure apparatus introduced in Chapter 3 was a developed for the purpose of this research and can be used to measure local impact pressure of the droplets for variety of purposes, most notably, local heat transfer.
3. The single-phase heat transfer correlation developed in this work was validated for wide range of fluid properties. This is in contrast with the earlier correlations in the literature that are valid for only a few liquids.
4. Local and area-averaged critical heat flux was shown to occur at around the same temperature for a given liquid/surface pair regardless of spray characteristics. This is a remarkable discovery that greatly facilitates the prediction of boiling heat transfer in spray cooling.
5. Local critical heat flux values for PF-5060 were measured and a pressure-based correlation was developed to predict those values. This correlation was the first to use the two major findings of heat transfer driving parameter and T_{CHF} to predict the critical heat flux.
6. A correlation was proposed to predict the entire local spray cooling curve using a combination of single-phase and CHF correlations. The idea to combine the two regimes using a non-dimensional temperature weighting function was a new idea in this area and was made possible due to the observation of a constant T_{CHF}.

7-3- Recommendations for Future Research Areas

As it is common in science, answering a question opens the field to a variety of other problems. While this work can set the stage for the future spray cooling studies, there are a number of areas that need further attention and investigation. Some of the research ideas require more moderate efforts while others will need extensive endeavor.

1. Extending the validity range of correlations proposed in this work can be an important area of future work. The input power needed for spray cooling reduced for liquids with lower viscosity and surface tension. So it is desirable to investigate applicability of the current correlations for lighter fluids (Pr<12). In some applications, such as internal combustion engines cooling, the liquids are highly viscous and it is necessary to extend the correlation to that extreme as well. The experimental methodology will be similar to the present work and all that needs to be changed are the liquids and the nozzles.
2. Although measuring the local impingement pressure is not a major issue, it is very desirable to develop relations to the impingement pressure using easy-to-measure parameters, such as, standoff distance, flow rate through the nozzle, nozzle orifice diameter, nozzle cone angle, etc. While this research idea might sound relatively trivial, it should noted that basing the correlations on droplet velocity, size, and number concentration has to be avoided because it further complicates problem. This limitation introduces major challenges to make the correlations independent of the mentioned parameters.
3. This work established that T_{CHF} is independent of spray characteristics and recorded the CHF temperature for PF-5060. However, it is necessary to develop a

database of T_{CHF} for various liquid/surface pairs. The future research can be targeted for the specific needs of the industry. Operating fluids such as FCs, HFEs, water and surfaces with different roughnesses, straight-finned surfaces can be good candidates to conduct the experiments. For the smooth flat surfaces T_{CHF} is anticipated to be independent of spray orientation, this is not necessarily true for extended surfaces. The possible effect of nozzle inclination on T_{CHF} for extended surfaces is another important question.

4. Discovering the underlying heat transfer mechanisms in two-phase spray cooling is tremendously important for the future studies. There are number of viable theories, however, no work has been presented to unify those ideas and bring consensus among the researchers. One suggested method for doing that is similar to that of Delgoshaei and Kim (2010) for pool boiling. A very high speed photography system (100,000+ fps) with a synchronized data acquisition system are needed to take local heat transfer data and simultaneously visualize the process. The peaks and drops in the heat flux along with the visual clues from the high speed camera can be very effective to make breakthroughs in identifying the basic heat transfer mechanisms.

APPENDIX 1: PRESSURE AND HEAT TRANSFER DATA

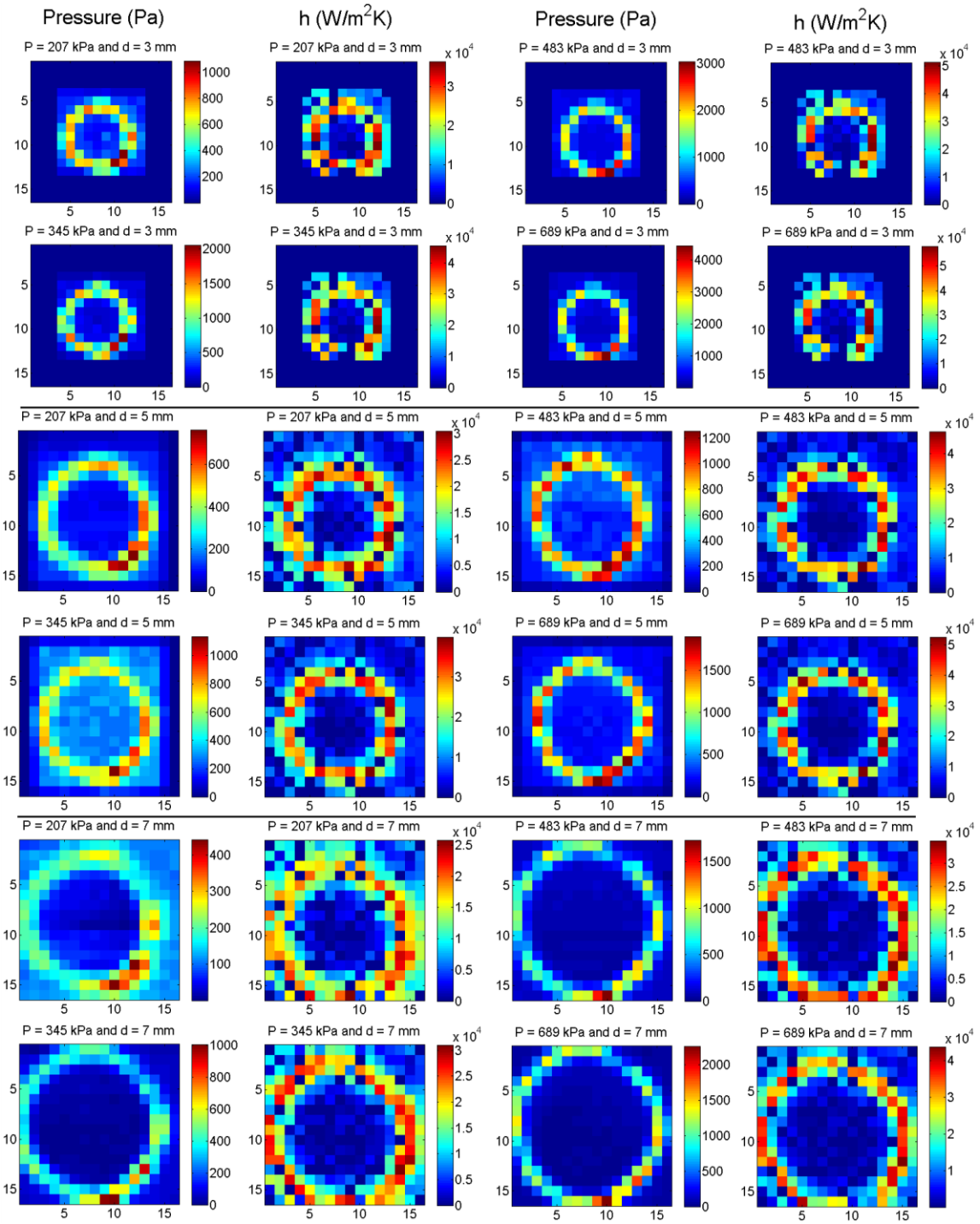

Figure 43. Pressure and heat transfer coefficient distribution for normal PF-5060 hollow cone spray

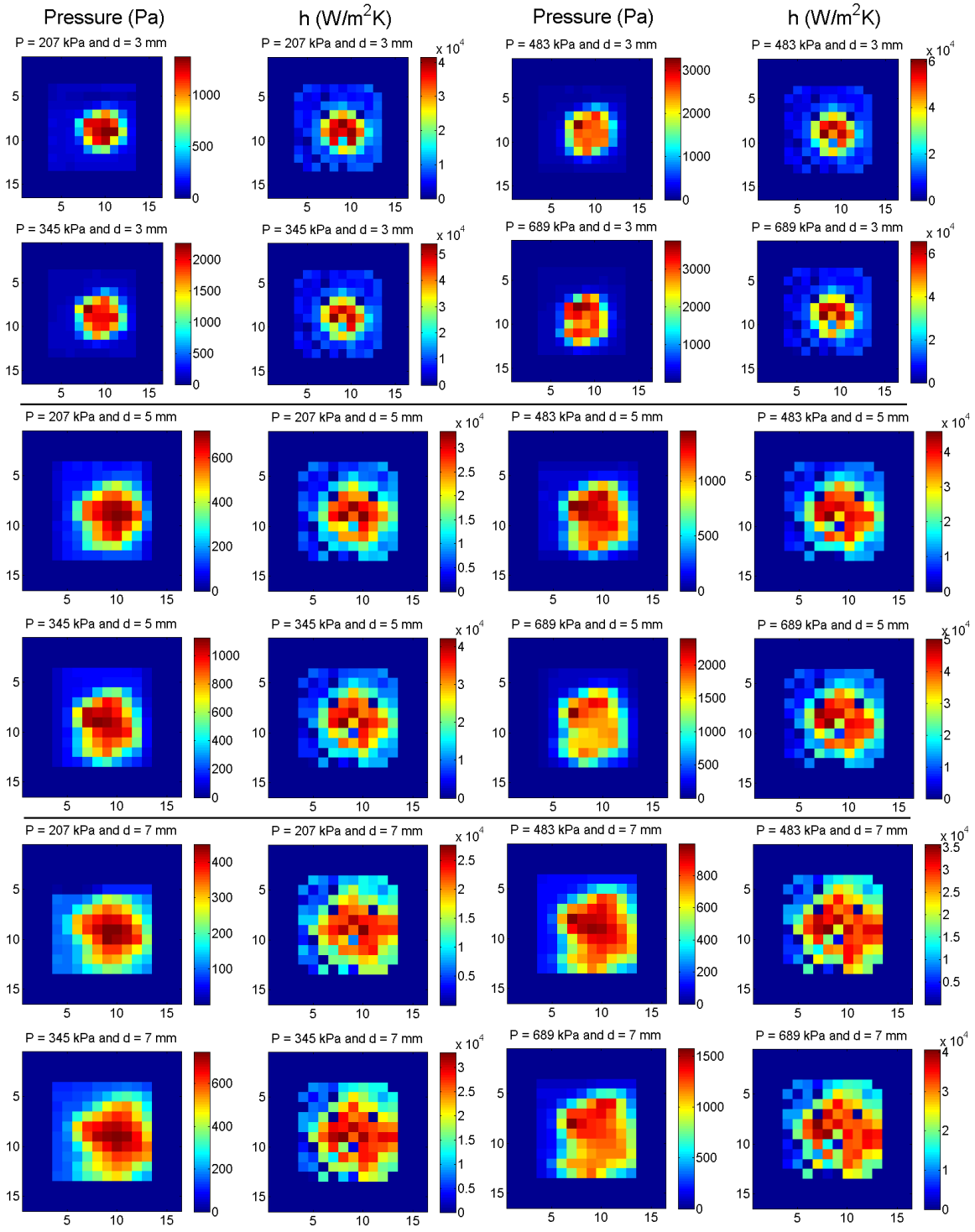

Figure 44. Pressure and heat transfer coefficient distribution for normal PF-5060 full cone spray

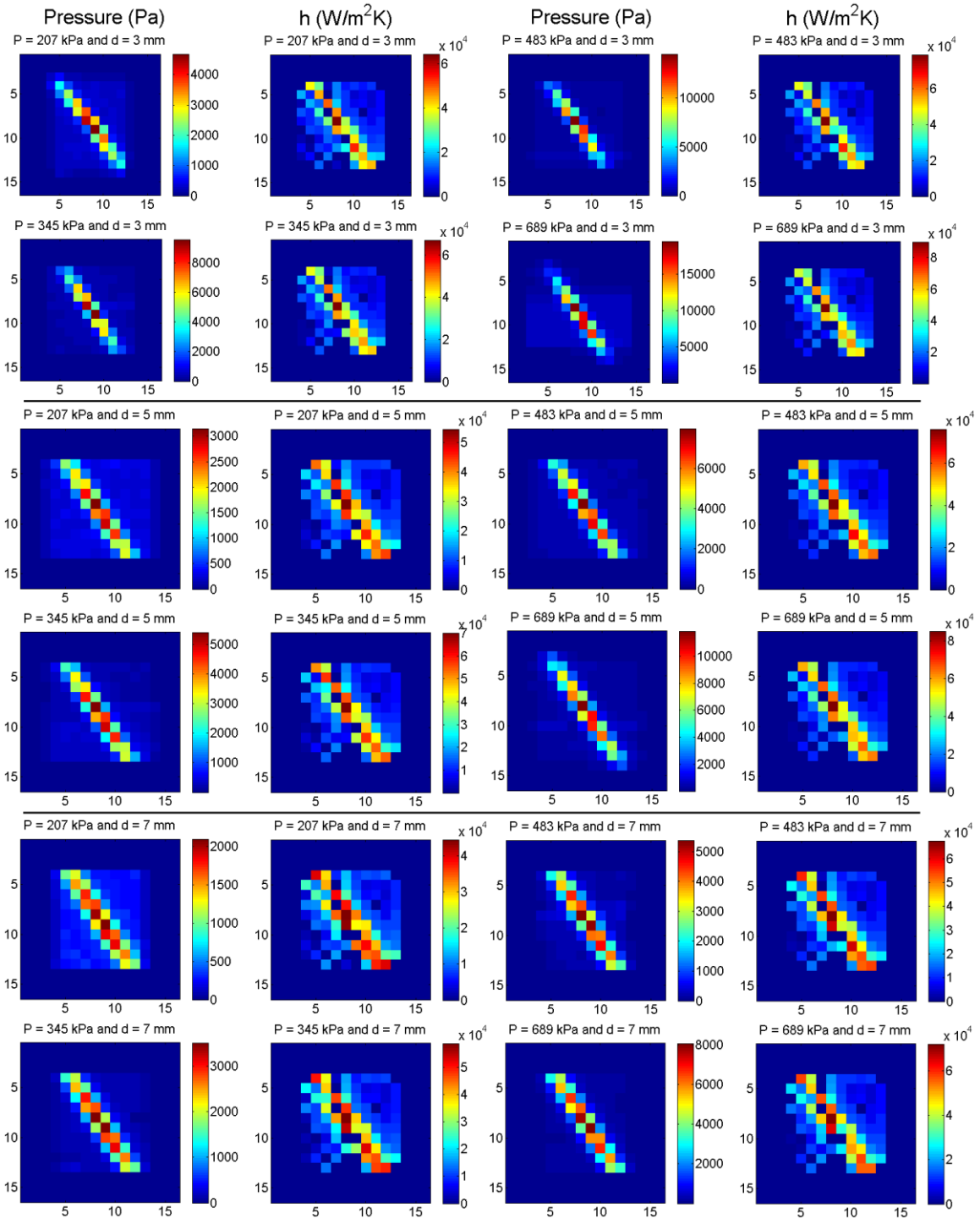

Figure 45. Pressure and heat transfer coefficient distribution for normal PF-5060 flat fan spray

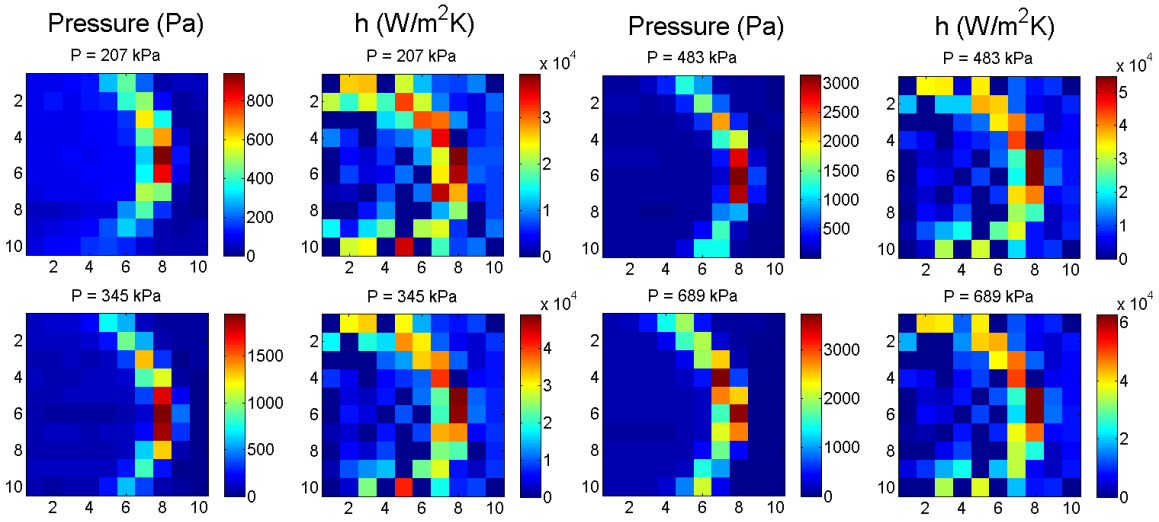

Figure 46. Pressure and heat transfer coefficient distribution for 45° inclined PF-5060 hollow cone spray

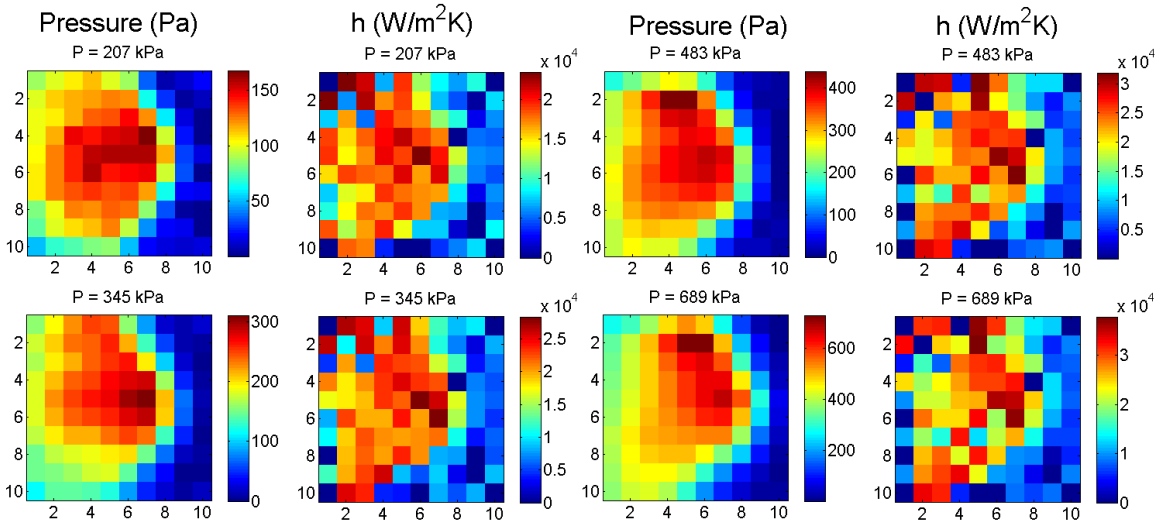

Figure 47. Pressure and heat transfer coefficient distribution for 45° inclined PF-5060 full cone spray

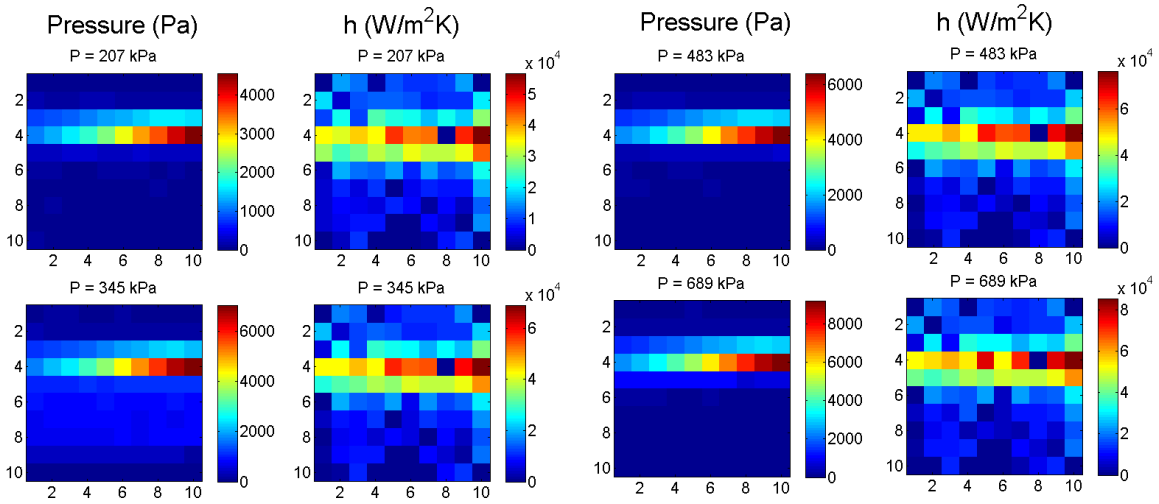

Figure 48. Pressure and heat transfer coefficient distribution for 45° inclined PF-5060 horizontal flat cone spray

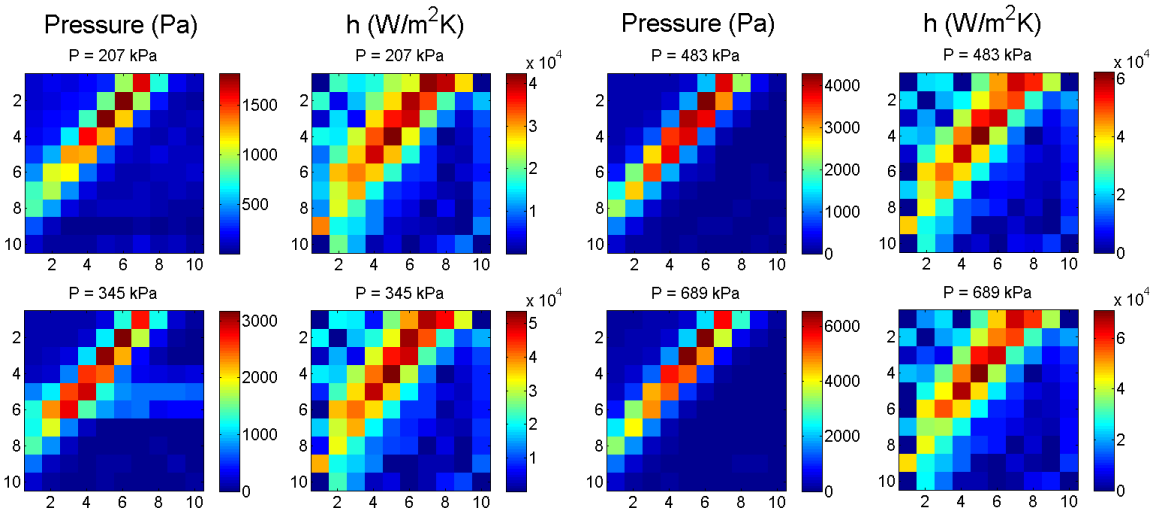

Figure 49. Pressure and heat transfer coefficient distribution for 45° inclined PF-5060 rotated flat cone spray

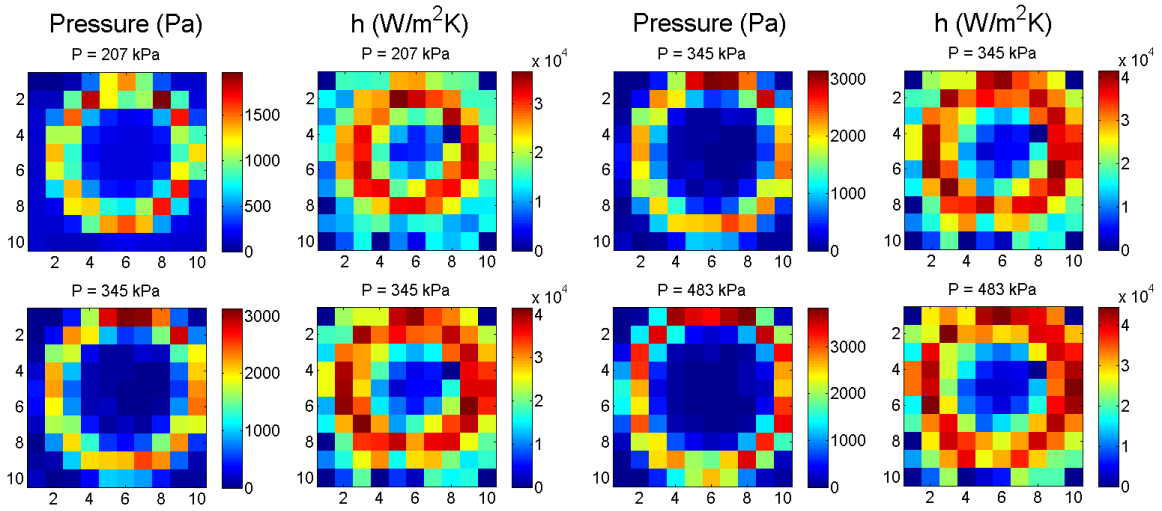

Figure 50. Pressure and heat transfer coefficient distribution for normal PAO-2 hollow cone spray at 5 mm standoff distance

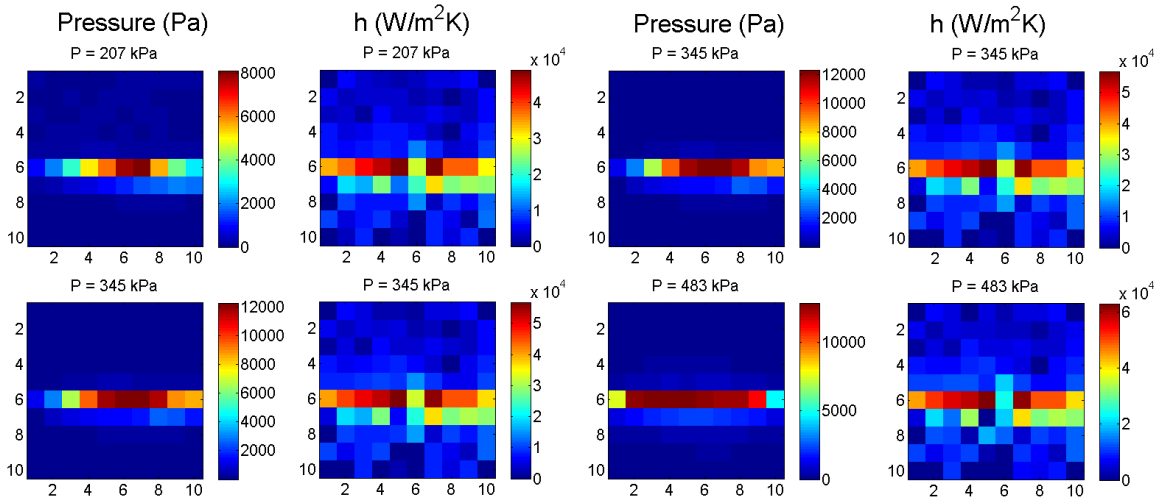

Figure 51. Pressure and heat transfer coefficient distribution for normal PAO-2 flat cone spray at 3 mm standoff distance

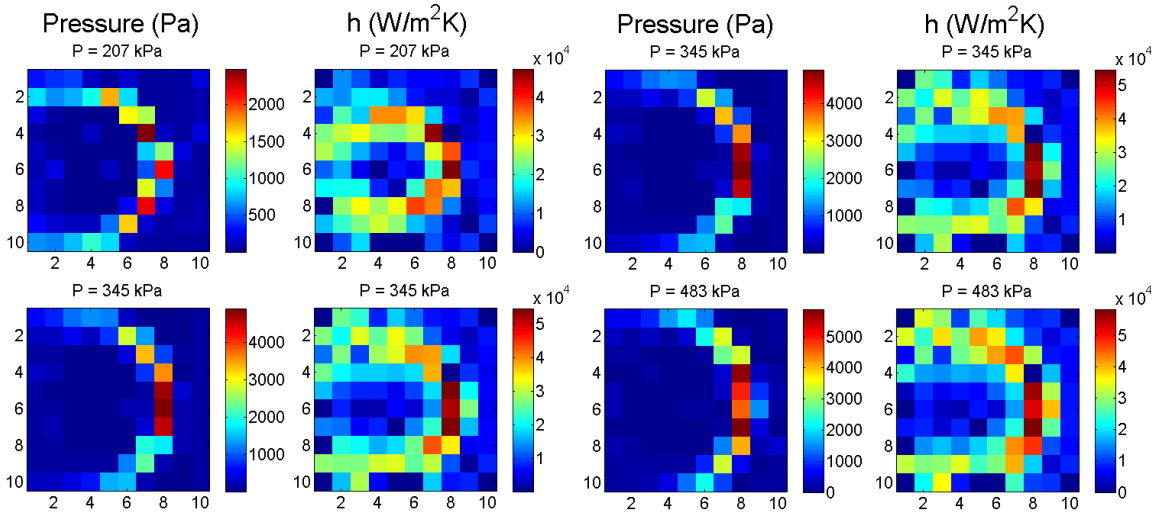

Figure 52. Pressure and heat transfer coefficient distribution for 45° inclined PAO-2 hollow cone spray

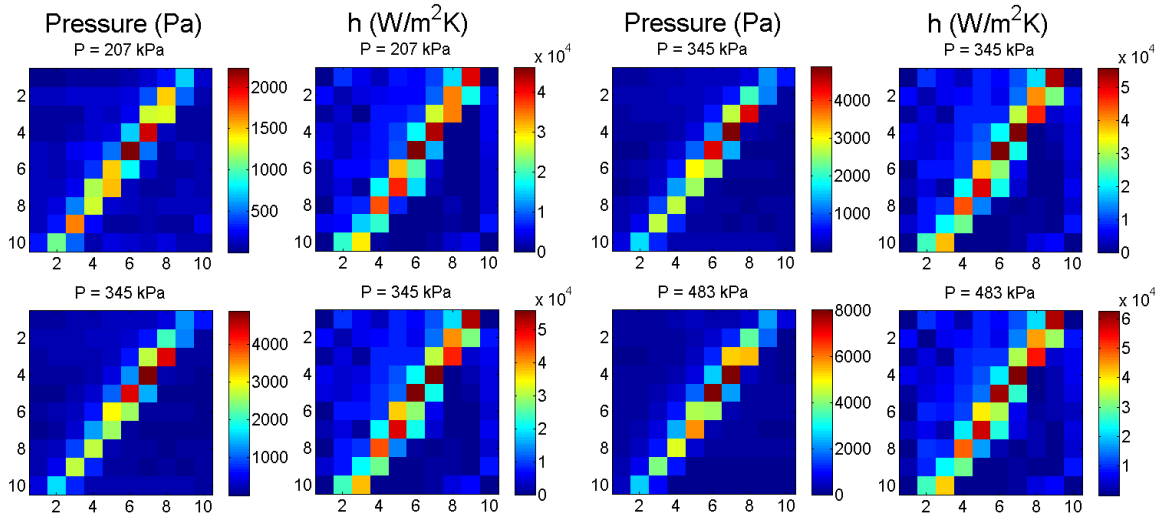

Figure 53. Pressure and heat transfer coefficient distribution for 45° inclined PAO-2 rotated flat spray

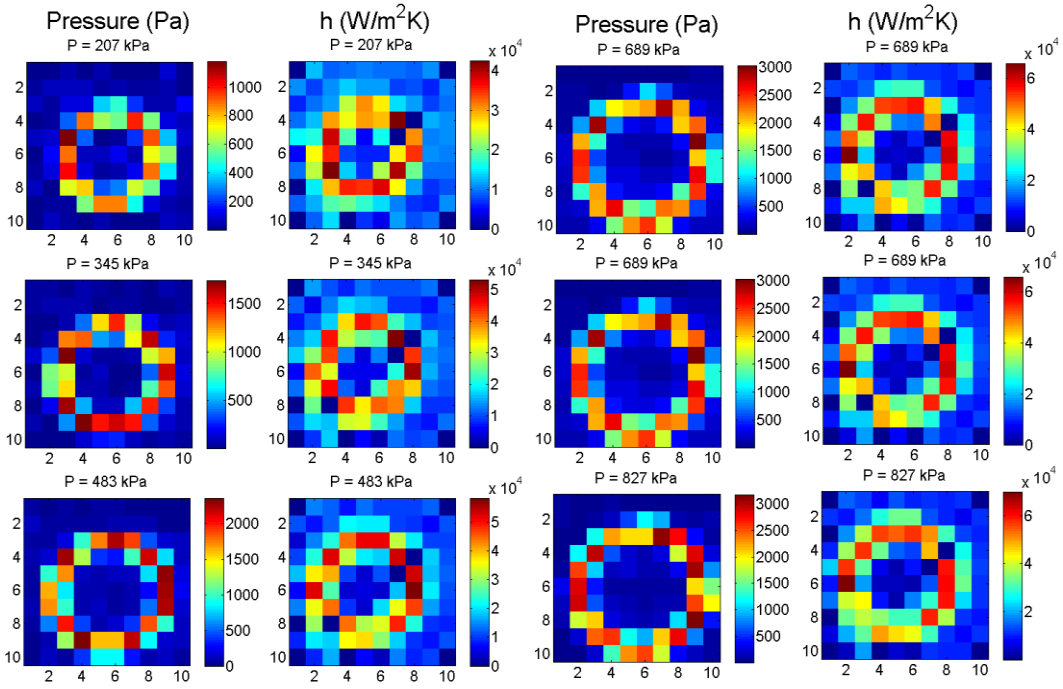

Figure 54. Pressure and heat transfer coefficient distribution for normal PSF-3 hollow cone spray at 3 mm standoff distance

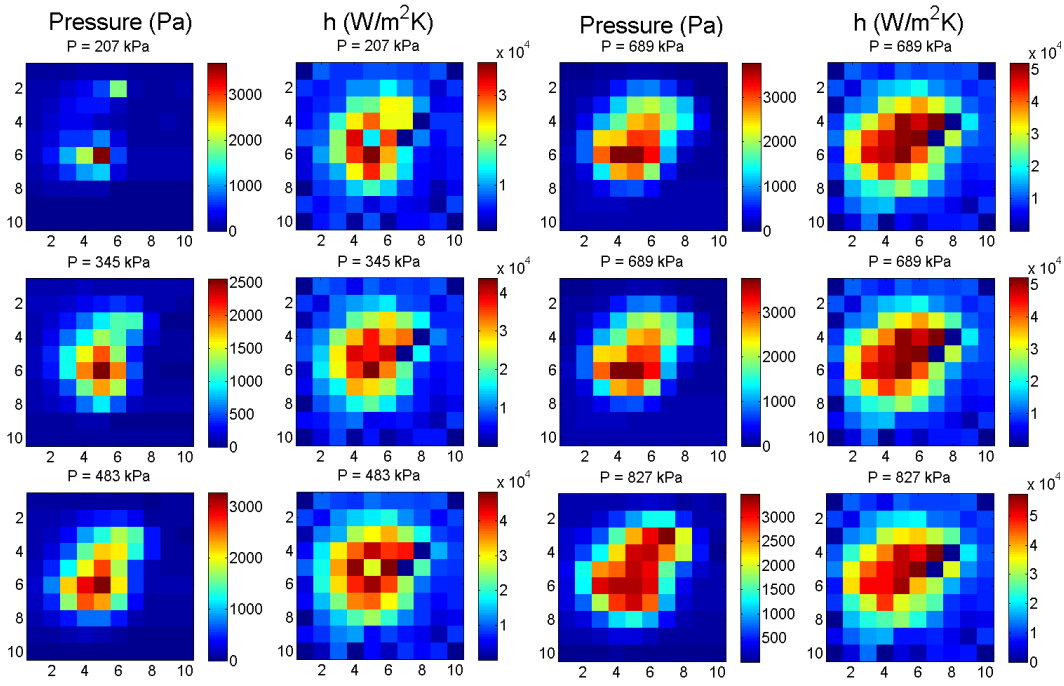

Figure 55. Pressure and heat transfer coefficient distribution for normal PSF-3 full cone spray at 5 mm standoff distance

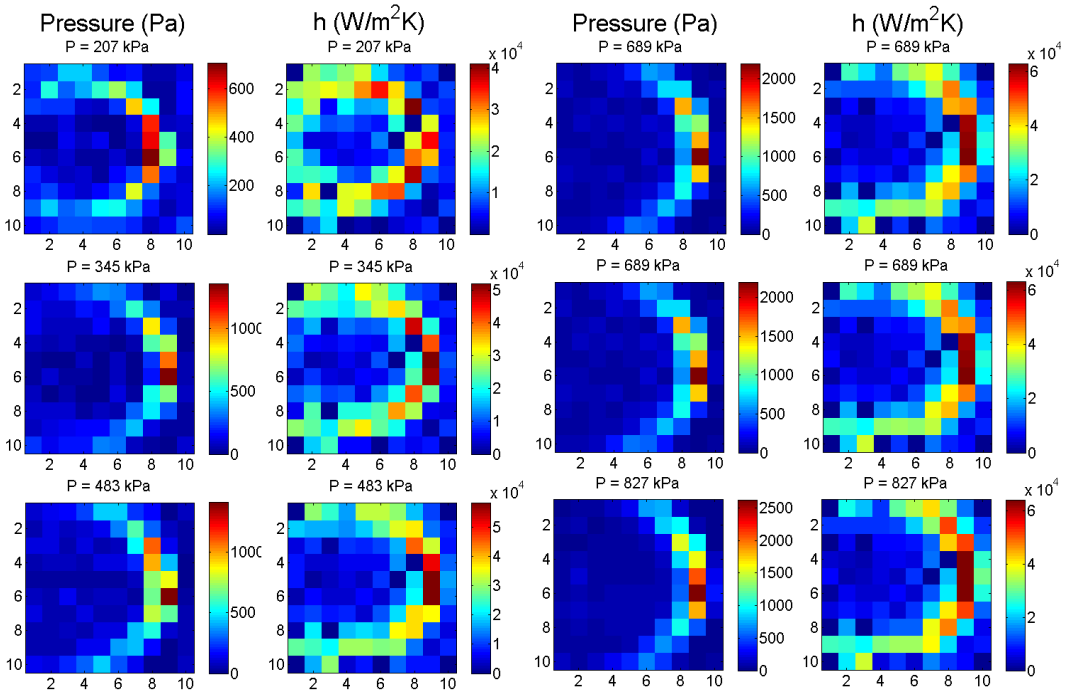

Figure 56. Pressure and heat transfer coefficient distribution for 45° inclined PSF-3 hollow cone spray

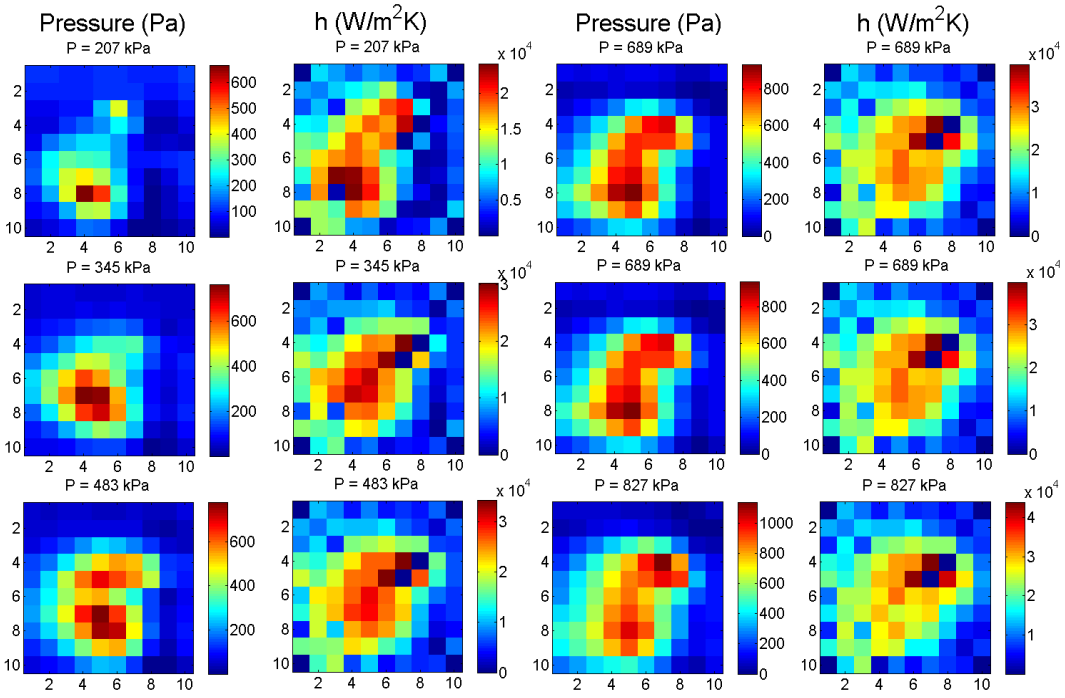

Figure 57. Pressure and heat transfer coefficient distribution for 45° inclined PSF-3 full cone spray

APPENDIX 2: SPRAY COOLING CURVES

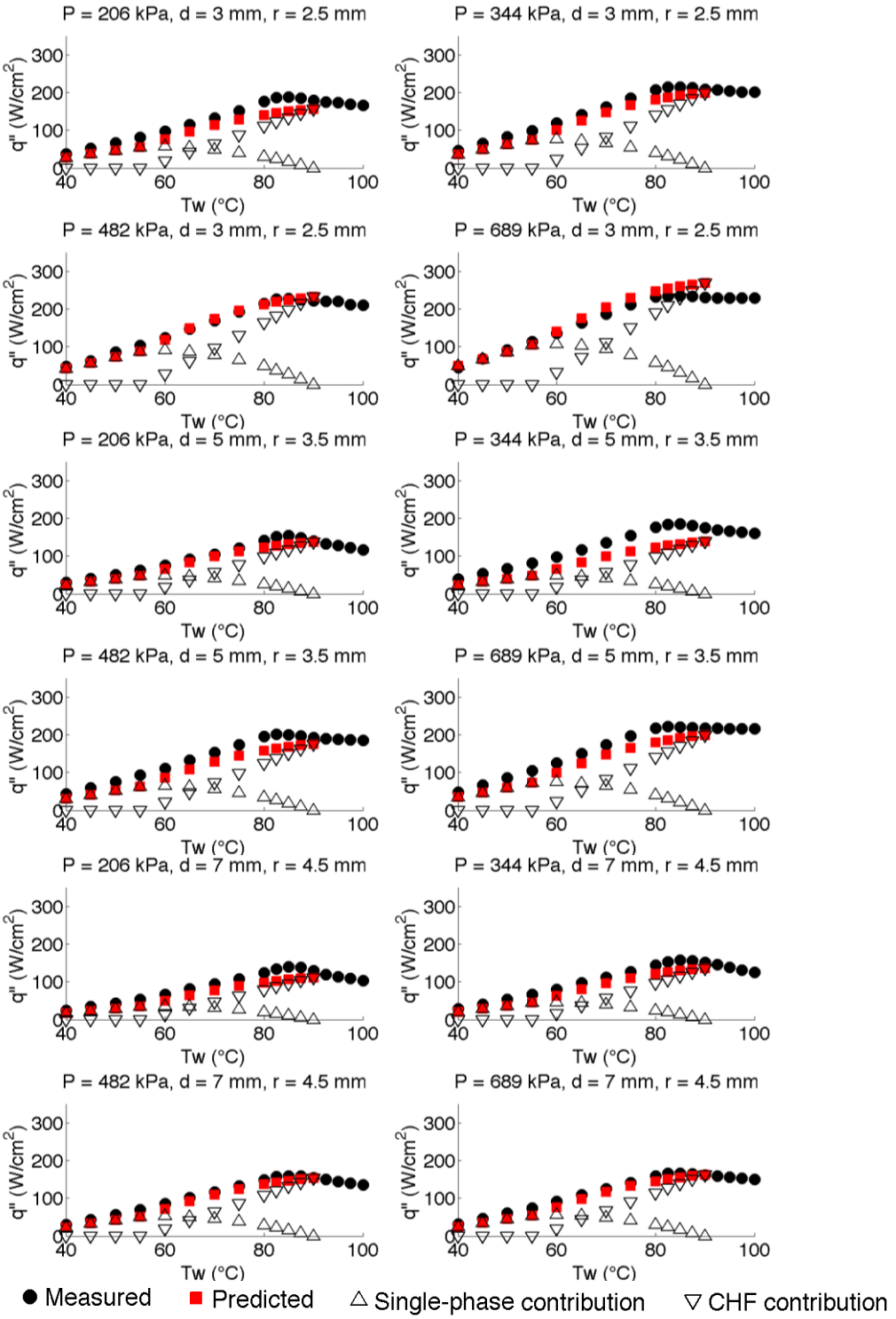

Figure 58. Measured and predicted local spray cooling curves over the impingement area of hollow cone sprays at 25°C

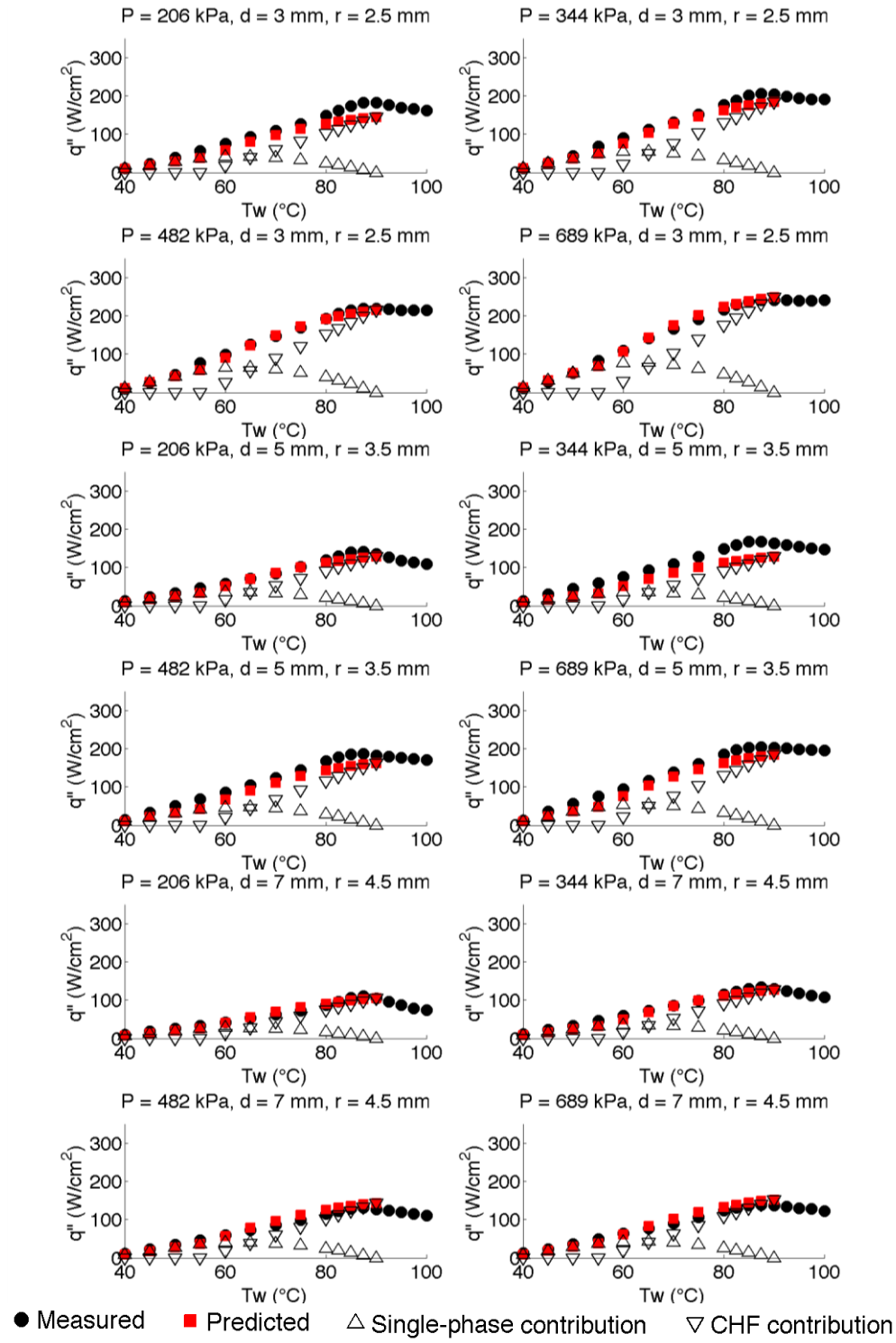

Figure 59. Measured and predicted local spray cooling curves over the impingement area of hollow cone sprays at 35°C

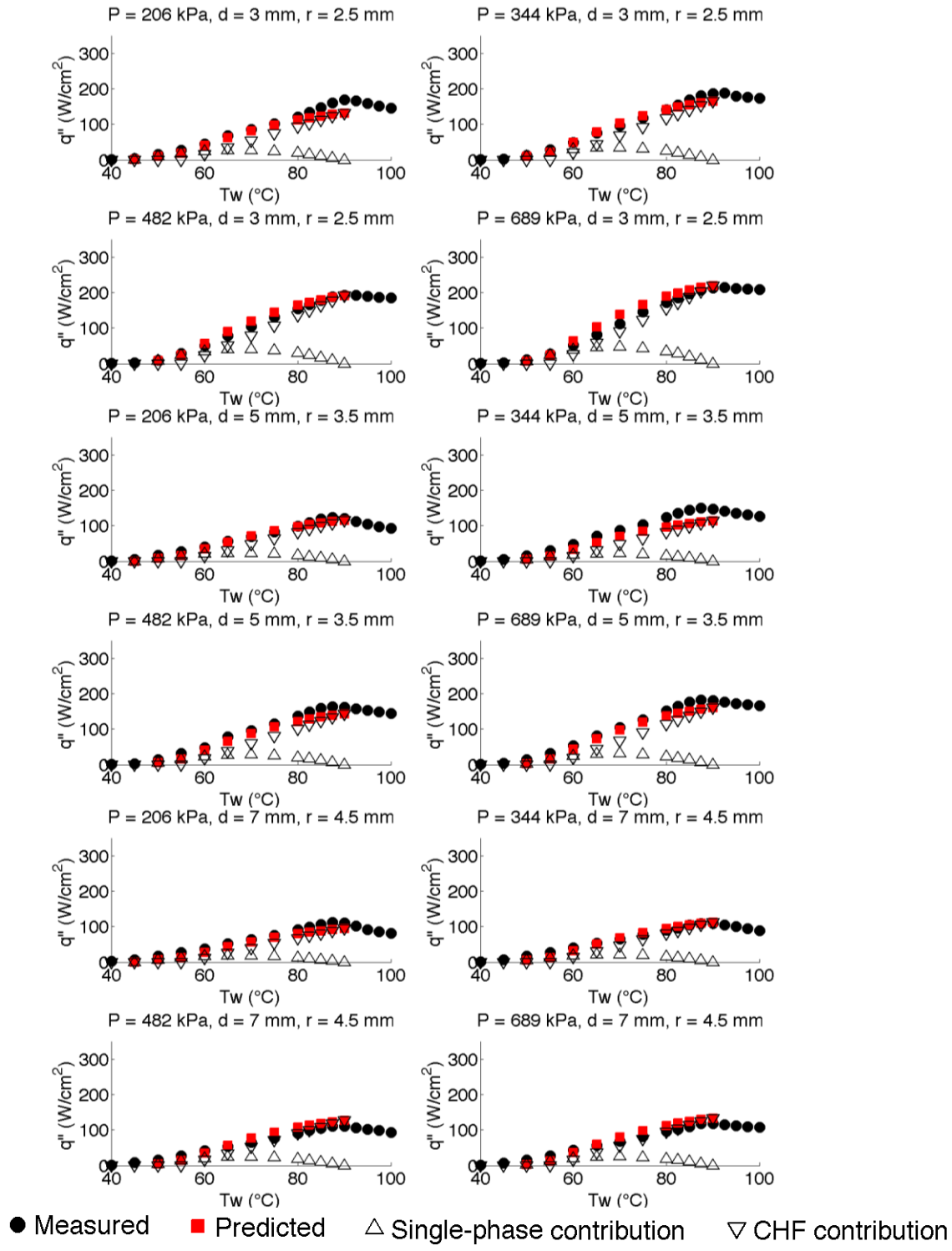

Figure 60. Measured and predicted local spray cooling curves over the impingement area of hollow cone sprays at 45°C

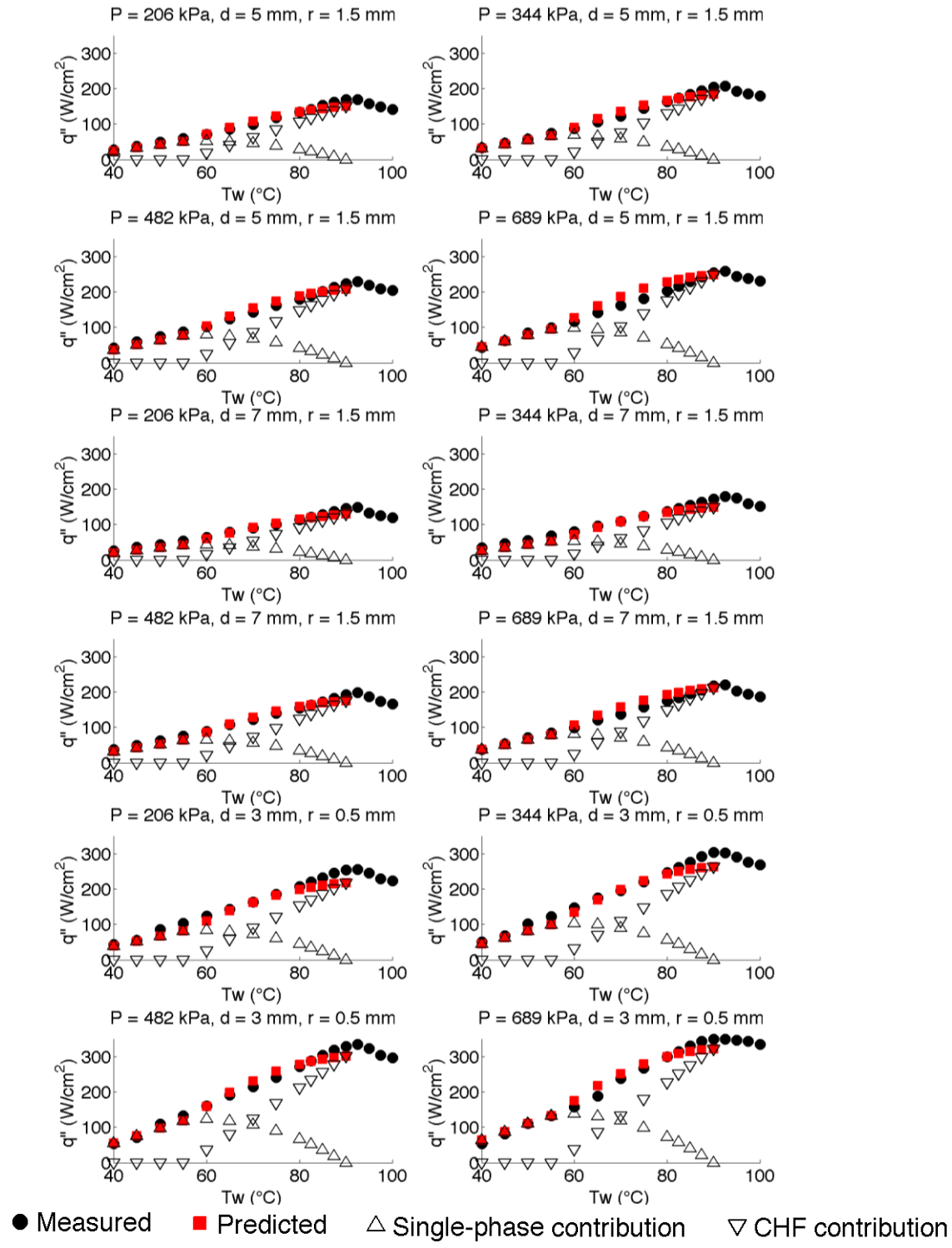

Figure 61. Measured and predicted local spray cooling curves over the impingement area of full cone sprays at 25°C

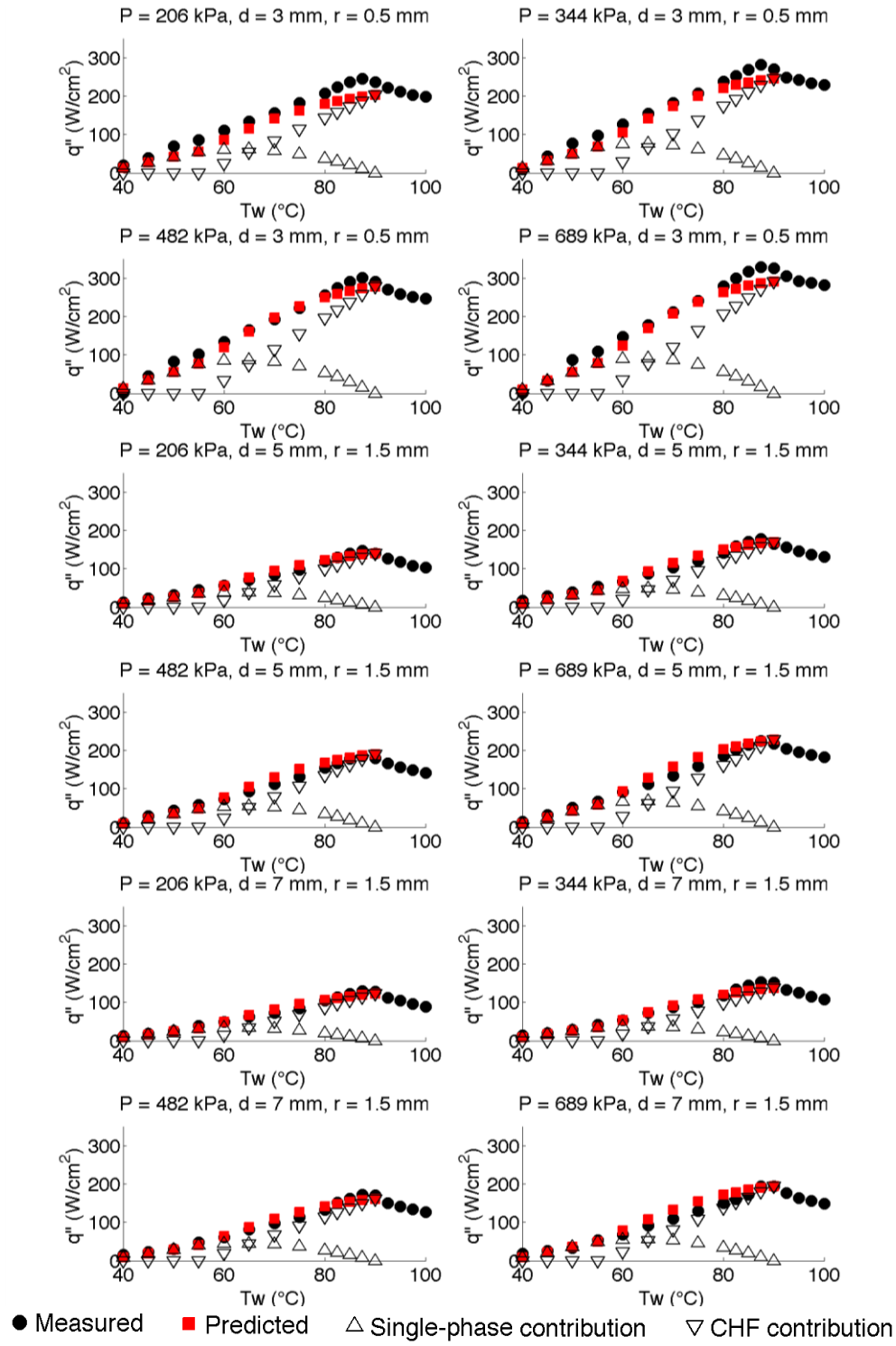

Figure 62. Measured and predicted local spray cooling curves over the impingement area of full cone sprays at 35°C

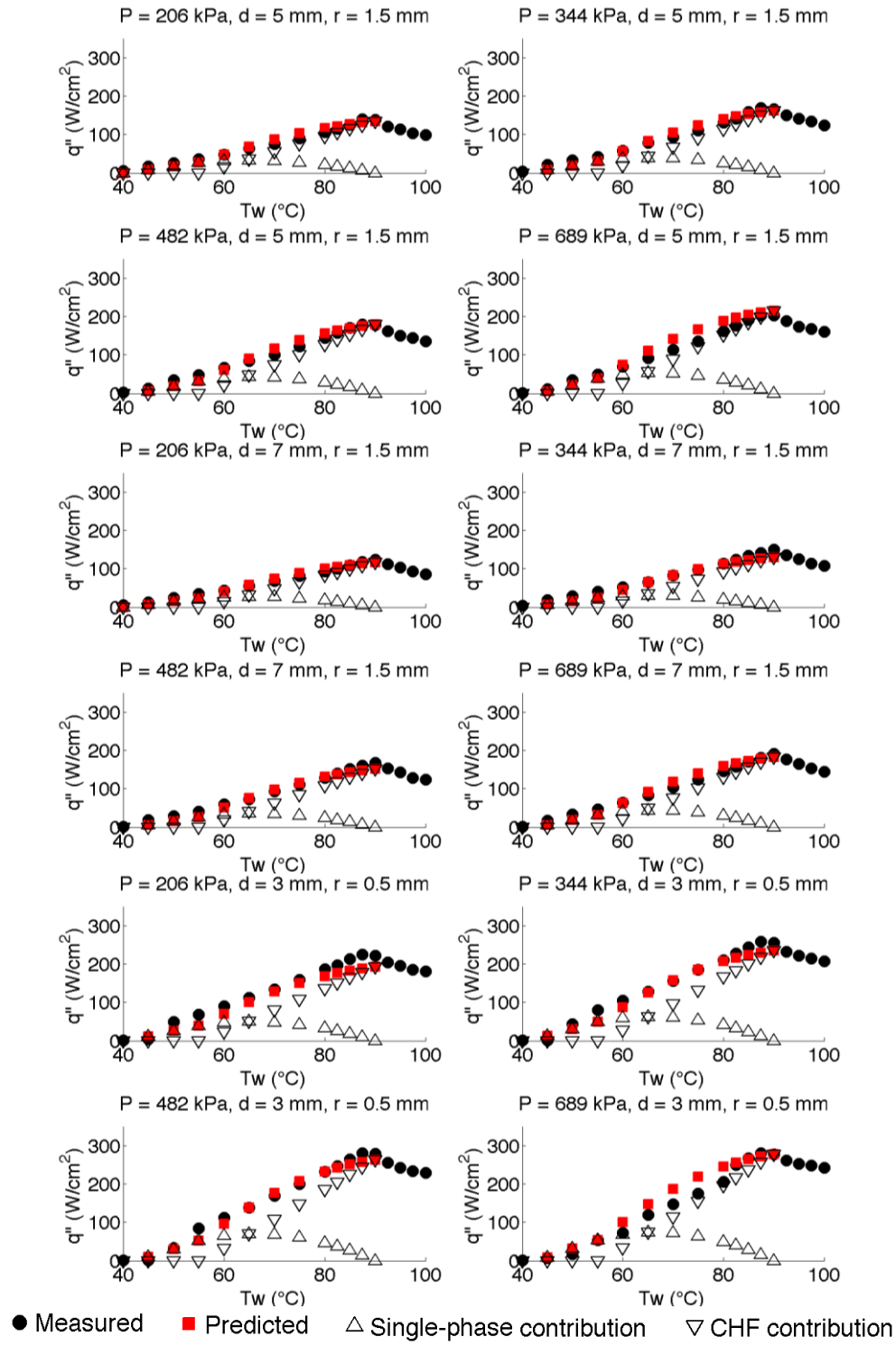

Figure 63. Measured and predicted local spray cooling curves over the impingement area of full cone sprays at 45°C

REFERENCES

Abbasi, B., Kim, J., Marshall, A., 2010, "Dynamic Pressure based prediction of spray cooling heat transfer coefficients," International Journal of Multiphase Flow, vol. 36, no. 6., pp. 491-502.

Abbasi, B., Kim, J., 2010, "Pressure-based prediction of single phase spray cooling heat transfer coefficient for low Prandtl number liquids," Proceedings of the 14th International Heat Transfer Conference – IHTC14, August 8-13 2010, Washington, DC.

Arcoumanis, C., Chang, J. C., 1993, "Heat transfer between a heated plate and an impinging transient diesel spray," Experiments in Fluids, vol. 16, pp. 105-119.

Arik, M., Bar-Cohen, A., 2003, "Effusivity-based correlation of surface property effects inpool boiling CHF of dielectric liquids," International Journal of Heat and Mass Transfer, vol. 46, pp. 3755-3764.

Ashwood, A. C., Shedd, T. A., 2007, "Spray cooling with mixtures of dielectric fluids," 23rd IEEE SEMI-THERM Symposium, pp. 144-149.

Bae, S., Kim, M. H., and Kim, J., 1999, "Improved technique to measure time and space resolved heat transfer under single bubbles during saturated pool boiling of FC-72," Experimental Heat Transfer, vol. 12 (3), pp. 265-278.

Bang, I. C., Chang, S. H., Baek, W., 2005, "Visualization of a principal mechanism of critical heat flux of pool boiling," International Journal of Heat and Mass Transfer, vol. 48, pp. 5371-5385.

Bernardin, J. D., Stebbins, C. J., Mudawar, I., 1997, "Mapping of impact and heat transfer regimes of water drops impinging on a polished surface," International Journal of Heat and Mass Transfer, vol. 40, no. 2, pp. 247-267.

Bostanci, H., Saarloos, B. A., Rini, D. P., Kizito, J. P., Chow, L. C., 2008, "Spray cooling with ammonia on micro-strauctured surfaces," IEEE transactions 2008, pp. 290-295.

Bratuta, E. G., Ivonowsky, A. Y., 1982, "Intensification of heat and mass transfer during cooling by dispersed fluids," Energa-Ma-chinotroenia, vol. 33, pp. 98-101.

Cabra R., Dibble, R. W., Chen, J. Y., 2002, "Characterization of liquid fuel evaporation of a lifted methanol spray flame in a vitiated coflow burner," National Aeronautics and Space Administration Report, NASA/CR-2002-212083, December 2002.

Cabrera, E., Gonzalez, J. E., 2003, "Heat flux correlation for spray cooling in the nucleate boiling regime," Experimental Heat Transfer, vol. 16, pp. 19-44.

Carey, V. P., 2007, “Liquid-vapor phase-change phenomena,” second edition, Taylor & Francis, Inc.

Chen R. H., Chow, L. C., Navedo, J. E., 2002, Effects of spray characteristics on critical heat flux in subcooled water spray cooling,” International Journal of Heat and Mass Transfer, vol. 45, pp. 4033-4043.

Chen R. H., Tan, D. S., Lin, K. C., Chow, L. C., Griffin, A. R., Rini, D. P., 2008, “Droplet and bubble dynamics in saturated FC-72 spray cooling on a smooth surface,” Journal of Heat Transfer, vol. 130, pp. 101501-1 – 101501-8.

Chow, L. C., Sehmbey, M. S., Pais, M. R., 1996, “Critical heat flux in spray cooling,” AIAA 33rd Aerospace Sciences Meeting and Exhibit, January 1996, Reno, NV.

Coursey, J., Kim, J., Kiger, K. T., 2005, “Spray cooling of small-pitched, straight-finned, copper heat sinks,” Proceedings of 2005 ASME International Mechanical Engineering Congress and Exhibition – IMECE2005, November 5-11 2005, Orlando, FL.

Coursey, J., Kim, J., Kiger, K. T., 2007, “Spray cooling of high aspect ration open microchannels,” Journal of Heat Transfer, vol. 129, pp. 1052-1058.

Coursey, J. S., Kim, J., 2007, “Critical heat flux enhancement through improved surface wettability with surface oxides and nano-fluids,” Proceedings of the ASME/JSME Thermal Engineering Summer Heat Transfer Conference – HT 2007, vol. 2, pp. 171-178.

Coursey, J. S., Kim, J., 2008, “Nano-fluid boiling: The effect of surface wettability,” International Journal of Heat and Fluid Flow, vol. 29, pp. 1577-1585.

Demiray, F., Kim, J., 2004, “Microscale heat transfer measurements during pool boiling of FC-72: effect of subcooling,” International Journal of Heat and Mass Transfer, vol. 47, pp. 3257-3268.

Delgoshaei, P., Kim, J., 2010, “Microscale heat transfer measurements during subcooled pool boiling of pentane: effect of bubble dynamics,” Proceedings of the 14th International Heat Transfer Conference – IHTC14, August 8-13, 2010, Washington, DC.

Dhiman, R., Chandra, S., 2008, “Rupture of radially spreading liquid films,” Physics of Fluids, vol. 20, pp. 092104-1 – 092104-9.

Duursma, G., Sefiane, K., Kennedy, A., 2009, “Experimental studies of nano-fluid droplets in spray cooling,” Heat Transfer Engineering, vol. 30, no. 13, pp. 1108-1120.

El-Genk, M. S., Parker, J. L., 2004, "Pool boiling in saturated and subcooled HFE-7100 dielectric fluid from a porous graphite surface," IEEE 2004 Inter Society Conference on Thermal Phenomena, pp. 655-662.

Elbaum, M., Lipson, G., Wettlaufer, J. S., 1995, "Evaporation preempts complete wetting," Europhysics Letters, vol. 29, no. 6, pp. 457-462.

Estes, K. A., Mudawar, I., 1995, "Correlation of Sauter Mean Diameter and critical heat flux for spray cooling of small surfaces," International Journal of Heat and Mass Transfer, vol. 38 (16), pp. 2985-2996.

Fedorchenko, A. I. and Wang, A. B., 2004 "On some common features of drop impact on liquid surfaces," Physics of Fluids, Vol. 16, No. 5, pp. 1349-1365.

Gulder, O. L., 1990, "Multiple scattering effects in dense spray sizing by laser diffraction," Aerosel Science and Technology, vol. 12, pp. 570-577.

Ha, S. J., No, H. C., 1997, "A dry-spot model of critical heat flux in pool and forced convection boiling," International Journal of Heat and Mass Transfer, vol. 41, no. 2, pp. 303-311.

Hede, P. D., Bach, P., Jensen, A. D., 2008, "Validation of the flux number as scaling parameter for top-spray fluidized bed systems," Chemical Engineering Science, vol. 63, pp. 815-828.

Horacek, B., Kim. J., Kiger, K. T., 2003, "Effects of noncondensable gas and subcooling on the spray cooling an isothermal surface," Proceedings of ASME IMECE-2003, Washington, DC.

Horacek, B., Kim. J., Kiger, K. T., 2004, "Spray cooling using multiple nozzles: Visualization and wall heat transfer measurements," IEEE Transactions on Device and Materials Reliability, vol. 4, no. 4, pp. 614-625.

Horacek, B., Kiger, K. T., Kim. J., 2005, "Single nozzle spray cooling heat transfer mechanisms," International Journal of Heat and Mass Transfer, vol. 48, pp. 1425-1438.

Hsieh, S., Tien, C., 2007, "R-134a spray dynamics and impingement cooling in non-boiling regime," International Journal of Heat and Mass Transfer, vol. 50, pp. 502-512.

Jia, J., Guo, Y., Wang, W., Zhou, S., 2008, "Modeling and experimental research on spray cooling," 24th IEEE SEMI-THERM Symposium, pp. 118-123.

Josserand, C. and Zaleski, S., 2003, "Droplet splashing on a thin film," Physics of Fluids, Vol. 15, No. 6, pp. 1650-1657.

Karwa, N., Kale, S., Subbarao, P. M. V., 2007, "Experimental study of non-boiling heat transfer from a horizontal surface by water sprays," Experimental Thermal and Fluid Science, vol. 32, pp. 571-579.

Kim, J., 2007, "Spray cooling heat transfer: The state of the art," International Journal of Heat and Fluid Flow, vol. 28, pp. 753-767.

Kim, J., 2009, "Review of nucleate pool boiling bubble heat transfer mechanisms," International Journal of Multiphase Flow, vol. 35, pp. 1067-1076.

Kim, J., 2009, "Nucleate pool boiling: The dominant bubble heat transfer mechanisms," Proceedings of the Seventh International ASME Conference on Nanochannels, Microchannels, and Minichannels, ICNMM2009, June 22-24 2009, Pohand, South Korea.

Kheshgi, H. S., Scriven, L. E., 1991, "Dewetting: Nucleation and growth of dry regions," Chemical Engineering Science, vol. 46, pp. 519-526.

Landero, J. C., Watkins, A. P., 2008, "Modeling of steady-state heat transfer in a water spray impingement onto a heated wall," Atomization and Spray, vol. 18, pp. 1-47.

Lefebvre, A. H., 1989, "Atomization and Sprays," Taylor & Francis.

Leong, M. Y., McDonell, V. G., Samuelsen, G. S., 2000, "Mixing of an airblast-atomized fuel spray injected into a crossflow of air," National Aeronautics and Space Administration Report, NASA/CR-2000-210467, October 2000.

Lin, S. P., Jiang, W. Y., 2003, "Absolute and convective instability of a radially expanding liquid sheet," Physics of Fluids, vol. 15, no. 6, pp. 1745-1754.

Manglik, R. M., Jog, M. A., 2009, "Molecular-to-large-scale heat transfer with multiphase interfaces: current status and new directions," Journal of Heat Transfer, vol. 131, pp. 121001-1 – 121001-11.

Mikic, B. B., Rosenhow, W. M., 1969 "A new correlation of pool boiling data including the effect of heating surface characteristics," Journal of Heat Transfer, vol. 9, pp. 245-250.

Moreira, A. L. N., Carvalho, J., Panao, M. R. O., 2006, "An experimental methodology to quantify the spray cooling event at intermittent spray impact," International Journal of Heat and Mass Transfer, vol. 28, pp. 191-202.

Moreira, A. L. N., Panao, M. R. O., 2007, "Heat transfer at multiple-intermittent impacts of a hollow cone spray," International Journal of Heat and Mass Transfer, vol. 49, pp. 4132-4151.

Moreira, A. L. N., Caravalho, J., Panao, M. P. O., 2007, "An experimental methodology to quantify the spray cooling event at intermittent spray impact," International Journal of Heat and Fluid Flow, vol. 28, pp. 191-202.

Moreno, G., You, S., Steinthorsson, E., 2007, "Spray cooling performance of single and multi-jet spray nozzles using subcooled FC-72," Proceedings of HT2007, ASME-JSME Thermal Engineering Summer Heat Transfer Conference, July 8-12 2007, Vancouver, British Columbia, Canada.

Mudawar, I., Bharathan, D., Kelly, and Narumanchi, S., 2009, "Two-phase spray cooling of hybrid vehicle electronics," IEEE Transaction on Components and Packaging Technologies, vol. 32, no. 2, pp. 501-512.

Mzad, H., Tebbal, M., 2009, "Thermal diagnostics of highly heated surfaces using water-spray cooling," Heat and Mass Transfer, vol. 45, pp. 287-295.

Nishio, S., Gotoh, T., Nagal, N., 1998, "Observation of boiling structures in high heat-flux boiling," International Journal of Heat and Mass Transfer, vol. 41, pp. 3191-3201.

Oguz, H. N., Prosperetti, A., 1990, "Bubble entrainment by the impact of drops on liquid surfaces," Journal of Fluid Mechanics, Vol. 219, pp. 143-179.

Panao, M. R. O., Moreira, A. L. N., 2005, "Thermo- and fluid dynamics characterization of spray cooling with pulsed spray," Experimental Thermal and Fluid Science, vol. 30, pp. 79-96.

Panao, M. R. O., Moreira, A. L. N., 2009, "Heat transfer correlation for intermittent spray impingement: A dynamic approach," International Journal of Thermal Sciences, vol. 48, pp. 1853-1862.

Prosperetti, A. and Oguz, H. N., 1993, "The impact of drops on liquid surface and the underwater noise of rain," Annual Reviews of Fluid Mechanics, Vol. 25, pp. 577-602.

Puterbaugh, R. L., Yerkes, K. L., Michalak, T. E., 2007, "Cooling performance of a partially-confined FC-72 spray: The effect of dissolved air," 45th AIAA Aerospace Sciences Meeting and Exhibit, January 8-11 2007, Reno, NV.

Rule, T. D., Kim, J., 1999, "Heat transfer behavior on small horizontal heaters during pool boiling of FC-72," Journal of Heat Transfer, vol. 121 (2), pp. 386-393.

Rybicki, J. R., Mudawar, I., 2006, "Single-phase and two-phase cooling characteristics of upward-facing and downward-facing sprays," International Journal of Heat and Mass Transfer, vol. 49, pp. 5-16.

Silk, E. A., Kim. J., Kiger, K. T., 2006, "Spray cooling of enhanced surfaces: Impact of structured surface geometry and spray axis inclination," International Journal of Heat and Mass Transfer, vol. 49, 4910-4920.

Silk, E., Kim, J., Kiger, K., 2007, "Energy conservation based spray cooling CHF correlation for flat surfaces small area heaters," ASME/JSME Thermal Engineering Summer Heat Transfer Conference, July 8-12 2007, Vancouver, British Columbia, Canada.

Sharma, A., Ruckenstein, E., 1989, "Dewetting of solids by formation of holes in macroscopic liquid films," Journal of Colloid and Interface Science, vol. 133, no. 2, pp. 358-368.

Shedd, T. A., 2007, "Next generation spray cooling: High heat flux management in compact space," Heat Transfer Engineering, vol. 28 (2), pp. 87-92.

Sodtke, C., Stephan, P., 2007, "Spray cooling on micro structured surfaces," International Journal of Heat and Mass Transfer, vol. 50, 4089-4097.

Some, T., Lehmann, E., Sakamoto, H., Kim, J., Chung, J. T., Steinthorssen, 2007 "Pressure based prediction of spray cooling heat transfer coefficient," Proceedings of IMECE2007, November 11-15, 2007, Seattle, WA, USA.

Visaria, M., Mudawar, I., 2007, "A systematic approach to predicting critical heat flux for inclined sprays, Journal of Heat Transfer," vol. 129, pp. 452-459.

Visaria, M., Mudawar, I., 2008, "Theoretical and experimental study of spray inclination on two-phase cooling and critical heat flux," International Journal of Heat and Mass Transfer, vol. 51, pp. 2398-2410.

Visaria, M., Mudawar, I., 2008, "Application of two-phase spray cooling for thermal management of electronic devices," IEEE, pp. 275-283.

Visaria, M., Mudawar, I., 2008, "Effects of high subcooling on two-phase spray cooling and critical heat flux," International Journal of Heat and Mass Transfer, vol. 51, pp.5269-5278.

Wang, A., Lin, C., Chen, C., 2000, "The critical temperature of dry impact for tiny droplet impinging on a heated surface," Physics of Fluids, vol. 12, no. 6, pp. 1622-1625.

Weiss, D. and Yarin, A., 1999, "Single drop impact onto liqud films: neck distortion, jetting, tiny bubble entrainment, and crown formation," Journal of Fluid Mechanics, Vol. 385, pp. 229-254.

Wendelstrof, J., Spitzer, K. H., Wendelstrof, R., 2008, “Spray water cooling heat transfer at high temperatures and liquid mass fluxes,” International Journal of Heat and Mass Transfer, vol. 51, pp. 4902-4910.

Yang, J., Pais, M. R., Chow, L. C., 1993, “Critical heat flux limits in secondary gas atomized liquid spray cooling,” Experimental Heat Transfer, vol. 6., pp. 55-66.
Zhu, Y., Oguz, H. N., Prosperetti, A., “On the mechanism of air entrainment by liquid jets at a free surface,” Journal of Fluid Mechanics, Vol. 404, pp. 151-177, 2000.